Polymeric Membranes for Super Critical Carbon Dioxide ($scCO_2$) Separations

A Dissertation
Presented to
The Academic Faculty

By

Madhava R. Kosuri

In Partial Fulfillment
Of the Requirements for the Degree
Doctor of Philosophy in the
School of Chemical & Biomolecular Engineering

Georgia Institute of Technology

May 2009

Polymeric Membranes for Super Critical Carbon Dioxide ($scCO_2$) Separations

Approved by:

Dr. William Koros, Advisor
School of Chemical & Biomolecular Engineering
Georgia Institute of Technology

Dr. Carson Meredith
School of Chemical & Biomolecular Engineering
Georgia Institute of Technology

Dr. Sankar Nair
School of Chemical & Biomolecular Engineering
Georgia Institute of Technology

Dr. Amyn Teja
School of Chemical & Biomolecular Engineering
Georgia Institute of Technology

Dr. Wallace Carr
Polymer, Textile & Fiber Engineering
Georgia Institute of Technology

Date Approved: January 27, 2009

A Dedication to
My dearest sisters (Anu and Suji)
& my dearest Parents

ACKNOWLEDGEMENTS

First and foremost, I would like to thank Prof. Koros for his constant encouragement, support, and guidance during my entire course of study. His utmost dedication and his unfaltering enthusiasm towards research has been a great inspiration to me. He is a great mentor who considers student's growth as the topmost priority and I am very fortunate to have him as an advisor. I would also like to thank all my other committee members: Sankar Nair, Amyn Teja, Carson Meredith, and William Carr for evaluating my thesis and giving me some valuable suggestions.

I am utmost indebted to my parents for their unconditional love and support. They have given constant encouragement in every step I have taken and thereby helped realize my dreams. I would also like to thank both my sisters, Anooradha and Sujatha, for their absolute love and encouragement in every phase of my life.

I would like to thank all my friends for their wonderful company, help and encouragement throughout my doctoral studies. Among them, I specifically want to thank my B.Tech buddy and my room mate, Venkata Nori for patiently listening to my complaints and giving me strong moral support. I would also like to thank my dearest friends and colleagues, Justin Johnson, Imona Omole and Ryan Adams for making my stay at Gatech a pleasant memorable experience. I want to thank all the Koros group members for their tremendous help in my research and also for creating a nice working atmosphere and lunches together. Among them, I would like to mention Mita Das, Jong Suk Lee, Dhaval Bhandari, Neha Bighane, and Mayumi Kiyono. I would also like to acknowledge Laurent Nassif, Jyoti Gupta, and Suchitra Konduri, who have been good friends since my first year.

TABLE OF CONTENTS

LIST OF TABLES

Page

LIST OF FIGURES

SUMMARY

Providing an energy efficient recycle for the Teflon® synthesis process is of great interest due to environmental and economic reasons. This recycle step involves separating CO_2 from a stream containing $scCO_2$ and valuable monomer (C_2F_4). Membranes provide economical and environmental friendly separations compared to conventional methods (e.g. distillation, amine absorption). Therefore, I am investigating membrane materials that are well-suited for this important separation.

Developing a robust membrane that can withstand the aggressive $scCO_2$ environment (~1070 psi of CO_2) is a key challenge. Supercritical CO_2 swells traditional polymeric membrane materials, thereby increasing segmental mobility of the polymer chains which leads to a decrease in separation capacity. There have been no polymeric membrane materials identified in the literature which are suitable for this separation. In this work, I have identified an advanced polymer, Torlon® (a polyamide-imide), that solves this problem.

After determining the appropriate material, it is important to choose a membrane morphology that is industrially desirable. The asymmetric hollow fiber membrane morphology provides the highest productivity compared to other membrane types. I have successfully produced defect-free asymmetric hollow fiber membranes using Torlon® that withstand high pressure feeds. These membranes have been shown to provide selective separations under $scCO_2$ conditions without being plasticized.

To further improve the separation performance of Torlon® membranes, the mixed matrix concept was explored. Zeolite 4A, which is relatively more permeable and selective compared to Torlon®, was chosen as the sieve material. Mixed matrix

membranes from Torlon® and zeolite 4A were made and their separation performance was measured. Based on these experimental measurements and Maxwell modeling, challenges in making successful mixed matrix membranes were identified and feasible solutions for these challenges are suggested.

CHAPTER 1

INTRODUCTION AND MOTIVATION

1.1. Motivation

The motivation of this project is to provide a membrane to enable an economical energy efficient recycle process technology for a new Teflon® production process that uses supercritical carbon dioxide ($scCO_2$) as a solvent.

1.1.1. Background on Teflon® production

Currently Teflon® is produced by free-radical polymerization of tetrafluoroethylene (C_2F_4) in an aqueous medium. In this polymerization process, perfluorooctanoic acid (PFOA), also known as "C8", is used as a dispersing agent.[1, 2] This dispersing agent/surfactant is identified by the Environmental Protection Agency (EPA) as a persistent organic pollutant and could potentially have adverse environmental and health effects in humans.[3, 4] Because of these concerns, Dupont® (the leader in Teflon® production) is trying to find alternative methods of producing Teflon®. Extensive studies are being performed by Dupont® to identify alternate dispersing agents, but to date no viable substitute has been found.

Recently a new process has been identified to produce Teflon® using $scCO_2$, an environmentally benign solvent.[3, 4] This new polymerization process does not require the use of the potentially hazardous surfactant C8. This method of producing Teflon® has been successful in lab scale batch production. To economically produce this polymer in

large quantities, a continuous process with a recycle is required. Such a continuous reactor-recycle system is shown in Figure 1.1.

1.1.2. Need for recycle in $scCO_2$ based Teflon® production

Tetrafluoroethylene reacts explosively in the presence of molecular oxygen (which acts like an initiator) to form a rubbery semi-crystalline polymer, $(CF_2\text{-}CF_2)_n$.[5] To prevent explosive reactions, C_2F_4 is stored and transported along with carbon dioxide.[6] Safety regulations state that C_2F_4 should be transported along with CO_2 as a gas mixture containing at least 30 mole% of CO_2.[6] Therefore, the highest C_2F_4 feed concentration that can be sent to the Teflon® reactor will be 70 mole%.

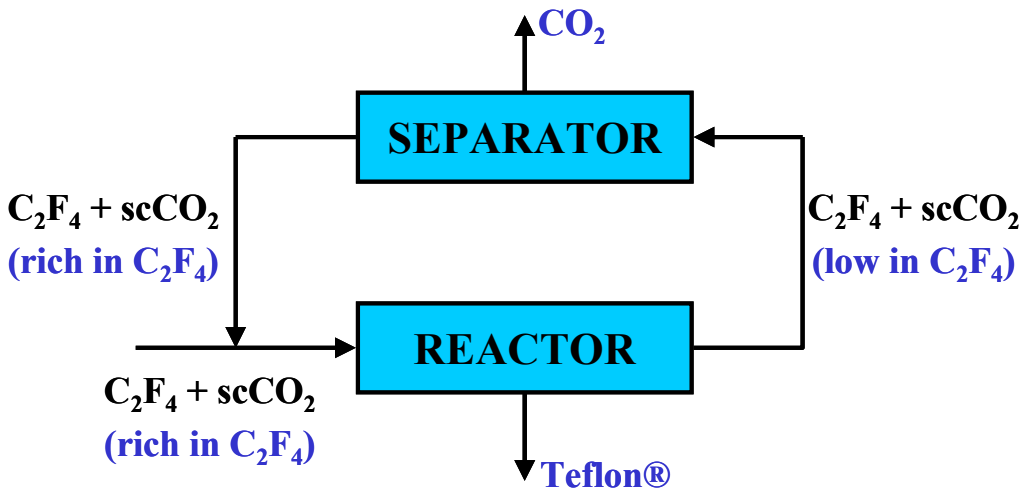

Figure 1.1: Coupled reactor-separation unit for super critical carbon dioxide based Teflon® production.

The feed mixture, C_2F_4 and CO_2, enters the reactor where some of the tetrafluoroethylene polymerizes and forms Teflon®, which precipitates. The remaining un-reacted C_2F_4, along with CO_2, exits the reactor. This un-reacted and valuable C_2F_4 need to be recycled for economic and environmental reasons. This is done by selectively removing CO_2 from the exit stream and the resulting enriched C_2F_4 stream is sent back to the reactor. An overall mass balance indicates that the amount of CO_2 that needs to be separated from the exit stream is the same as the amount of CO_2 that is fed to the reactor. So, the reason for CO_2 separation arises because of the addition of CO_2 to the reactor along with the monomer, C_2F_4.

1.1.3. Comparison of various separation techniques for CO_2 removal

Cryogenic distillation, amine absorption, and membrane separation are three techniques primarily used for CO_2 removal. These three techniques are briefly reviewed and compared in the following paragraphs.

1.1.3.1 Cryogenic Distillation[7]

A distillation process separates components based on the differences in their boiling points. The boiling points of CO_2 and C_2F_4 are -78.5 °C and -75.6 °C respectively. Since the boiling points are quite close, many stages may be required to perform the separation effectively. To estimate the required number of stages, one needs the equilibrium data for CO_2 and C_2F_4 gas pair. This information is not available in the literature. However, if one takes an analogy with respect to propane and propylene gas mixture, the boiling points of propane and propylene are -42.1 °C and -47 °C,

respectively. For this difference of -4.9 °C, typically about 100-300 stages are used to perform the separation.[8] So clearly in our case as the difference in the boiling points for CO_2 and C_2F_4 is 2.9 °C, which is smaller than in the case of propane/propylene, one could expect even more number of stages than 100-300.

Such large number of stages makes the installation costs for distillation expensive. Moreover, the gases need to be condensed to low temperatures of -78.5 °C for separation and then after the separation they have to be heated back to the reactor conditions of 35 °C. These cooling and heating steps add additional energy costs to the distillation process. Because of these high installation and high operational costs, distillation is not an attractive economic solution for separating CO_2 and C_2F_4 mixture.

1.1.3.2. Absorption[7]

In this process an organic liquid is used to selectively absorb CO_2 from the gas mixture. This process generally takes place in a tower, similar to a distillation column. For this process to be effective the organic liquid must have a higher affinity for CO_2 than the other component.

In our desired separation, both CO_2 and C_2F_4 gases have different chemical properties. Because of the inert characteristics of fluorine molecules, C_2F_4 is relatively more inert compared to CO_2. Even though CO_2 has net zero polarity, the individual oxygen's of CO_2 are slightly negative. This difference in chemical properties can be captured by choosing an appropriate liquid.

The main drawback of the absorption process is the regeneration step. Once the organic liquid is saturated with CO_2, it needs to be heated to strip the absorbed CO_2. This

regeneration step is energy intensive and increases the operational costs of the absorption process. This separation process is economical if the amount of CO_2 to be separated is small, as in such a case, not much liquid needs to be regenerated. However, in our intended separation, at least 30% of the feed flow rate is CO_2 and this entire amount needs to be separated. This means high regeneration costs will be encountered. Because of such high anticipated operational cost, the absorption process is not an attractive option.

1.1.3.3. Membrane Separation[9]

Membranes separate gases by selectively allowing a particular gas to pass through them. The membranes differentiate gases based on their size, shape and chemical properties. Since CO_2 and C_2F_4 gases differ on all of these three factors, membrane separations are ideal for this CO_2/C_2F_4 separation.

Compared to distillation and absorption processes, membrane separations are very energy efficient. There is no regeneration step involved as in the case of absorption process and there is no cooling and heating of gases as in the case of distillation process. In addition to energy efficiency, membranes have low installation costs and operating costs. This is evident from the picture shown in Figure 1.2. The two big amine towers (used in absorption process) are completely replaced by a small membrane unit (shown towards the bottom of the figure). Since the membrane unit is quite small, the installation costs are also quite low. There are no moving parts in the membrane unit, so it is easy to operate and has low operational costs. Membranes are also environmentally friendly (because no organic liquids are used as in the case of absorption process).

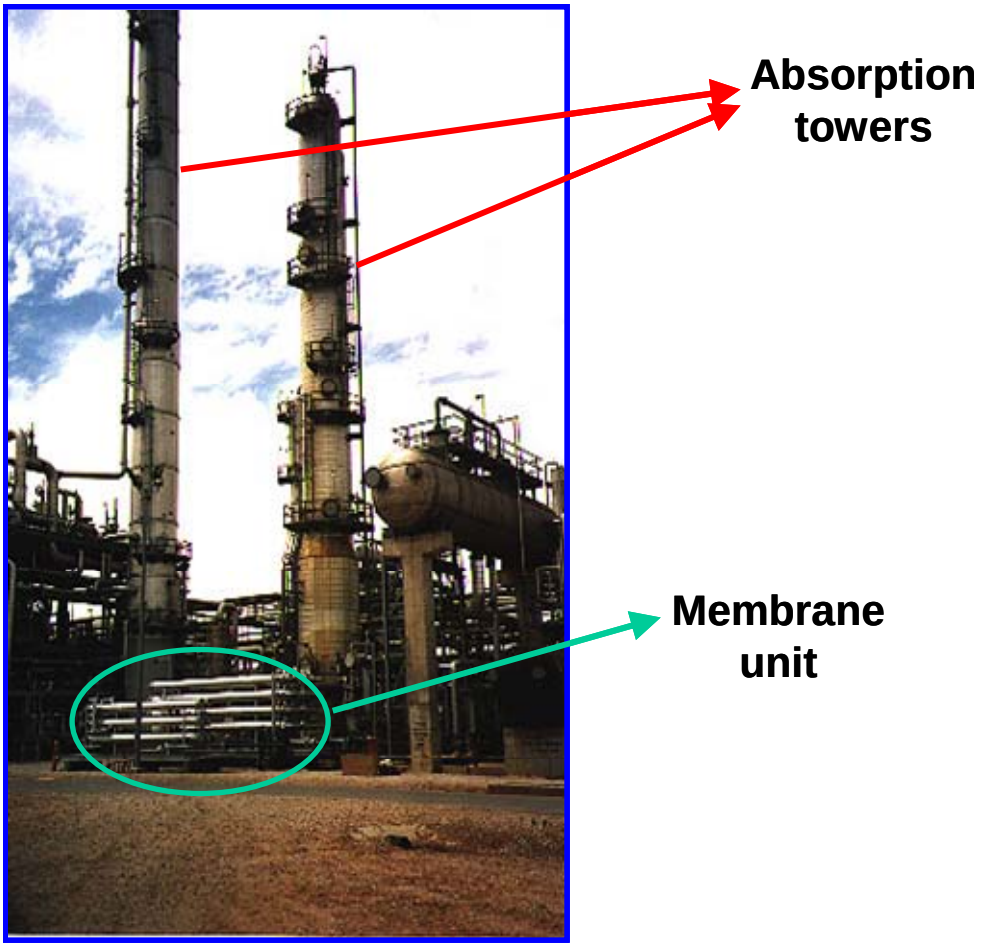

.

Figure 1.2: Comparison between membrane separation process and amine absorption process. This picture is a courtesy of Medal inc.

Because of the above mentioned advantages, the membrane technology was selected for our desired separations. The next section covers the background, introduction, and challenges of membrane separations in CO_2 and C_2F_4 application.

1.2. Gas Separation Membranes

As mentioned in the previous section, membranes separate gases based on the relative differences in the gas diffusion rates. These diffusion rates in turn depend on the differences in shape, size and chemical nature of the gas molecules. Depending on the type of membrane material and separation mechanism, membranes are classified into various categories. The principal ones are: polymeric membranes, inorganic membranes, carbon molecular sieves, and liquid membranes. A brief description of these different membrane types and their pros and cons are described in the following sections.

1.2.1. Polymeric Membranes[10]

Polymeric membranes separate gases by the sorption-diffusion mechanism. In this process, gas molecules are absorbed into the membrane and then the absorbed molecules diffuse through it. The sorption (absorption) depends on the chemical nature of the molecules whereas the diffusion depends on the shape and size of the molecules.

These membranes are relatively easy to process and are inexpensive. They can be scaled up to industrial applications relatively easily; however, they have moderate gas separation capabilities compared to some other membrane types (discussed in the following sections). The advantages of these polymeric membranes outweigh their shortcomings and as such these membranes are widely used industrially.

1.2.2. Inorganic Membranes[9]

Inorganic molecular sieve membranes have precise openings which allow small gas molecules (smaller than the sieve openings) to permeate while rejecting larger ones. The

separation performance of these membranes can surpass polymeric membranes not only in their separation efficiency but also in the rate of separation. These membranes are chemically more inert and thermally more stable compared than polymeric membranes. Unlike current polymeric membranes, they can be used in aggressive feed separations (example: high CO_2 concentration feeds) and high temperature separations. However these membranes are quite expensive (roughly about two orders of magnitude or more) and are hard to handle and process. Because of these drawbacks, the applications of these membranes are limited to small scale applications.

1.2.3. Carbon Molecular Sieves[10]

Similar to inorganic membranes, carbon molecular sieve (CMS) membranes operate primarily on the size exclusive mechanism. These membranes also have better separation performance both in terms of efficiency and rate of separation compared to polymeric membranes. However, defect-free CMS membranes are hard to make in large scale batches. Moreover, these membranes are brittle and cannot withstand mechanical shocks, so CMS membranes were not yet employed in industrial applications.

1.2.4. Liquid Membranes[9]

Liquid membranes consist of carrier components (often ionic liquids are used). The gases are separated based on the differences in interactions between the carrier components and the gases. The fluxes through such membranes can be considerably higher than polymers, and in certain separations, they could also have much higher separation efficiencies compared to polymeric counterparts. The long term stability of

these membranes is an important issue, since the ionic liquids or other carrier can be lost (either due to evaporation or leakage) over time, jeopardizing the membrane performance. In addition, these membranes are unstable under high pressures. Due to these reasons, the industrial application of these membranes has not yet been realized.

Because of the economics and the ease in scale up of polymeric membranes to industrial application, polymeric membranes are pursued in this project for separating CO_2 and C_2F_4. A brief history, introduction and challenges to polymeric gas separations are detailed in the following section.

1.3. Polymeric Gas Separation Membranes

1.3.1. History and introduction to polymeric membranes[9, 10]

Researchers have been working on gas separation membranes since as early as 1850, roughly for the past 150 years. However, only recently (about 30 years ago), membranes have been used industrially for major gas separations. Most of the early work (1850-1960) was spent on understanding the transport through the membranes. During this time, membranes were not attractive for industrial applications because the fluxes through them are very low; however a great breakthrough in terms of industrial application occurred when Loeb and Sourirajan made asymmetric membranes[11] in 1962 and it formed the basis for modern molecularly selective membrane technology.

Asymmetric membranes consist of a thin separating layer on a porous substructure. A schematic of such a membrane is shown in Figure 1.3. The thin outer layer does the separation of the gases whereas the porous substructure provides mechanical strength to

the membrane for high pressure applications. Since the separating layer is quite thin, the resistance to gas transport is greatly reduced, thereby largely increasing the gas fluxes.

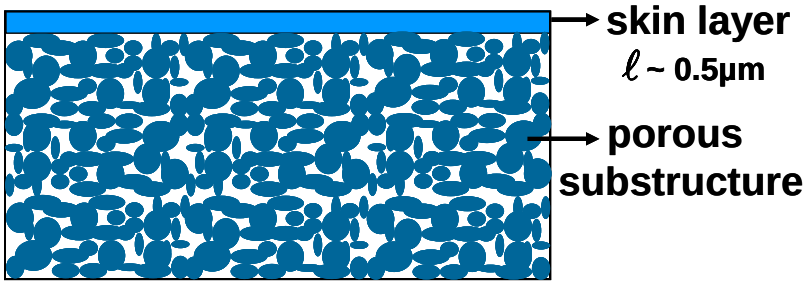

Figure 1.3: Cross-section of an asymmetric flat membrane showing the separating layer (skin layer) and the porous substructure.

Another breakthrough in membrane technology took place when asymmetric membranes were made in hollow fiber form. The schematic of such a fiber is shown in Figure 1.4. These fibers can be packed in small volume units (Figure 1.5) resulting in high surface area to volume ratios. This considerably decreased the cost of a membrane unit, which is particularly important for high pressure feeds. A comparison of surface-to-volume ratios of asymmetric hollow fiber membranes with other membrane types (spiral wound and dense film) is shown in Figure 1.6.[9]

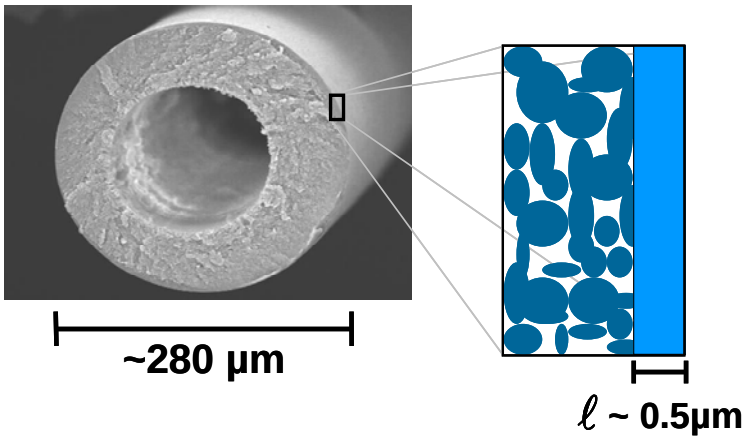

Figure 1.4: Cross-section of an asymmetric hollow fiber membrane showing the separating layer and the support layer.

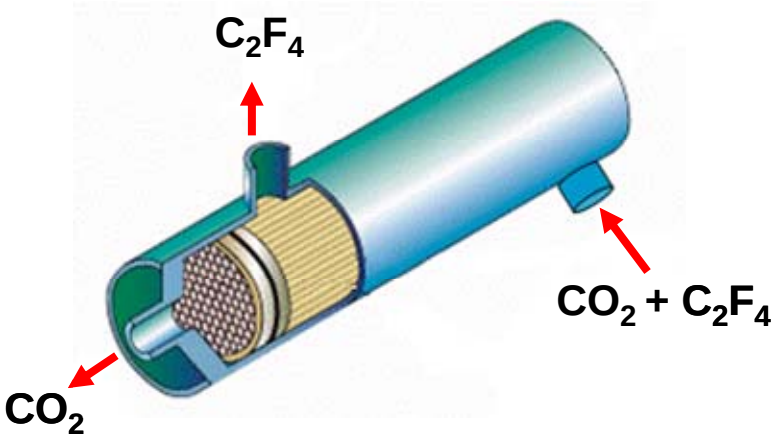

Figure 1.5: A schematic of a membrane module showing tight packing of hollow fiber membranes.

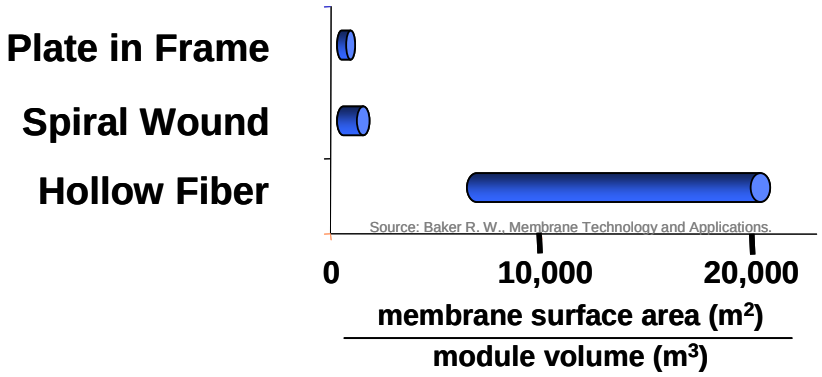

Figure 1.6: Comparison of membrane surface area to volume ratios of different module types: plate in a frame, spiral wound, and hollow fiber. Hollow fibers show the highest surface to volume ratio compared to other forms.

Because of the advantages associated with asymmetric hollow fiber form, I have used a membrane with such productive morphology in this work.

1.3.2. Challenge of using polymeric membranes for CO_2/C_2F_4 separations

The current technology in polymeric membranes is limited to separating non-interacting gas molecules (gases that do not have strong interactions with polymers) or low concentrations of interacting gas molecules. Examples of non-interacting gas separations include air separations[12] (nitrogen & oxygen production) and hydrogen/nitrogen purification in ammonia synthesis. An example of an interacting gas separation is natural gas purification by selectively removing CO_2. The current technology removes CO_2 from a natural gas stream only if CO_2 partial pressure is less than 200psi,[13] since above this 200psi, the membrane becomes unstable and loses selective separations. Such polymers are not suitable for separating high partial pressures of CO_2 that would be encountered in the exit stream of the Teflon® reactor (refer to

Figure 1.1 for the process). The stream coming out of the Teflon® reactor has CO_2 in supercritical conditions (P_{CO2} > 1070psi) and as such existing polymer membranes cannot be used directly. To use the existing membrane technology, one needs to de-pressurize the exit stream to low pressures and use membranes to separate CO_2 and the resulting stream would need to be re-pressurized and sent back to the reactor. The schematic of such a process is shown in Figure 1.7.

Such a process requires additional expander and compressor units which increase the capital costs. More importantly, large energy costs are involved in compressing the gas from 200psi to supercritical pressures. Because of these high capital and operational costs, current polymeric membrane technology is uneconomical for the desired $scCO_2$ separations.

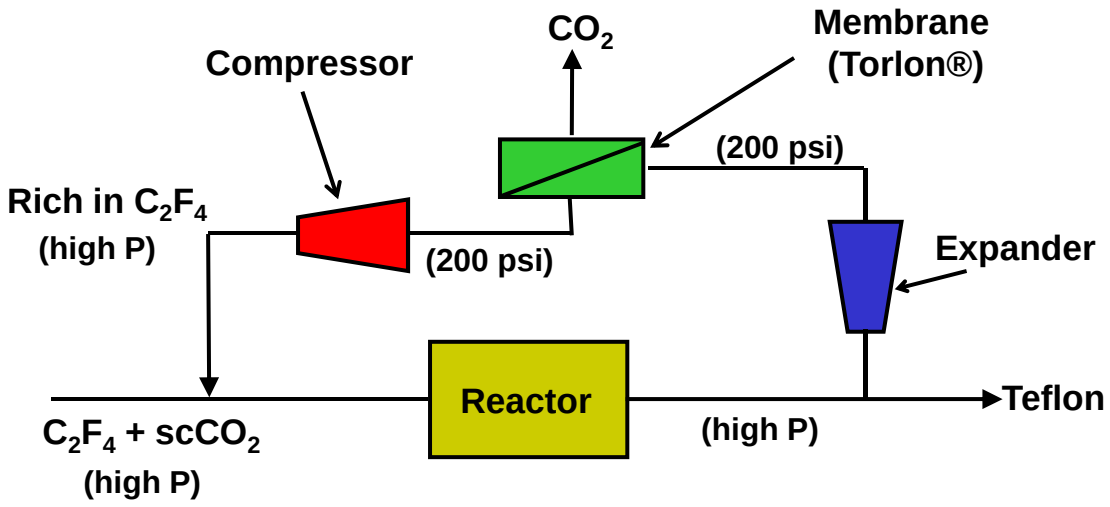

Figure 1.7: Reactor-separation unit for Teflon® production using the existing membrane technology for CO_2 separation.

If a new membrane material is identified that can provide selective separations under supercritical conditions, then such a membrane could separate CO_2 directly from the exit stream of the reactor and the resulting enriched C_2F_4 stream can be sent to the reactor without any compression. Such a technology will not only eliminate the unnecessary compressor and expander units but also the large compression costs. The schematic of such a simplified process is shown in Figure 1.8, and such an approach will make the recycle process less energy intensive and improve overall Teflon® production economics.

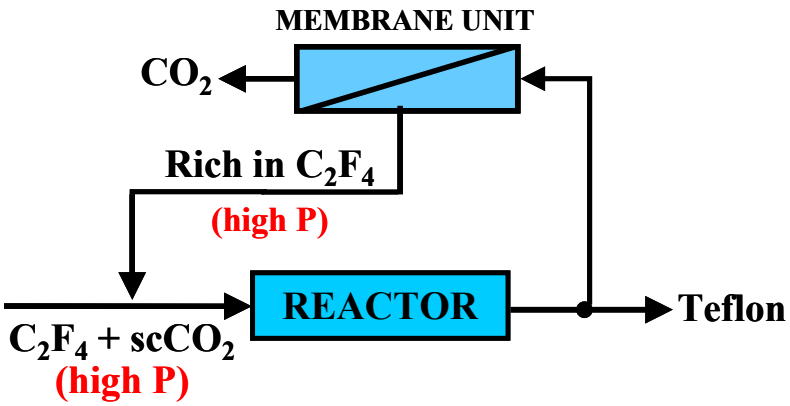

Figure 1.8: Reactor-separation unit for Teflon® production using the ideal membrane technology.

The motivation of this project is to identify such a robust material and to develop a productive membrane (asymmetric hollow fiber membrane) from this material. Such a membrane could also be used in other recycle systems encountered in similar $scCO_2$ based polymerization processes (such as vinylidene fluoride and vinyl fluoride synthesis processes[2]) and also for purification of high CO_2 content natural gas streams[14].

1.4. Mixed Matrix Technology

Once a successful polymer membrane technology is identified for $scCO_2$ separations, studies involved in further improving its separation properties will also be investigated.

As mentioned earlier, polymeric membranes have low separation performance characteristics compared to inorganic molecular sieving materials (zeolites). The separation performance of polymers is bounded by a tradeoff line as shown in Figure 1.9.[15] The figure shows the separation characteristics of various polymers (each black dot corresponds to a different polymer) in separating CO_2 and CH_4. This type of trend would be applicable to CO_2 and C_2F_4 separations, but such data do not exist for this pair to show the tradeoff between the intrinsic rate of separation (permeability, x-axis in the figure) and the efficiency of separation (selectivity, y-axis in the figure). Inorganic molecular sieves are not bounded by this tradeoff and as such they have superior separation performance compared to the polymers. For comparison, the potential zeolite permeabilities and selectivities are also plotted in Figure 1.9. As noted earlier, difficulty and cost in handling and processing such zeolites limits their utility in large scale membranes, whereas polymeric membranes are easy to handle and process.

Since the two material types have opposite pros and cons, the idea of combining the pros of the two materials has evolved into the mixed matrix concept, which has gained a lot of attention in the recent years.[16-20] These mixed matrix materials combine the efficient separation of zeolites and the processability of polymers.

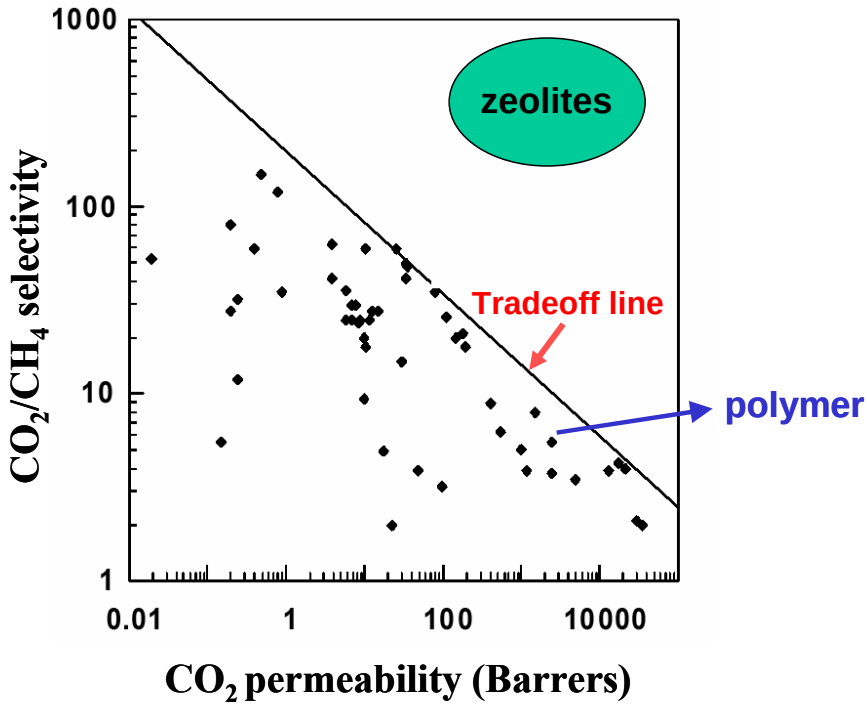

Figure 1.9: Tradeoff line between permeability and selectivity for polymeric membranes. The data is obtained at 35 °C, at pressures less than 10atm and with pure gases.

Having a good polymer-zeolite interface is critical in making a good mixed matrix membrane. If there is a bad interface (i.e. a gap exists between the polymer and zeolite), then the gas molecules could go through this gap and bypass the sieve and as such the advantage of the zeolite will be lost. Indeed achieving a good polymer-sieve interface is a key challenge of such mixed matrix membranes.

1.5. Research Objectives

As explained in the above motivation and introduction sections, I intend to provide productive and selective separations of CO_2 and C_2F_4 using polymeric and/or composite (mixed matrix) membranes. This overall objective was approached in a systematic manner and has been divided into three sub-objectives.

Objective 1: To produce an asymmetric hollow fiber membrane from Torlon® with a defect free skin layer that could withstand high pressures.

Torlon®, a polyamide-imide polymer, was identified as a candidate polymer for $scCO_2$ separations. After choosing the polymer, we must identify the experimental procedures and conditions for making a defect-free asymmetric hollow fiber membrane. A major requirement for this membrane is the ability to withstand high pressures that are encountered in supercritical conditions (P > 1070psi). Methods of making such a fiber are investigated in this objective.

Objective 2: Study the performance of the membranes for separating CO_2 from the $scCO_2$ and C_2F_4 gas mixture.

Once a high strength membrane with a defect-free skin layer is prepared, it is tested for actual CO_2 and C_2F_4 separations. Since C_2F_4 is explosive, we could not study CO_2/C_2F_4 separations in our laboratories for safety reasons. Instead, we have chosen CO_2/C_2H_4 and $CO_2/C_2H_2F_2$ gas pairs to predict the separation performance of CO_2/C_2F_4. The CO_2/C_2H_4 and $CO_2/C_2H_2F_2$ separation performance is evaluated at various partial pressures of CO_2.

Objective 3: To produce a mixed matrix membrane from Torlon® and zeolite 4A.

To further improve the properties of polymeric membranes, the concept of mixed matrix membranes is investigated. Zeolite 4A, is chosen because it has a pore dimension of 3.8Å which is ideal for CO_2 transport but not for C_2F_4. Making a good polymer-zeolite interface is the central aim of this objective.

1.6. Dissertation Overview

This dissertation is divided into seven chapters including this chapter. The description of each of the chapters is as follows:

Chapter 2 explains the gas transport mechanisms through the polymer and the zeolite materials. Challenges in making successful polymeric and mixed matrix membranes are also covered.

Chapter 3 describes the materials used and the reasons for selecting those materials. The experimental methods in making dense membranes and asymmetric hollow fiber membranes are described in detail. The characterization techniques used to measure the properties of polymer, zeolite and the membranes are also explained.

Chapter 4 identifies the experimental conditions for making a successful asymmetric hollow fiber membrane from Torlon®.

Chapter 5 discusses the characterization results of the produced Torlon® hollow fiber membrane for the separation of CO_2 and C_2F_4.

Chapter 6 describes the challenges encountered in making good Torlon®-zeolite 4A mixed matrix membranes. The methods taken to improve the interface and the outcome of these methods will also be disclosed.

Chapter 7 reviews the accomplishments of this research and will address the areas where future work needs to be done to further advance the project.

1.7. References

1. Tan, L.S. and R.S. Buckanin, Emulsion polymerization of fluorinated monomers, 2007, U.S. Patent, US 7,262,246 B2.

2. Kennedy, K.A., G.W. Roberts, and J.M. DeSimone, *Heterogeneous polymerization of fluoroolefins in supercritical carbon dioxide.* Advanced Polymer Science, 2005. 175: p. 329.

3. Cooper, A.I. and J.M. DeSimone, *Polymer synthesis and characterization in liquid / supercritical carbon dioxide.* Current Opinion in Solid State & Materials Science, 1996. 1: p. 761.

4. DeSimone, J.M., Method of making fluoropolymers, 1996, U.S. Patent, 5,496,901.

5. Gozzo, F. and G. Camaggi, *Oxidation reactions of tetrafluoroethylene and their products-I (Auto-oxidation).* Tetrahedron, 1966. 22: p. 1765-1770.

6. Bramer, D.J.V., M.B. Shiflett, and A. Yokozeki, Safe handling of tetrafluoroethylene, 1994, U.S.Patent, 5,345,013.

7. Humphrey, J.L. and G.E.K. II, *Separation Process Technology*. 1997: McGraw-Hill.

8. Burns, R.L., *Investigation of Poly(pyrrolone-imide) Materials for the Olefin/Paraffin Separation*, in *Chemical Engineering*. 2002, The University of Texas at Austin: Austin. p. 1-15.

9. Baker, R.W., *Membrane Technology and Applications*. 2000, McGraw-Hill: New York. p. 87-157.

10. Mulder, M., *Basic Principles of Membrane Technology*. 2nd edition ed. 2003, Boston: Kluwer Academic Publishers. 71-156.

11. Loeb, S. and S. Sourirajan, *Sea water demineralization by means of an osmotic membrane.* Advances in Chemistry Series, 1962. 38: p. 117.

12. R., P., N. F., and T.D. R., *Evolution of membranes in commercial air separation.* Journal of Material Science, 1994. 94: p. 225.

13. Bos, A., et al., *Plasticization-resistant glassy polyimide membranes for CO2/CH4 separations.* Separation and Purification Technology, 1998. 14: p. 27.

14. Wind, J.D., D.R. Paul, and W.J. Koros, *Natural gas permeation in polyimide membranes.* Journal of Membrane Science, 2004. 228: p. 227.

15. Robeson, L.M., *Correlation of separation factor versus permeability for polymeric membranes.* Journal of Membrane Science, 1991. 62: p. 165.

16. Husain, S. and W.J. Koros, *Mixed matrix hollow fiber membranes made with modified HSSZ-13 zeolite in polyetherimide polymer matrix for gas separation.* Journal of Membrane Science, 2007. 288: p. 195.

17. Mahajan, R. and W.J. Koros, *Mixed matrix membrane materials with glassy polymers. Part 1.* Polymer Engineering and Science, 2002. 42(7): p. 1420.

18. Mahajan, R. and W.J. Koros, *Mixed matrix membrane materials with glassy polymers. Part 2.* Polymer Engineering and Science, 2002. 42(7): p. 1432.

19. Shu, S., S. Husain, and J.K. William, *A general strategy for adhesion enhancement in polymeric composites by formation of nanostructured particle surfaces.* The journal of physical chemistry C, 2007. 111(2): p. 652.

20. Shu, S., S. Husain, and J.K. William, *Formation of nanostructured zeolite particle surfaces via a halide/grignard route.* Chemistry of materials, 2007. 19(16): p. 4000.

CHAPTER 2

THEORY AND BACKGROUND

This chapter covers the basic concepts needed for understanding both the gas separation mechanisms and the challenges in making polymeric and mixed matrix membranes. The first section briefly recaps the gas transport through polymeric and inorganic molecular sieve materials. The second section describes the formation process involved in making asymmetric hollow fiber membranes from a polymeric solution. The challenges encountered in making a successful asymmetric hollow fiber membrane are also described. Finally in the last section, gas transport through mixed matrix membranes and the challenges in making a successful mixed matrix membrane are detailed.

2.1. Membrane Transport Theory

Membranes separate gas mixtures by selectively permeating a particular gas more rapidly than the other. Two different types of membranes are studied in this work: polymeric membranes and mixed matrix membranes. As described in Chapter 1, mixed matrix membranes are the combination of polymeric materials and inorganic molecular sieves. These two different types of materials separate gases based on the same general mechanism and the overall separation performances of these materials are characterized using the same parameters. These parameters are described in the following section.

2.1.1. Separation Characteristics of a Membrane

The gas molecules that need to be separated are introduced to the upstream side of the membrane at relatively high pressures. Depending on the chemical nature of the gas molecules, the molecules adsorb/absorb (hence the term "sorb" is used) into the membrane in different amounts. These sorbed molecules then diffuse to the downstream side of the membrane (low pressure side) where they desorb to complete the permeation process. This process is schematically shown in Figure 2.1. During this gas transport process, it is assumed that the gas phases on either side of the membrane are in thermodynamic equilibrium with their respective membrane interfaces, and the interfacial adsorption and desorption processes are rapid compared to the rate of diffusion through the membrane.

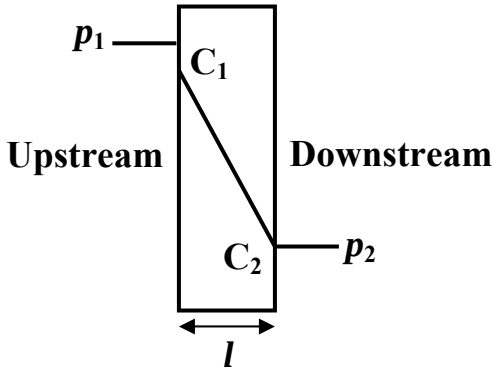

Figure 2.1: Schematic of gas permeation through a polymer film.

Permeability and selectivity are the two parameters used to characterize the membrane's separation performance. The permeability coefficient characterizes the productivity of the membrane and is defined as the flux of species A (N_A) through the membrane normalized by the membrane thickness (l), and the partial pressure difference

of species A (Δp_A) across the membrane (Equation 2.1). In the case of gases that show non-ideal gas phase effects, fugacity difference (Δf_A) is used instead of partial pressure difference (Δp_A).

$$P_A = \frac{N_A * l}{\Delta p_A} \tag{2.1}$$

The most common units for the permeability coefficient are "Barrers", where 1 $Barrer = 10^{-10}\,(cm^3_{STP} * cm)/(cm^2 * \sec * cmHg)$. In the case of asymmetric membranes, where the thickness of the membrane is not known unambiguously, permeance (instead of permeability) is used to characterize the membrane separation. Permeance is defined as

$$\left(\frac{P}{l}\right)_A = \frac{N_A}{\Delta p_A} \tag{2.2}$$

Permeance has units of "gas permeation units" (GPUs), where $1\,\mathrm{GPU} = 10^{-6}\,cm^3_{STP} / \left(cm^2 \cdot sec \cdot cmHg\right)$.

In the case of negligible downstream pressure $\left(p_A^{dowstram} \sim 0\right)$ and when the Fickian diffusion is the rate determining transport through the membrane, the permeability is given as the product of the average solubility coefficient of the gas $\left(S_A\right)$, and the average diffusion coefficient of the gas $\left(D_A\right)$, viz.,

$$P_A = D_A \times S_A . \tag{2.4}$$

Both the diffusion and sorption coefficients depend on the chemical and physical nature of the gas molecules and also on the type of membrane material. This dependence is described in the following sections. The permeability of a gas can be increased by

increasing either the sorption coefficient or the diffusion coefficient through the membrane.

The second parameter used to describe the separation performance of the membrane is the separation factor (SF) and is given by:

$$SF = \left(y_A / y_B\right) / \left(x_A / x_B\right). \tag{2.5}$$

Where y_A and y_B represent the mole fractions of components A and B in the down stream and x_A and x_B represent the mole fractions of components A and B in the upstream, respectively. The separation factor is a measure of membrane's ability to differentiate between two co-permeating gas species. When the downstream pressure is negligible compared to the upstream pressure, then the separation factor equals the ratio of the individual permeabilities (or permeances) of the components. This ratio is referred as the intrinsic selectivity of the membrane. The mathematical expression is given by:

$$SF = \alpha_{A/B} = \frac{P_A}{P_B} = \frac{\left(\frac{P}{l}\right)_A}{\left(\frac{P}{l}\right)_B} \tag{2.6}$$

2.1.2. Diffusion through polymers[1]

Molecules diffuse through a dense non-porous membrane by taking a random jump from one position to another. This jump is initiated when an opening (big enough for the molecule to jump) is created next to the existing gas molecule. The jump is completed when the molecule jumps into this new opening and the hole left behind by the displaced molecule is closed, thereby trapping the gas molecule in its new position. The schematic of this diffusion process is shown in Figure 2.2.

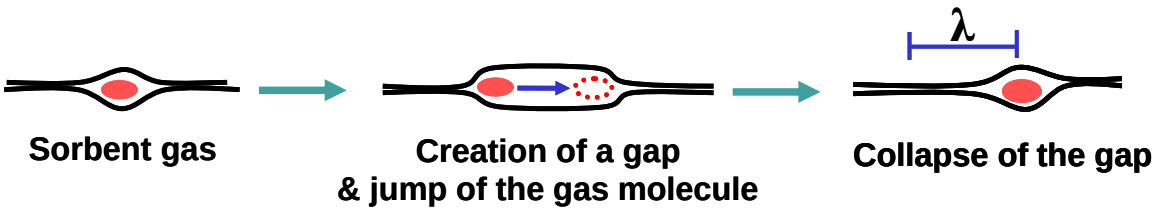

Figure 2.2: Schematics of diffusion through dense polymeric membrane, where λ is the average length of a random diffusion step.

The rate of diffusion is proportional to the length and frequency of the jumps. These parameters in turn depend on the length and frequency of the openings. In a given polymer, smaller openings are more frequent compared to bigger ones then in such a polymer, small size penetrants (which required only small openings) will diffuse faster compared to large size penetrants. This way the membrane provides size discrimination (diffusion selectivity) between the molecules.

The length and frequency of the openings are determined by thermal fluctuations of the polymeric chains. If these thermal fluctuations are large then the frequency of large openings will be similar to the frequency of small openings resulting in very little size discrimination. On the other hand, if these thermal fluctuations are small then the frequency of large openings will be low compared to the frequency of the small openings resulting in greater size discrimination. Glassy polymers with rigid back bone structures have low thermal volume fluctuations and therefore provide good diffusion selectivities. However, since they have low thermal fluctuations, the fluxes (diffusivities) through the glassy polymers tend to be small.

The gas diffusion through a polymeric membrane not only depends on the thermal fluctuations but also depend on free volume of the material. The free volume of the polymer is defined as the difference between the specific volume of the polymer (v) and the specific volume occupied by the polymeric chains (v_o). This free volume comprises the sum of the many small spaces between the polymeric chains and is increased when the polymeric chain segments are not well packed. Bulky pendant groups and backbone rigidity of the polymer can promote greater free volume in the amorphous state. If a material has higher free volume, gases diffuse faster through that material.

Therefore, by structural engineering, a material can have both higher diffusivities (fluxes) and higher diffusion selectivities if it has a higher free volume and also has low thermal fluctuations.

1.2.3. Sorption in Polymers[2]

Equilibrium sorption coefficient (S) of a gas in a polymer is defined as the ratio of the concentration of dissolved gas in the polymer (c) to the pressure of gas in the continuous gas phase (p):

$$S = \frac{c}{p}. \tag{2.7}$$

Equilibrium gas sorption in glassy polymers is well described by dual mode sorption model. According to this model, glassy polymeric membranes have two kinds of sorption sites. In one kind, the polymer segments are in packing equilibrium with each other, and in the other kind, the polymer segments are not in packing equilibrium with each other. In the non-equilibrium state, gaps or voids exist between the chains, thereby providing low energy sorption sites.

Sorption occurs at the two different sites via different mechanisms. In the well-packed sites, sorption shows a simple behavior as in liquids and is described by Henry sorption coefficient, so these equilibrium sites are often referred as Henry's sorption sites. The concentration of the dissolved gas (c_D) in the polymer in these sites is given by

$$c_D = K_D \times p\,. \tag{2.8}$$

Where K_D and p represent the Henry's (or Bunsen) sorption coefficient and partial pressure of the gas respectively.

In the non-equilibrium segmental packing sites, sorption follows Langmuir sorption model described by the following expression:

$$c_H = \frac{C_H^{'} \times b \times p}{1 + b \times p}\,. \tag{2.9}$$

Where c_H, $C_H^{'}$, and b represents the concentration of the dissolved gas in the polymer in the non-equilibrium sites, Langmuir sorption capacity, and the Langmuir affinity parameter respectively. Since the sorption occurs in these non-equilibrium sites via Langmuir adsorption model, these sites are often referred as Langmuir sorption sites, and since these sites are limited in number, the sorption becomes saturated once all the sites are filled.

The net sorption in the polymer at a pressure, p, is the sum of the sorptions at both these sites:

$$c = c_D + c_H = K_D p + \frac{C_H^{'} \times b \times p}{1 + b \times p}\,. \tag{2.10}$$

2.1.4. Sorption and diffusion through zeolites[3]

Zeolites are ultra-microporous and consist of large cavities interconnected by narrow channels. During the sorption process, the gas molecules enter through these narrow channels and sorb in the large cavities. The sorption follows the Langmuir sorption model similar to the sorption in the Langmuir sites of the polymer. The concentration of the absorbed gas in the zeolites is given by:

$$c_Z = \frac{C'_{HZ} \times b_Z \times p}{1 + b_Z \times p}. \tag{2.11}$$

Where C'_{HZ}, and b_Z represent the Langmuir sorption capacity, and the Langmuir affinity parameter for the zeolite. Since the number of sorption sites in the large cavities is limited, the sorption in these sites are also becomes saturated at high pressures.

During steady state permeation process, the sorbed molecules diffuse through the zeolites by making random jumps through the interconnected channels. The schematic illustrating the diffusion through the zeolite membranes is given in Figure 2.3.

The rate of jumps through these narrow channels determines the diffusion coefficient through the zeolites. The frequency of the jumps depends on the shape and size of the molecules relative to the shape and size of the interconnected channels. The frequency is lowered when the size of the gas molecule approaches the size of the channel or when the molecule has to orient itself in a particular direction to traverse the channel. So zeolites separate gases based on the relative differences in the shapes and sizes of the gas molecules.

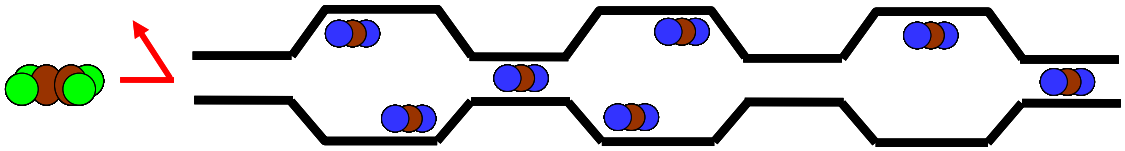

Figure 2.3: Schematics illustrating molecular sieving by zeolites.

2.2. Asymmetric hollow fiber membranes and their formation

As explained in the previous chapter, asymmetric hollow fiber membranes have the most productive form compared to other types of membranes (Figure 1.6). They consist of a thin dense selective skin layer supported on a porous substructure (Figure 1.4). These membranes are made using dry-wet spinning process, which is explained in the following section.

2.2.1. Spinning procedure for hollow fiber membranes

Asymmetric hollow fiber membranes are formed by a "dry-wet" spinning process.[4] and is schematically shown in Figure 2.4. In this process, a polymeric solution is coextruded along with the bore fluid through the spinneret. The spinneret is an annular die (shown in Figure 2.4) in which the polymeric solution is extruded through the outer annular region and the bore fluid is extruded through the inner one. Bore fluid is a neutral fluid to the polymeric solution and it creates the bore of the fiber. The extruded polymer solution is then drawn through the air gap ("dry") and then into the water quench bath ("wet") where the polymer solution phase separates. These phase separated fibers are then collected on a take-up drum.

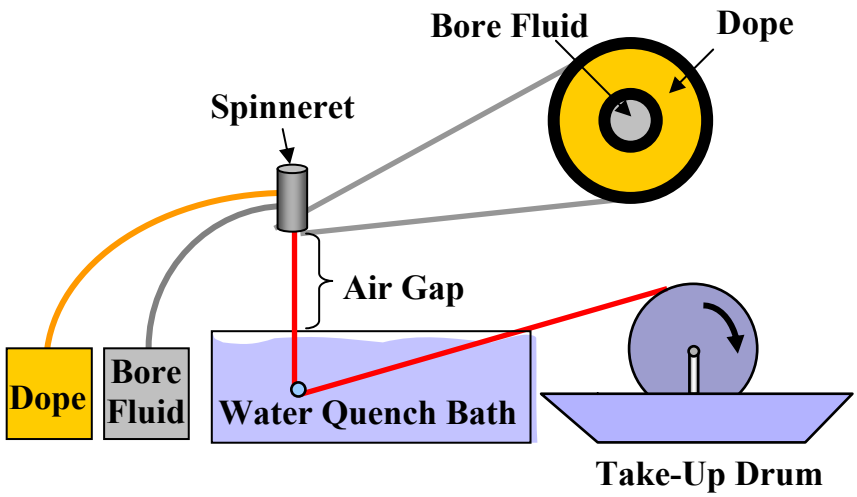

Figure 2.4: Schematic of the experimental setup for spinning asymmetric hollow fiber membranes.

A qualitative ternary diagram for the polymer (Torlon®), solvents (NMP and THF) and non-solvent (ethanol) system is shown in Figure 2.5. The ternary plot is divided into three different regions: homogeneously stable 1-phase region, 2-phase region and the vitrified region. In the 2-phase region, the polymer solution is unstable and it phase separates into two different phases: polymer rich phase and polymer lean phase. In the vitrified region, the polymer concentration is so high that the solution behaves like a dense polymeric material. These three regions are divided by the binodal curve and the vitrification line[2], as shown in the figure.

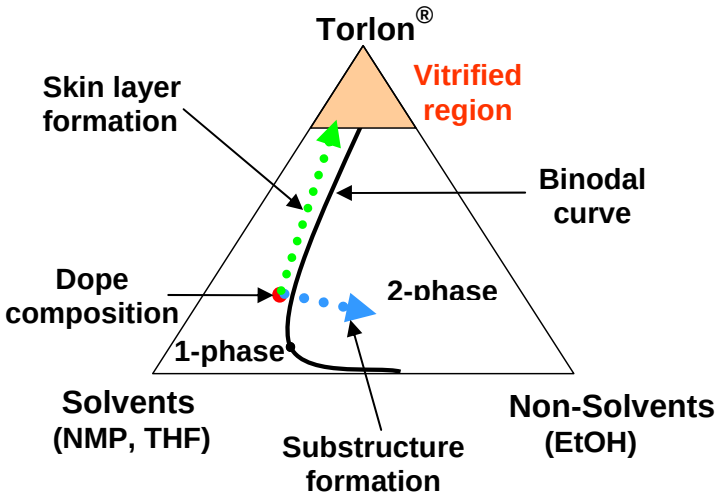

Figure 2.5: Ternary diagram showing the asymmetric membrane formation process.

Dope composition is chosen to be close to the binodal curve to facilitate faster phase separation during the quenching process. When the dope is extruded through the air gap, volatile solvents and non-solvents evaporate from the outer surface of the fiber driving the outer dope composition closer to the vitrified region. This results in the formation of a skin layer.[4] When the fiber is quenched in the water bath, water from the bath enters the nascent fiber and brings the composition into the 2-phase region, where the solution phase separates forming the substructure. The qualitative composition paths during the skin layer and the substructure formation are also shown in Figure 2.5.

Various parameters can be tuned in the spinning process. These parameters are the dope extrusion rate, bore fluid extrusion rate, temperature of the dope, air gap, temperature of the quench bath and the take-up rate. These process parameters along with the dope and bore fluid compositions can be changed to obtain a successful hollow fiber membrane. The main challenges encountered in making these membranes are detailed in the next section.

2.2.2. Key challenges in making asymmetric hollow fiber membranes

A successful asymmetric hollow fiber membrane consists of a defect-free skin layer with no macrovoids, and negligible substructure resistance. The description of each of these characteristics and the parameters that affect them are discussed in the following sections.

2.2.2.1. Defect free skin layer

The skin layer needs to be defect free to provide intrinsic selectivity. Small pores of even 5Å size covering as little as one millionth of the skin surface cause a fiber to become defective by allowing high flux, low selectivity, Knudsen flow.[5, 6] The common method that is employed industrially to cure such defective fibers is to "caulk" the pores by using a post treatment method[5, 7]; however, this treatment may not withstand high pressures that are encountered in supercritical separations, so a defect free skin layer is preferred.

The skin layer is formed while the fiber is being drawn in the air gap during the fiber formation process. In the air gap, the volatile components of the dope leave the spin line, thereby driving the outer surface composition into the vitrified region. [4, 8] This process, if performed successfully, will result in a defect free skin layer. The thicker the nascent skin formed via this process, the higher is the chance of getting a defect free skin;[9] however, the lower the permeance (Equation 2.2)

The amount of volatile solvents in the dope[9], time spent by the spin line in the air gap (evaporation time)[10, 11], and the polymer concentration in the dope[11] have been shown to have a significant impact on the formation of defect free skin layer.

Higher amounts of volatile solvents, longer evaporation time, and higher polymer concentrations assist in producing defect free skin layer. Clausi et al. have noted that the formation of defect free fibers can be further aided by enhancing the evaporation of solvents by increasing the temperature of the dope.[11]

2.2.2.2. Macrovoids

Large voids (10-50 micron) in the substructure of the fiber are termed "macrovoids". Such voids decrease the mechanical strength of the fibers and as a result they collapse under high pressures as shown in Figure 2.6. Macrovoids are clearly unfavorable and should be minimized especially for high pressure applications such as supercritical CO_2 separations.

Figure 2.6: SEM picture showing the fiber collapse at high pressures due to the presence of macrovoids.[12]

Macrovoids are formed during the quenching step of the fiber formation process.[13-16] The influx of water from the quench bath drives the dope composition

into the metastable region, where nucleation of the polymer-lean phase occurs. This nucleated polymer-lean phase could grow into a macrovoid if the osmotic pressure inside the nucleus is high enough to displace the polymeric solution before it vitrifies.[17] This osmotic pressure exists due to the movement of water (from the quench bath) and solvent (from the surrounding polymer solution) into the nucleus.

Various strategies have been pursued by others to decrease the macrovoid growth.[18] Among these various strategies, two of them are quite prominent. The first strategy is to reduce the diffusion of both water and solvents into the nucleus by increasing the viscosity of the polymeric solution.[19] The second strategy is by formulating the dope solution closer to the binodal so that the polymer solution phase separates much faster and suppresses the time available for macrovoid growth.[18]

2.2.2.3. Substructure Resistance[20, 21]

Ideally, the substructure needs to be porous and offer negligible resistance to gas transport through the membrane. If the substructure is not sufficiently porous (especially in the transition layer, just beneath the skin layer) and the substructure resistance is comparable to the skin layer resistance, then the overall gas permeance through the membrane is reduced. Moreover, the permeance of fast gas is reduced more than the slow gas, lowering the selectivity of the membrane, so, the substructure resistance reduces both the permeance and selectivity of the membrane.

In reality, some substructure resistance always exists in asymmetric hollow fiber membranes. This resistance is considered negligible (acceptable) as long as the selectivity of the membrane is greater than 90% of its intrinsic value.

2.3. Background on mixed matrix membranes

Mixed matrix membranes have the advantage of the easy processability of polymers and superior separation performance of inorganic molecular sieves. The separation performance of this composite membrane is often modeled using the following "Maxwell model":

$$P_{MM} = P_C \left[\frac{P_D + 2P_C - 2\phi_D (P_C - P_D)}{P_D + 2P_C + \phi_D (P_C - P_D)} \right], \tag{2.12}$$

where P_{MM}, P_C, P_D, and ϕ_D represent the effective permeability of the mixed matrix membrane, permeability of polymer, permeability of molecular sieves, and the volume fraction of molecular sieves, respectively.

Controlling the polymer-zeolite interface is a crucial challenge in making successful mixed matrix membranes for gas separations.[22] Undesirable polymer-zeolite interfaces occur if there are voids between the polymer-zeolite interfaces or if the polymer gets overly rigidified around the sieve particle.[23] These two phenomena are called "sieve in a cage" and "polymer rigidification" respectively. "Sieve in a cage" morphology is detrimental to mixed matrix effect, as it allows gas molecules to bypass the sieve by providing a less resistance path through the voids. Moreover, the presence of large voids in the "sieve in a cage" morphology would lower the mechanical strength of the fiber. "Polymer rigidification" is also detrimental to mixed matrix effect as it decreases the polymer chain mobility around the sieve surface thereby decreasing the overall permeability of the membrane and potentially blocking the access to the selective sieve.

Various factors have been identified that influence the formation of a defect free polymer-zeolite interface in dense mixed matrix membranes.[23-25] The "sieve in a cage" morphology is formed when the polymer-solvent, zeolite-solvent interactions are greater than the polymer-zeolite interactions.[25] Apart from the polymer-zeolite interactions, the flexibility of polymeric chains plays a crucial role in influencing the polymer-zeolite interface.[25] Successful mixed matrix membranes are obtained more easily with flexible polymers (rubbery polymers) compared to rigid (high Tg) polymers. [26] Popular strategies to improve the interface for rigid polymers include: modifying the zeolite external surface[27], covalently attaching the polymer and zeolite using a coupling agent[22], heat treatment[27], and modifying the membrane formation conditions[28]. By applying these strategies, prior workers were able to improve the adhesion between the polymer and the zeolite.[24, 28] Recently a new surface modification technique has been reported by Shu et al[29-31] and Husain[29] that showed selectivity enhancement for glassy polymers. This surface modification technique involves growing $Mg(OH)_2$ nano-whiskers on the zeolite surfaces. This treatment procedure is complex and the exact mechanism of the formation of the $Mg(OH)_2$ nano-whiskers is still under investigation. While this approach is being investigated by other researchers in our group, I have taken a new approach of modifying the zeolite surface with phosphonic acid (PA) ligands which is relatively simple and easy to scale up. Using this technique the surface chemistry of the zeolite can be tuned accordingly to promote good interactions with the polymer.

In addition to the factors that are identified in dense film work; asymmetric hollow fiber formation process adds additional challenges that need to be addressed to

form a good polymer-zeolite interface.[32] Some of the additional factors arise due to the incorporation of volatile solvents, non-solvents, and other additives in the dope formulation. These additional components introduce various additional interactions involving the zeolite and the polymer that can influence the formation of a higher integrity "polymer-zeolite" interface. Apart from the effect of the additional dope components, phase separation of the fiber in the water quench bath brings additional complications: for example excessive nucleation of the polymer lean phase on the sieve surface will result in "sieve in a cage" morphology. These challenges can be addressed by using the phosphonic acid technique which is explored in this thesis. By choosing an appropriate phosphonic acid ligand that has good interactions with the polymer and weak interactions with the solvents and non-solvents, the above mentioned challenges can be resolved.

2.4. References

1. Baker, R.W., *Membrane Technology and Applications*. 2000, McGraw-Hill: New York. p. 87-157.

2. Mulder, M., *Basic Principles of Membrane Technology*. 2nd edition ed. 2003, Boston: Kluwer Academic Publishers. 71-156.

3. Auerbach, S.M., K.A. Carrado, and P.K. Dutta, *Zeolite Science and Technology*. 2003, New York: Marcel Dekker, Inc.

4. Pesek, S.C. and W.J. Koros, *Aqueous quenched asymmetric polysulfone hollow fibers prepared by dry/wet phase separation.* Journal of Membrane Science, 1994. 88: p. 1.

5. Henis, J.M.S. and M.K. Tripodi, *Composite hollow fiber membranes for gas separation: the resistance model approach.* Journal of Membrane Science, 1981. 8: p. 233.

6. Koros, W.J. and G.K. Fleming, *Membrane-based gas separations.* Journal of Membrane Science, 1993. 83: p. 1.

7. Ekiner, O.M., R.A. Hayes, and P. Manos, Reactive post treatment for gas separation membranes, 1992, U.S. Patent, 5,091,216.

8. Carruthers, S.B. and J.K. William, *Integral-skin formation in hollow fiber membranes for gas separations*, in *Department of Chemical Engineering*. 2001, University of Texas at Austin: Austin. p. 140-188.

9. Niwa, M., et al., *Fabrication of an asymmetric polyimide hollow fiber with a defect-free surface skin layer.* Journal of Membrane Science, 2000. 171: p. 253.

10. Carruthers, S.B., G.L. Ramos, and W.J. Koros, *Morphology of integral-skin layers in hollow-fiber gas separation membranes.* Journal of Applied Polymer Science, 2003. 90: p. 399.

11. Clausi, D.T. and W.J. Koros, *Formation of defect-free polyimide hollow fiber membranes for gas separations.* Journal of Membrane Science, 2000. 167: p. 79.

12. McKelvey, S.A. and J.K. William, *Formation and Characterization of Hollow Fiber Membranes for Gas Separation*, in *Department of Chemical Engineering*. 1997, University of Texas at Austin: Austin.

13. Albrecht, W., et al., *Formation of hollow fiber membranes from poly(ether imide) at wet phase inversion using binary mixtures of solvents for the preparation of the dope.* Journal of Membrane Science, 2001. 192: p. 217.

14. Paulsen, F.G., S.S. Shojaie, and W.B. Krantz, *Effect of evaporation step on macrovoid formation in wet-cast polymeric membranes.* Journal of Membrane Science, 1994. 91: p. 265.

15. Smolders, C.A., et al., *Microstructures in phase-inversion membranes. part 1. formation of macrovoids.* Journal of Membrane Science, 1992. 73: p. 259.

16. Van de Witte, P., et al., *Phase separation processes in polymer solutions in relation to membrane formation.* Journal of Membrane Science, 1996. 117: p. 1.

17. McKelvey, S.A. and W.J. Koros, *Phase separation, vitrification, and the manifestation of macrovoids in polymeric asymmetric membranes.* Journal of Membrane Science, 1996. 112: p. 29.

18. Ekiner, O.M. and G. Vassilatos, *Polyaramide hollow fibers for H_2/CH_4 separation II. Spinning and properties* Journal of Membrane Science, 2001. 186: p. 71.

19. Pereira, C.C., et al., *Hollow fiber formation using lewis acid: base complex in the polymer solution.* Journal of Applied Polymer Science, 2001. 81: p. 908.

20. Clausi, D.T., S.A. McKelvey, and W.J. Koros, *Characterization of substructure resistance in asymmetric gas separation membranes.* Journal of Membrane Science, 1999. 160: p. 51.

21. Pinnau, I. and W.J. Koros, *Relationship between substructure resistance and gas separation properties of defect-free integrally skinned asymmetric membranes.* Industrial and Engineering Chemistry Research 1991. 30: p. 1837.

22. Mahajan, R. and W.J. Koros, *Mixed matrix membrane materials with glassy polymers. Part 1.* Polymer Engineering and Science, 2002. 42(7): p. 1420.

23. Moore, T.T. and W.J. Koros, *Non-ideal effects in organic-inorganic materials for gas separation membranes.* Journal of Molecular Structure, 2005. 739: p. 87.

24. Mahajan, R., et al., *Challenges in forming successful mixed matrix membranes with rigid polymeric materials.* Journal of Applied Polymer Science, 2002. 86: p. 881.

25. Mahajan, R. and W.J. Koros, *Factors controlling successful formation of mixed-matix gas separation materials.* Industrial and Engineering Chemistry Research, 2000. 39: p. 2692.

26. Vankelecom, I.F.J., et al., *Incorporation of zeolites in polyimide membranes.* Journal of Physical Chemistry, 1995. 99: p. 13187.

27. Duval, J.-M., et al., *Preparation of zeolite filled glassy polymer membranes.* Journal of Applied Polymer Science, 1994. 54: p. 409.

28. Mahajan, R. and W.J. Koros, *Mixed matrix membrane materials with glassy polymers. Part 2.* Polymer Engineering and Science, 2002. 42(7): p. 1432.

29. Husain, S. and W.J. Koros, *Mixed matrix hollow fiber membranes made with modified HSSZ-13 zeolite in polyetherimide polymer matrix for gas separation.* Journal of Membrane Science, 2007. 288: p. 195.

30. Shu, S., S. Husain, and J.K. William, *A general strategy for adhesion enhancement in polymeric composites by formation of nanostructured particle surfaces.* The journal of physical chemistry C, 2007. 111(2): p. 652.

31. Shu, S., S. Husain, and J.K. William, *Formation of nanostructured zeolite particle surfaces via a halide/grignard route.* Chemistry of materials, 2007. 19(16): p. 4000.

32. Husain, S. and J.K. William, *Mixed matrix dual layer hollow fiber membranes for natural gas separation*, in *Department of Chemical and Biomolecular Engineering*. 2006, Georgia Institute of Technology: Atlanta.

CHAPTER 3

MATERIALS AND EXPERIMENTAL METHODS

3.1. Materials

3.1.1. Polymer

Torlon® 4000T, a polyamide-imide polymer, was chosen as the membrane material for supercritical carbon dioxide ($scCO_2$) separations. The reason behind this selection is explained in chapter 4. This polymer was provided by Solvay Advanced Polymers (Alpharetta, GA) and its chemical structure[1] is shown in Figure 3.1. It is a random co-polymer and is prepared by reacting TMACl (trimellitic anhydride acid chloride) with the two diamines: ODA (4,4'-oxydianiline) and m-PDA (m-phenylenediamine). The structures of these monomers are shown in Figure 3.2. The detailed polymerization procedure is provided by Yokelson et.al.[2] The number average (Mn) and the weight average (Mw) molecular weights of the polymer are 18,400 and 43,700 Da, respectively. These molecular weights are determined using Gel Permeation Chromatography in 1-methyl-2-pyrrolidone (NMP). The inherent viscosity of the polymer is 56 cm^3/g. The reported glass transition temperature (Tg) of this polymer is 273 °C. To remove any absorbed water, the polymer was dried overnight under vacuum at 120 °C before use.

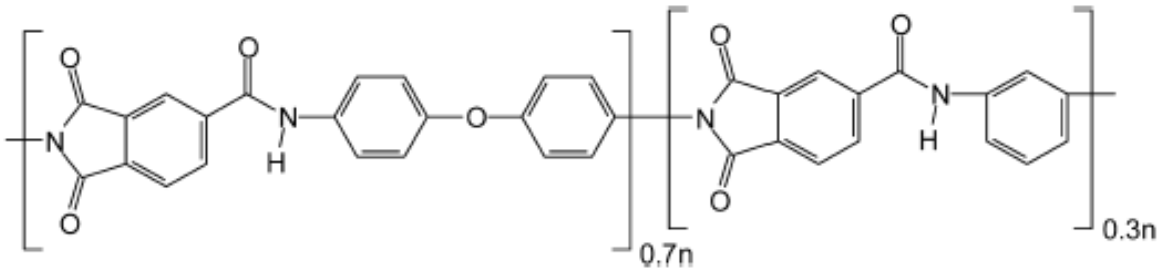

Figure 3.1: Molecular structure of Torlon 4000T.

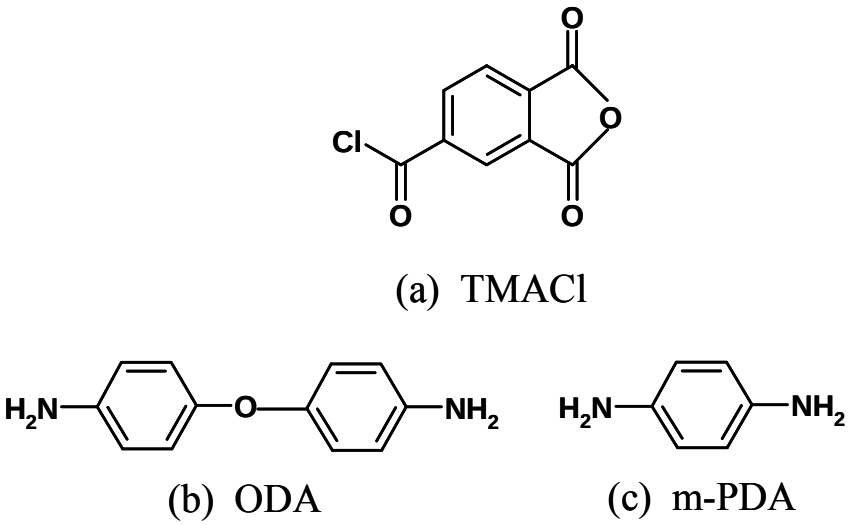

Figure 3.2: Monomers for Torlon® , 4000-T, synthesis. TMACl: trimellitic anhydride acid chloride, ODA: oxydianiline, m-PDA: m-phenylenediamine.

3.1.2. Molecular Sieves

Molecular sieve, zeolite 4A, is used in this work. The framework structure of this zeolite as viewed along [100] direction is shown in Figure 3.3, and it has a three-dimensional pore network in which the gas molecules can diffuse in all three dimensions. To have a better view of the pore window, the repeat unit of the zeolite is

also shown in Figure 3.3. The 8-ring window, which is shown in the figure, has a dimension approximately equal to 3.8 Å. Gas molecules smaller than this size would diffuse through the zeolite and molecules that are bigger are blocked.

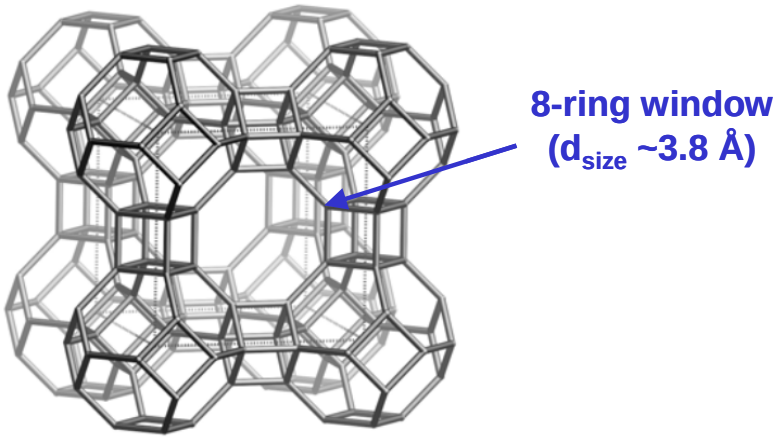

(a)

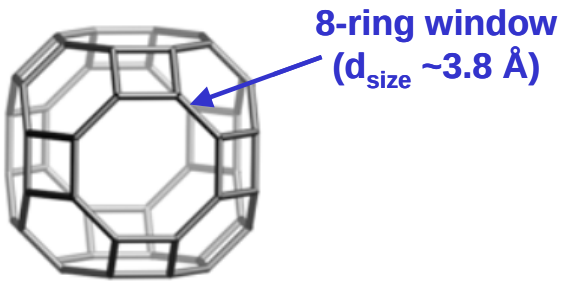

(b)

Figure 3.3: a) Framework structure of zeolite 4A. b) Building unit of 4A that shows an 8-ring pore window. The size of the window is ~3.8Å.

The chemical composition of the as-received 4A is $\left|Na_{96}\left(H_2O\right)_{216}\right|\left[Al_{96}Si_{96}O_{384}\right]$. This zeolite is hydrophilic in nature and so when left in ambient conditions it absorbs moisture from the air. This hydrophilic nature is due to the presence of sodium counter

ions which adsorbs water molecules. Moreover, the oxygen bonded to the aluminum has a slight negative charge and this slight polarity serves as a hydrogen bonding site to water. To remove the absorbed water, the zeolites are heated overnight at 150 °C before they are used in the experiments.

In this work, three different sizes of zeolites are used: 2-5 microns, 1-2 microns and 300nm zeolites. The 2-5 micron size zeolites are commercially obtained from Sigma-Aldrich. Both the 1-2 microns and 300nm sized zeolites are provided by Tae-Hyun, a PhD candidate with Prof. Chris Jones of Georgia Tech. These zeolites are synthesized according to the procedure developed by Larlus et al.[3]

3.1.3. Chemicals and gases

3.1.3.1. Chemicals for membrane formation

Torlon®, the polymer of our interest, is only soluble in aprotic solvents like N-methyl pyrrolidinone (NMP), dimethylsulfoxide (DMSO), dimethylacetamide (DMAc), and dimethylformamide (DMF). Among these different solvents, NMP is chosen because of its relatively environmentally benign nature. A mixture of NMP and tetrahydrofuran (THF) is used as an "effective solvent" in making asymmetric hollow fiber membranes. THF is added because of its high volatility, which facilitates the formation of a skin layer. The role of THF in forming skin layer is described later in this chapter. Ethanol is used as a non-solvent in the dope formulation. Methanol and hexane are the two non-solvents used in the solvent exchange process. All these chemicals are purchased from Sigma Aldrich and they are either anhydrous or reagent grade.

3.1.3.2. Chemicals for surface modification of zeolites

The zeolite surface is modified using phosphonic acid treatment. The ligands used in the phosphonic acid treatment are pentafluoro benzyl phosphonic acid ligands. These are purchased from Sigma Aldrich.

3.1.3.3. Gases

Both pure and mixed gas permeation studies are performed to characterize the separation properties of Torlon® membranes. Pure gas permeation studies are performed using oxygen (O_2), nitrogen (N_2), helium (He), ethylene (C_2H_4), and carbon dioxide (CO_2). The mixed gas permeation studies are performed using CO_2/C_2H_4 (90/10), and $CO_2/C_2H_2F_2$ (94/6) gas mixtures. All the pure and mixed gases are research grade and are purchased from Air Gas, except CO_2 and $C_2H_2F_2$ mixture, which is purchased from Matheson gas.

3.2. Membrane Preparation

3.2.1. Dope Preparation

All the membranes in this work are solution casted from a polymer solution (often referred as dope). Dope formulations and membrane formation procedures for dense film membranes (both pure polymer and mixed matrix membranes) and asymmetric hollow fiber membranes are described in the following sections.

3.2.1.1. Dope for polymeric dense films

Dense polymeric films are made from a dope solution of 20 wt% polymer in NMP. A day prior to making the dope solution, the polymer is dried in a vacuum oven overnight at 120 °C to remove any absorbed water. The dried polymer is then added to a vial containing anhydrous NMP and shaken immediately to form homogeneous slurry of polymer and solvent. The vial is then placed on a roller with heat (approximately at 50 °C) for polymer dissolution to make a homogeneous polymer solution. This process may take 2-4 days.

3.2.1.2. Mixed matrix dope for dense films

Mixed matrix films with 20 wt% zeolite loading are investigated. So the relative amounts of polymer and zeolite used in making the dope are 4:1 by weight. A solution of 20 wt% of solids (the solids constitute both the polymer and zeolite) in NMP is used in making a mixed matrix dope.

The polymer and the zeolite are dried overnight at 120 °C and 150 °C respectively before they are used in the dope formulation. Solvent, NMP, is added to the dried zeolites to from 8 wt% zeolite solution in NMP. The zeolites are dispersed in the solvent by sonicating overnight in a sonication bath (70 watt sonication bath from Branson Ultrasonics Corporation, model number: 1510R-MTH). After the sonication, the dispersed solution looks milky and no visual agglomerates are observed. To keep this dispersion stable, a priming polymer solution is added. A 15 wt% polymer in NMP is used as a priming solution. This low polymer concentration is used for priming because it facilitates rapid dissolution of the polymer into the dispersion. This dissolved polymer

then sterically shields the particles from coming close to each other and thereby prevent agglomeration. Roughly one-third of the total polymer is added during the priming step. Once the priming solution is added, the vial is rigorously shaken and during this shaking, the polymer dissolves readily and a homogeneous solution is formed. The remaining polymer (two-thirds of the total polymer) is then added and the vial is kept on a roller at room temperature to form a mixed matrix dope. The polymer dissolution process takes about 5-7 days.

To give an idea of the actual amounts of the components added during each step of the dope formulation process, an example of a mixed matrix dope formulation is provided in this paragraph. First, a solution of 8 wt% of zeolites in NMP is formed by adding 3.45 grams of NMP to 0.3 grams of dried zeolites, and then the zeolites are dispersed overnight in a sonication bath. To stabilize this dispersion, 3 grams of priming solution (15 wt% Torlon® in NMP) is added. After rigorous shaking, the rest of the polymer, 0.75 grams of Torlon®, is added and the solution is rolled to form a mixed matrix dope. The final concentration of the dope and the total amounts added are shown in Table 3.1.

Table 3.1: Polymer, zeolite and solvent concentrations in a mixed matrix dope. The amounts of these components are also provided as an example.

Component	Weight percent	Weight in grams
Torlon®	16	1.2 g
Zeolite 4A	4	0.3 g
NMP	80	6.0 g

3.2.1.3. Dope for polymeric hollow fiber membranes:

Dope for hollow fiber membrane formation contains a non-solvent in addition to solvents. The reason for adding the non-solvent is explained later in this chapter. Both the solvents and non-solvents are added in a 250 or a 500 ml Quorpak jar and is shaken to mix. Then the desired amount of dried polymer is added to the mixture and is rolled under heat (roughly about 50 °C) for polymer dissolution. Typically in about 2-4 days, the polymer is completely dissolved forming a homogeneous dope solution.

3.2.2. Film Preparation

Once the polymer solution is completely dissolved, the dope is degassed in a vacuum oven before it is knife cast on a hot glass plate. The glass plate is pre-heated and maintained at 120 °C during the casting process. At this temperature of 120 °C, NMP evaporates, and in about 3.5 hrs, most of the solvent leaves the system forming a film. To remove any residual solvents from the film, the membrane is heated under vacuum at 220 °C for about 3 days.[4] This film is then tested for its permeation properties.

3.2.3. Hollow Fiber Membrane Formation[5-8]

3.2.3.1. Cloud point technique for binodal curve determination

Fibers are spun from a polymeric solution (dope) consisting of polymer, solvents and non-solvents, whose composition is chosen close to the binodal curve for faster phase separation. As such, one must first estimate the binodal curve for the polymer/solvent/non-solvent ternary system. The cloud-point technique, schematically shown in Figure 3.4, allows locating the binodal curve. In this technique, a series of dope

samples are prepared with the same polymer concentration but with varied non-solvent and solvent concentrations. The initial sample is made with only two components (polymer and solvent) to ensure that the solution is in 1-phase, and consecutive samples are made by adding non-solvent in small incremental steps till the solution becomes two distinct phases. These dope samples are then carefully observed visually to determine the composition at which the solution first turns slightly cloudy indicating the onset of phase separation. The so determined dope composition defines a binodal point. Such binodal points are determined at various polymer concentrations to yield the binodal curve with sufficient accuracy to select an appropriate dope composition. The length of the incremental step determines the accuracy of the binodal curve. In our experiments 1% increase in non-solvent concentration in the overall dope is used as an incremental step.

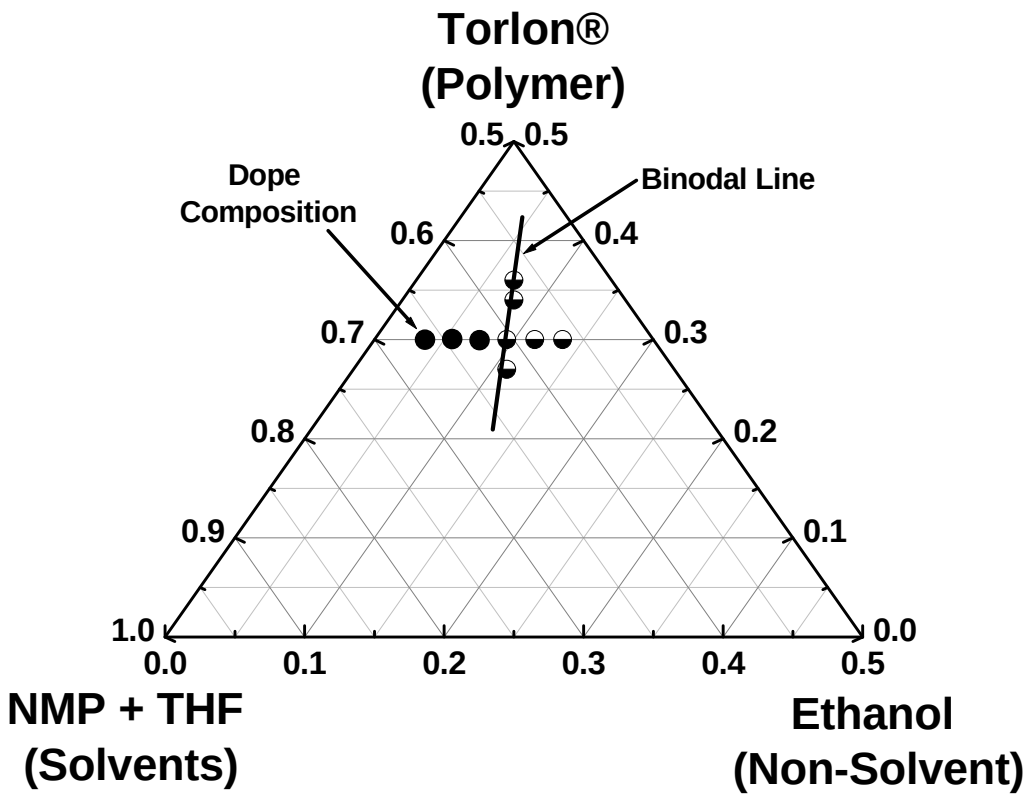

Figure 3.4: Ternary diagram for Torlon®, NMP/THF (4/1),and ethanol system. The figure also shows the cloud point technique to determine the binodal composition. Multiple dope compositions are prepared at a particular polymer composition as shown in the picture. The solid black dot indicates homogeneous solution and the half-filled black dot indicates the 2-phase region. The composition at which it starts becoming 2-phase is the binodal composition.

3.2.3.2. Formation of fibers and solvent exchange procedure

Asymmetric hollow fiber membranes are formed by a "dry-wet" spinning process,[7] which is described in the previous chapter (section 2.2). The extruded fibers are solvent exchanged with water for a period of about 3-5 days by changing the water daily. This is performed to remove the solvents and non-solvents from the wall of the fiber and also to remove the bore fluid from the bore of the fiber. The absorbed water was removed from the fibers without any capillary collapse of the substructure by exchanging the water with low surface tension liquids, methanol and hexane[9]. The

fibers are washed with three successive 20 minute methanol baths (500 ml each) followed by three successive 20 minute hexane baths (500ml each). To remove the hexane, the fibers were dried at room temperature for one hour followed by heating the fibers under vacuum at 120 °C for another hour. Even after this extensive solvent exchange process, the fibers still have some residual NMP. The method of removing this residual NMP is described in the following sections.

3.2.3.2.1. Presence of residual NMP in the fibers:

The TGA analysis on the Torlon® fibers, after usual solvent exchange process, is shown in Figure 3.5. There is a 10 percentage weight loss between 220 °C and 250 °C and this can be attributed to NMP loss, as its boiling point is near that temperature (boiling point of NMP is 205 °C).

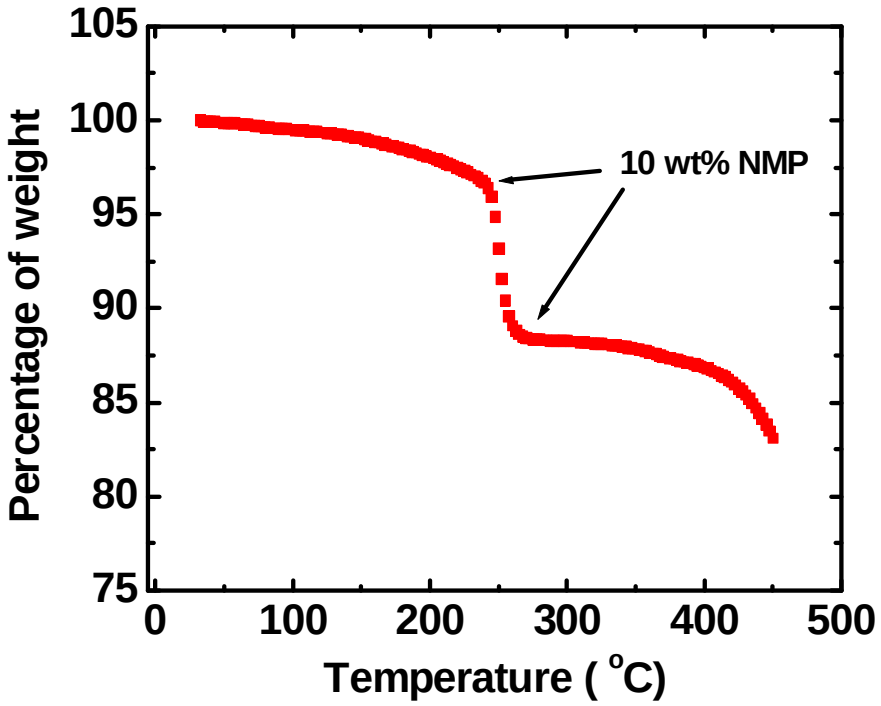

Figure 3.5: Thermal gravimetric analysis (TGA) of the spun fibers after the standard solvent exchange procedure.

To make sure that the weight loss is not because of polymer degradation or because of some impurities in the polymer, a blank TGA is done on the as-received Torlon® and the plot is shown in Figure 3.6. No weight loss is observed between 220 °C to 250 °C indicating that neither of the above mentioned phenomena is occurring and the weight loss observed in the fibers is due to the residual NMP. This residual NMP, in such large quantities (10 weight percent), could act like a plasticizer and could significantly influence the separation performance of the membranes. So this residual solvent needs to be removed from the fibers before using them for actual separation.

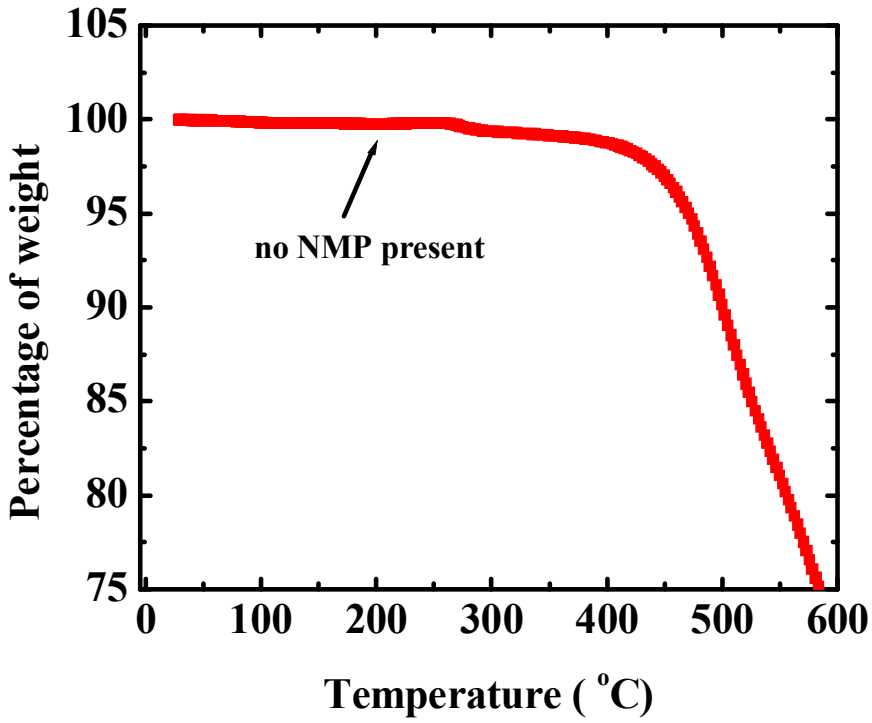

Figure 3.6: Thermal gravimetric analysis (TGA) of the as-received Torlon®.

3.2.3.2.2. *Removal of NMP from the fibers*

The reason for the presence of NMP even after the solvent exchange process is that it forms hydrogen bonds with the amide groups of Torlon® (see Figure 3.7). These hydrogen bonds are difficult to break during regular solvent exchange procedure. Therefore, aggressive solvent exchange procedures were investigated to remove the NMP.

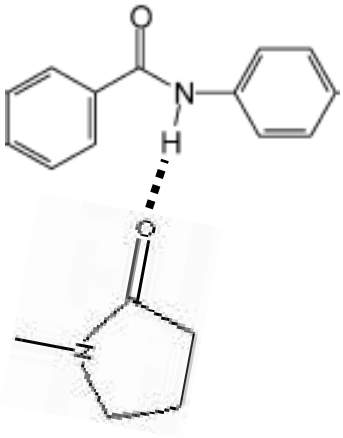

Figure 3.7: Pictorial representation of NMP hydrogen bonding with the amide groups of Torlon®.

Instead of a regular solvent exchange procedure using room temperature water, the fibers are treated with hot water at 90 °C for 3 days. The idea here is to break the hydrogen bonding between NMP and amide groups with high temperatures and then exchange this unbounded NMP with water. However, this strategy was not successful as TGA on these solvent exchanged fibers still show considerable amount of NMP left in them (about 8-10 weight percentage). Additional similar strategies of removing the NMP were employed. One of them is heating the fibers with methanol at 50 °C for 3 days and the other is treating the fibers with supercritical carbon dioxide for 3 days. Both these strategies were also similarly un-successful in removing the NMP.

One reason for the failure of the above strategies is the low diffusion coefficient of NMP through Torlon®. Because of the inter chain hydrogen bonding, Torlon® forms a membrane with low thermal fluctuations of polymeric chains. This makes Torlon® less permeable. Moreover, the bulky nature of NMP makes it hard to diffuse through the

Torlon® fibers. Because of the low diffusion coefficient of Torlon®, the free NMP molecules (after the hydrogen bond cleavage) take a long time to come out of the fibers.

NMP can be successfully removed from the fibers if its diffusion coefficient through the membrane is enhanced. To increase this diffusion coefficient, we opted to treat the fibers at 180 °C. High temperatures increase the polymer chain mobility and hence increases the NMP diffusion coefficient. To prevent the fibers from being oxidized (or to prevent any unwanted reactions), the fibers are treated at 180 °C in vacuum. The vacuum also eliminates any external mass transfer resistances that may occur i.e., it maintains the zero NMP concentration on the outside of the fibers and thereby maximizes the driving force for NMP removal. Thus, heating in vacuum helps in decreasing both the internal (low diffusion coefficient) and external mass transfer resistances.

The fibers are treated at 180 °C for 3 days in vacuum and then are analyzed using TGA. No weight loss between 220 °C to 250 °C was observed, indicating that the heating procedure completely removed all the NMP from the fibers. The NMP free fibers are then used to study gas transport characteristics.

3.2.3.3. Post Treatment Procedure

To eliminate defects in the skin layer, reactive post treatment procedure described by Ekiner et al. was carried out on the fibers.[10, 11] This procedure involves treating the fibers with a solution of 0.2 wt% diethyl-toluene-diamine in iso-octane for 30 mins, draining the solution and then finally treating the fibers with a solution of 0.2% trimesolychloride and 2% sylgard 184 (polydimethylsiloxane) in iso-octane. This above treatment ensures that the defects are plugged by two independent mechanisms. In the

first mechanism, a low permeable oligomer is polymerized in the defects of the fiber via a reaction between diethyl-toluene-diamine and trimesoylchloride monomers. The second mechanism further ensures that the defects are plugged by coating the outside surface of the fiber with a highly permeable amorphous polydimethylsiloxane polymer (PDMS) that contributes negligible additional transport resistance to the defect free regions of the skin. This PDMS coating also helps stabilizing the oligomer caulking agent.

3.3. Membrane Testing Methods

3.3.1. Permeation system

3.3.1.1. Dense Film Permeation

The intrinsic permeability and selectivity of a gas pair through the membrane are determined by measuring dense film permeation. Typical dimensions of the membrane used for testing are 1-2 mills in thickness and 4-9 cm^2 in area. This membrane is then attached (masked) to a permeation cell. The details of the permeation cell and the experimental procedure for masking are described in previous publications[12, 13].

The cell is loaded in a "constant volume and variable pressure" permeation system[13] to measure the gas transport properties. The schematic of the permeation system is shown in Figure 3.8, and it consists of an upstream volume and a downstream volume. The upstream volume contains the feed gas to the membrane and the downstream volume collects the permeate from the membrane. After loading the cell, both the volumes are evacuated for two days to remove any absorbed gases from the film. After degassing the film, the downstream leak rate is measured. The feed gas is then introduced to the membrane at a constant pressure. Permeate from the membrane is

collected in the downstream volume and the rate of increase in pressure is monitored with time using a pressure transducer. After ten time lags from the start of the experiment, a steady state permeation rate is obtained. This permeation rate is corrected for the leaks by subtracting the leak rate. In order to minimize the error introduced by the leaks, the leak rate is kept less than 10% of the steady state permeation rate. To account for any variations in the leak rate during different permeation tests, the leak rates are measured before the permeation of each gas. From the steady state permeation rate information (after the leak rate correction), the permeability is calculated using the following equation:

$$Permeability(P_A) = \frac{N \times l}{\Delta p} = 22400 \frac{V_R \left(dp/dt \right) l}{RT(\Delta p)A}, \tag{3.1}$$

where P_A, N, dp/dt, Δp, A, l, V_R, R, and T represents permeability (barrers), steady state permeation flux (cc(STP) /(cm^2-sec)), rate of increase in downstream pressure (cmHg/sec), trans-membrane pressure difference (cmHg), total permeation area (cm^2), thickness of the membrane (cm) volume of the downstream (cm^3), universal gas constant (cm^3 cmHg K^{-1} mol^{-1}), and temperature (K) respectively. All the permeation measurements are carried at 35 °C. This temperature is maintained in the permeation system by using a temperature controller.

In the case of CO_2, where non-ideal gas phase effects exist, the trans-membrane fugacity (Δf) is used instead of the trans-membrane pressure difference (Δp) in calculating the permeabilities using Equation (3.1). Permeabilities are expressed in barrers where

$$1\ Barrer = 1\times 10^{-10}\ \frac{cm^3(STP).cm}{cm^2\ \sec cmHg}. \tag{3.2}$$

The pure gas selectivity of the two gases was obtained by taking the ratios of their permeabilities:

$$\alpha_{i/j} = \frac{P_i}{P_j}. \tag{3.3}$$

In the case of a mixed gas feed, different gases permeate at different rates through the membrane and this causes the upstream concentration to change. This effect is called concentration polarization. This is minimized by having a constant flow across the membrane which brings the fresh feed to the membrane and maintains the upstream concentration. This flow across the membrane is called the retentate flow. To minimize the concentration polarization, the retante flow is chosen to be 100times the fast gas flux through the membrane.[14] This flow is controlled by using a needle valve as shown in the Figure 3.8.

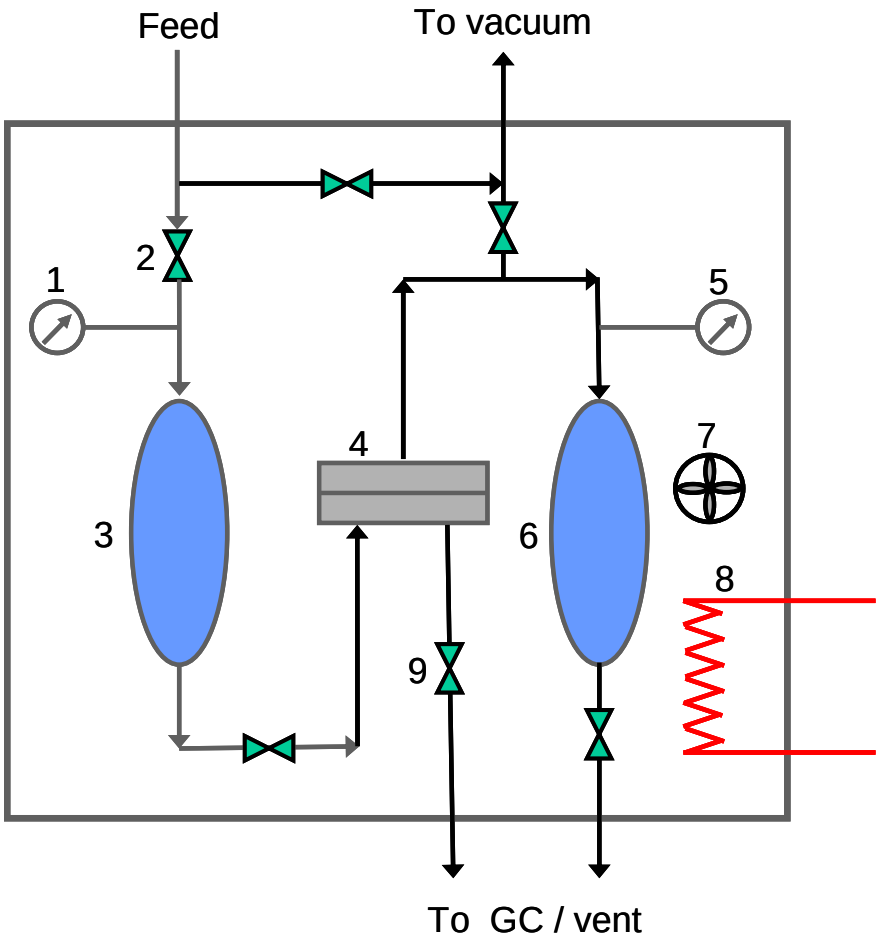

Figure 3.8:. Schematic of a permeation system to measure dense film/hollow fiber membrane permeabilities. 1.) upstream transducer, 2.) valve, 3.) upstream volume, 4.) cell in the case of a dense film / module in the case of a hollow fiber, 5.) downstream transducer, 6.) downstream volume, 7.) fan, 8.) heater, 9.) needle valve.

3.3.1.2. Asymmetric Hollow Fiber Membrane Permeation

To test the permeation properties of hollow fiber membranes, the fibers are packaged in a module[15]. Details of module making are given in earlier work [9, 15]. The module is loaded in a permeation system similar to the one shown in Figure 3.8. The procedure for running a permeation test is almost the same as the one described above for the dense film permeability measurements. The only differences are the evacuation time

and the time to reach steady state permeation. Since the actual separating thickness of a fiber is quite small compared to a dense film, the absorbed gases come quite readily from the fiber. Leak rate measurements at different times indicate that the overnight degassing is sufficient to remove the absorbed gases. Also, since the time lag is directly proportional to the square of the separating layer thickness, the "time lags" for all gases will be significantly lower for hollow fiber membranes. As such, steady state fluxes are obtained quite early during the experiment compared to dense film membranes.

In the case of high pressure permeation testing (example: supercritical CO_2 permeation), a syringe pump was used to feed the gas to the membrane. Commercially purchased pure CO_2 gas or CO_2 based mixed gases (CO_2/C_2H_4, $CO_2/C_2H_2F_2$ mixtures) come only in low pressures. For example, pure CO_2 is sold at 800-900 psi and a mixture of CO_2/C_2H_4 comes only at 500 psi. Such low pressure feed gases are pressurized to desired high pressures using a syringe pump. The pressurized gases are then fed directly to the membrane at a constant pressure.

3.3.1.2.1. Pure gas permeances and selectivities of hollow fibers

For permanent gases like O_2, N_2, He, and CH_4, permeance or pressure normalized flux (P/l) was calculated using the following expression.

$$\left(\frac{P}{l}\right) = \frac{N}{\Delta p} = 22400 \frac{V_R \left(dp / dt \right)}{RT(\Delta p)A}. \tag{3.4}$$

The permeate area (A) is determined by measuring the total external surface area of the fibers using the expression: $A = N\pi dL$, where N, d and L represents number of fibers used, outer diameter and length of the fibers respectively. The outer diameter of the fiber

is obtained from an SEM (scanning electron microscopy) measurement and is averaged over multiple fibers, approximately 10.

In the case of CO_2, where non-ideal gas phase effects exists, the trans-membrane fugacity (Δf) is used instead of the trans-membrane pressure difference (Δp) in calculating the permeances. Permeances are expressed in so-called "gas permeation units", GPUs, where

$$1\,GPU = 1\times 10^{-6}\,\frac{cm^3(STP)}{cm^2\,\sec cmHg}. \tag{3.5}$$

The pure gas selectivity of two gases was obtained by taking the ratios of their permeances:

$$\alpha_{i/j} = \frac{(P/l)_i}{(P/l)_j}. \tag{3.6}$$

For an ideal asymmetric membrane with negligible downstream pressure relative to the upstream, this selectivity equals the ratio of their skin permeabilities (P_i and P_j) and is independent of the effective skin thickness.

3.3.1.2.2. Mixed gas permeances and selectivities of hollow fibers[12]

Pressurization and depressurization permeation cycles are performed using a 90/10 mixture of CO_2/C_2H_4. Depressurization is carried out at a controlled rate that is slower than the CO_2 desorption from the fiber in order to prevent the fiber from being damaged due to rapid depressurization. Since the time lag of CO_2 in our Torlon® asymmetric membrane is less than 30 seconds, a depressurization rate of 1 psi per min is sufficient to prevent the fiber from being damaged.

The permeate gas was analyzed using gas chromatography (Model: 6890N, Agilent Technologies, CA) with a GS-Carbon plot column. Mixed gas separation factors were determined using the following expression[16].

$$SF(CO_2, CH_4) = \frac{y^d_{CO_2} \Big/ y^d_{CH_4}}{y^u_{CO_2} \Big/ y^u_{CH_4}}, \tag{3.7}$$

where $y^d_{CO_2}$, $y^d_{CH_4}$, $y^u_{CO_2}$, and $y^u_{CH_4}$ represent the mole fractions of the CO_2 and CH_4 in the downstream and upstream respectively. As noted in the previous chapter, ideally, separation factor is equal to intrinsic selectivity for cases where the downstream total pressure is negligible relative to the upstream total pressure.

Since CO_2/C_2H_4 gas mixtures show non-ideal effects, individual permeances are calculated using trans-membrane fugacity difference (Δf) instead of trans-membrane partial pressure difference (Δp). The equations that are used in determining the fugacity based permeances of CO_2 and C_2H_4 are:

$$\left(\frac{P^{\#}}{l}\right)_{CO_2} = \frac{N_{CO_2}}{\Delta f_{CO_2}}, \tag{3.8}$$

$$\left(\frac{P^{\#}}{l}\right)_{C_2H_4} = \frac{N_{C_2H_4}}{\Delta f_{C_2H_4}}, \tag{3.9}$$

where $\left(\frac{P^{\#}}{l}\right)$, N and Δf represent fugacity normalized permeance, steady state permeation flux and trans-membrane fugacity difference of a particular species respectively. The mixed gas selectivity of the membrane, taking into account non-ideal

gas phase effects, is the ratio of the individual fugacity normalized permeances and is defined as:

$$\alpha^{\#}_{CO_2/C_2H_4} = \frac{\left(P^{\#}/l\right)_{CO_2}}{\left(P^{\#}/l\right)_{C_2H_4}} = \frac{\left(N_{CO_2}/\Delta f_{CO_2}\right)}{\left(N_{C_2H_4}/\Delta f_{C_2H_4}\right)}. \tag{3.10}$$

In the case of negligible downstream pressure, the trans-membrane fugacity difference (Δf) is equal to the upstream fugacity (f^u) and the fluxes are proportional to downstream mole fractions (y^d). Incorporating these simplifications, equation 3.10 yields:

$$\alpha^{\#}_{CO_2/C_2H_4} = \frac{\left(P^{\#}/l\right)_{CO_2}}{\left(P^{\#}/l\right)_{C_2H_4}} = \frac{\left(y^d_{CO_2}/f^u_{CO_2}\right)}{\left(y^d_{C_2H_4}/f^u_{C_2H4}\right)}. \tag{3.11}$$

The above expression is used in our work to calculate the mixed gas selectivities, which takes into account of the non-ideal gas phase effects in the upstream.

Fugacities of CO_2 and CH_4 in a gas mixture are calculated using NIST SUPERTRAPP, a database for the prediction of thermodynamic properties of fluid mixtures. This database was obtained from the National Institute of Standards and Technology (Gaithersburg, Maryland) and uses the Peng and Robinson[17] equation of state. The calculated fugacities of CO_2 and C_2H_4 in a 90/10 mixture of CO_2/C_2H_4 are given in Figure 3.9.

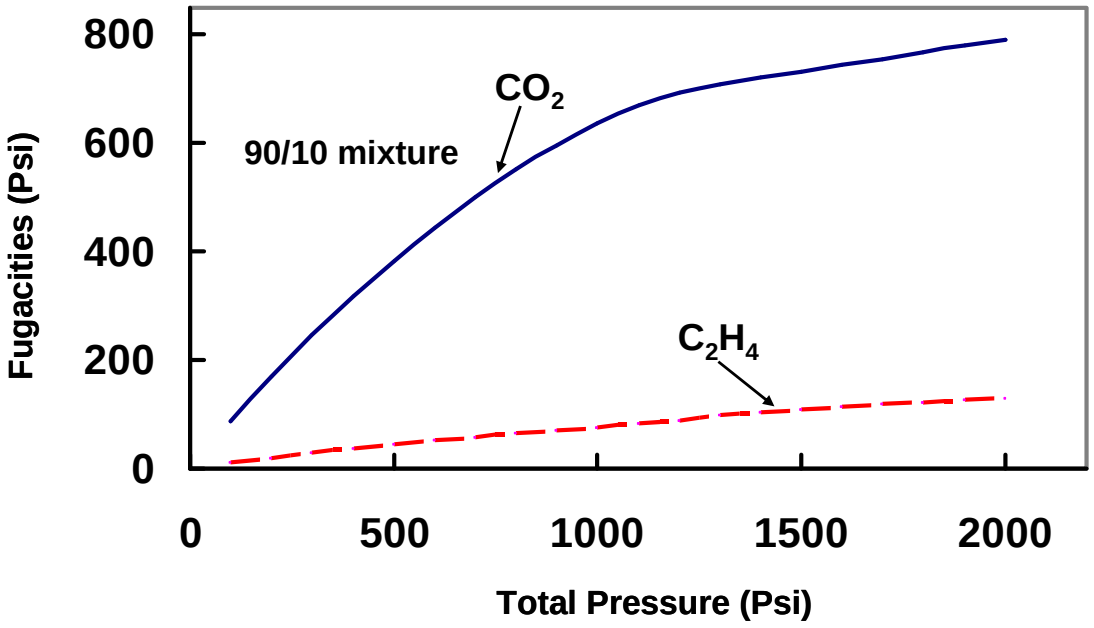

Figure 3.9: Fugacities of CO_2 and CH_4 at various pressures in a gas mixture containing 90 mole % CO_2 and 10 mole % C_2H_4 at 35 °C.

3.3.2. Sorption

This technique can be used to determine the diffusion and sorption coefficients of gases through a polymeric film or through inorganic molecular sieves. The apparatus used for this measurement is shown in Figure 3.10. It consists of a reservoir volume and a sample volume separated by a connecting valve (valve B in Figure 3.10). The pressures inside these volumes are measured using pressure transducers. Before the start of the experiment, both the volumes are evacuated using a vacuum pump. The reservoir is then isolated from the sample volume and a gas of pressure, p_{RI}, is introduced only to the reservoir volume. The reservoir volume is then isolated from the feed line, then the gas is expanded into the sample volume by opening the connecting valve for couple of seconds

before closing it. The final pressure in the reservoir volume (p_{RF}) is noted and the pressure decrease in the sample volume is monitored over time.

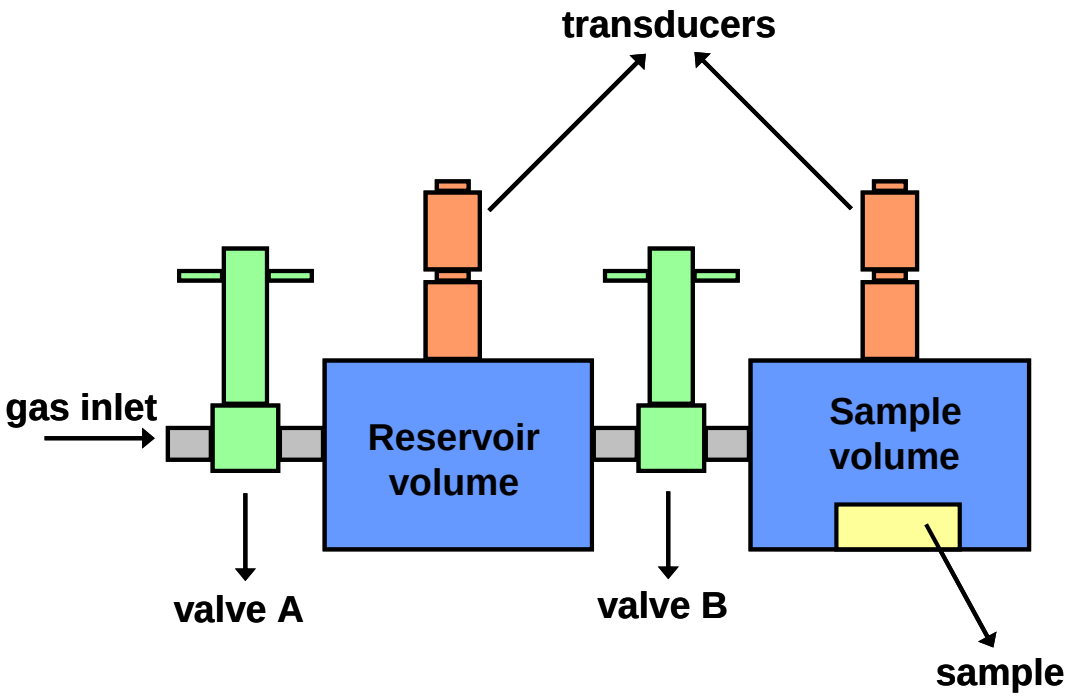

Figure 3.10: Apparatus set up for pressure decay sorption system.

3.3.2.1. Determining the sorption coefficient

The amount of gas absorbed by the material can be determined by knowing the initial and final pressures in the sample volume. It is calculated using the following expression:

$$amount.absorbed.by.the.film = \frac{(V_S - V_P) \times (p_{SI} \times Z(p_{SI}) - p_{SF} \times Z(p_{SF}))}{R \times T}. \quad (3.12a)$$

From this information, the sorption coefficient of the gas is determined using the following equation:

$$S = \frac{amount.absorbed.by.the.film}{V_P \times p_{SF}}, \tag{3.12b}$$

where S corresponds to the sorption coefficient ($moles/(cm^3 \times psi)$) at pressure, p_{SF} . R and T are the universal gas constant (1205.931 $cm^3.psi/(moles.K)$) and temperature in K respectively. The symbols V_S and V_P refer to the sample cell volume and polymer sample volume respectively in cm^3. p_{SI} and p_{SF} are the initial and final pressures in the sample cell volume in psi. $Z(p_{SI})$ and $Z(p_{SF})$ represent compressibility factors of the gas at pressures p_{SI} and p_{SF}, respectively. These compressibility factors take in to account of non-ideality of the gases and are calculated using either Peng-Robinson equation of state or virial equation of state. Details of these equations of state and the method of determining the compressibility factors for various gases of interest (CO_2, C_2H_4, and $C_2H_2F_2$) are given in Appendix A.

3.3.2.2. Determining the diffusion coefficient through a flat polymeric film

The rate of uptake of gas by a polymeric film from a finite source is given by the following equation[18]:

$$\frac{M_t}{M_\infty} = 1 - \sum_{n=1}^{\infty} \frac{2\alpha(1+\alpha)}{1+\alpha+\alpha^2 q_n^2} \exp\left(-Dq_n^2 t/l^2\right), \tag{3.13}$$

where M_t, M_∞ represent the amount of gas absorbed by the film up to time t and infinite times, respectively. α is the ratio of the amount of gas left in the sample volume to the amount of gas absorbed by the polymer. q_n s are the non-zero positive roots of

$$\tan(q_n) = -\alpha q_n . \tag{3.14}$$

The solution of this mathematic equation is plotted in Figure 3.11. The amount of uptake, $\left(\frac{M_t}{M_\infty}\right)$, is plotted against $\left(Dt/l^2\right)^{\frac{1}{2}}$. Numbers on the curves represent the percentage of the total sample gas that is absorbed by the film.

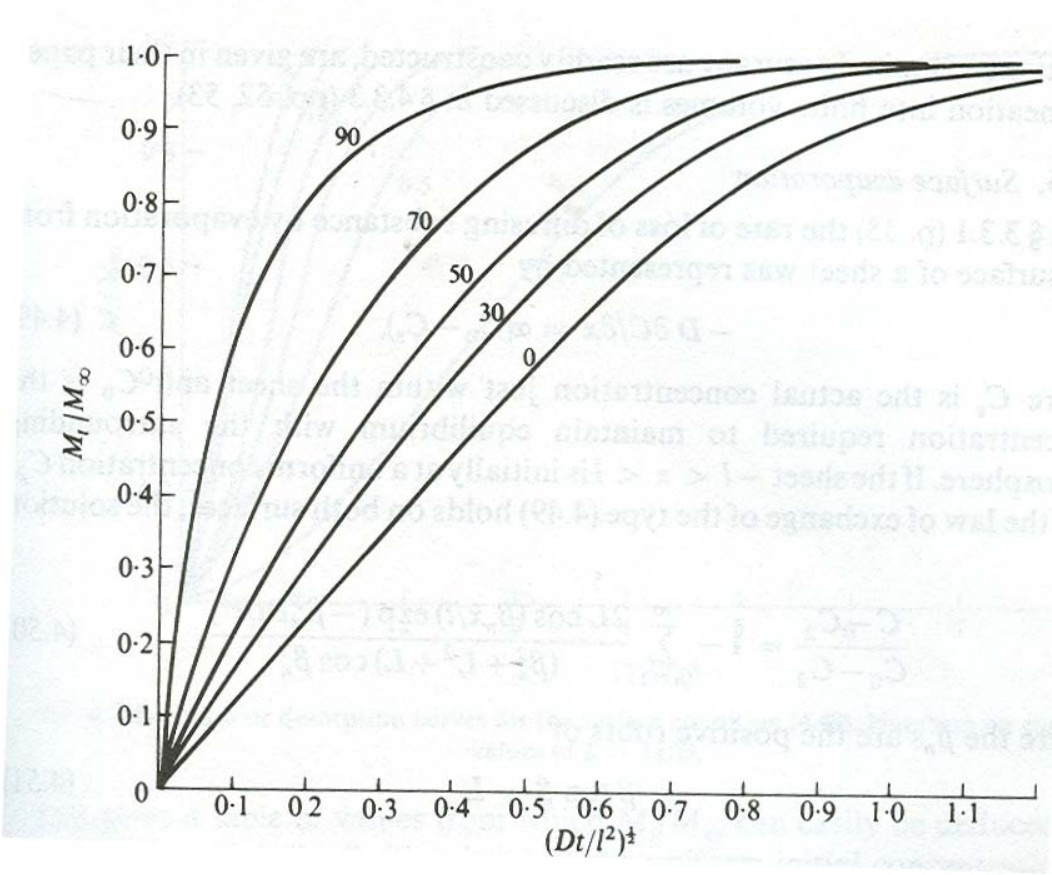

Figure 3.11: Gas uptake by a plane sheet (with thickness $2l$) from a finite source.[18]

From the measured pressure changes in the sample volume, the amount of gas absorbed by the film over time is determined using the following equation.

$$\frac{M_t}{M_\infty} = \left(\frac{p_{SI} \times Z_{SI} - p_{St} \times Z_{St}}{p_{SI} \times Z_{SI} - p_{SF} \times Z_{SF}} \right), \tag{3.15}$$

where p_{St} represent the pressure in the sample volume at time t. The fractional uptake by the film is determined by taking the ratio of the amount absorbed by the film and the total amount introduced to the sample volume. The amount of gas absorbed by the film is calculated using equation 3.12a. The overall percentage uptake by the film (numbers on the curves) is calculated using the following expression.

$$\left(\frac{amount.absorbed.in.the.film}{Total.amount.introduced}\right)=\frac{\left(p_{SI}\times Z\left(p_{SI}\right)-p_{SF}\times Z\left(p_{SF}\right)\right)}{\left(p_{SI}\times Z\left(p_{SI}\right)\right)}\times 100\%. \qquad (3.16)$$

By knowing the $\left(\frac{M_t}{M_\infty}\right)$ value at a particular time and also by knowing the overall percentage uptake by the film, the diffusion coefficient of the gas through the polymeric film is determined from Figure 3.11.[18]

3.4. Characterization Methods

3.4.1. Scanning Electron Microscopy

Fiber cross-sections were examined under a high resolution scanning electron microscope (Leo 1530, Cambridge, UK). The SEM samples were prepared by soaking the fibers in hexane for a couple of minutes and then shear fracturing in liquid N_2 using two fine point tweezers. Without using this approach, the tough Torlon® could not be broken cleanly. The samples were sputter coated with gold before they were examined.

3.4.2.. Infrared Measurements

Infrared spectra were recorded on a Tensor™ 27 model FT-IR (Fourier transform infrared) spectrometer from Bruker Optics. The spectra are taken at a resolution of $1cm^{-1}$ and are averaged our 350 scans.

3.4.3. Thermal Gravimetric Analysis (TGA)

This technique is used to determine the amount of residual solvents left in the membrane. The sample is heated at a desired temperature rate and the weight of the sample is monitored during this process. The measured weight profile provides the information for the residual solvents. In all the TGA experiments reported in this thesis, the sample is heated to 300 °C at rate of 10 °C per min. This heating is done in a controlled nitrogen atmosphere to prevent any oxidation of the sample that may occur at high temperature conditions.

3.4.4. Dynamic Scanning Calorimetry (DSC)

The glass transition temperature (T_g) of the polymer is determined using this technique by heating the sample to a desired temperature at a constant ramp rate. The energy flux required to heat the sample in that specified ramp rate is monitored. This measured energy flux is plotted against the corresponding temperature and a step increase in the energy flux occurs at the glass transition temperature. This is because at temperatures above the T_g, the polymer enters the rubbery state, and in the rubbery state, more chains are flexible and so more energy is required to raise the temperature of the sample. In all the DSC experiments, the sample is heated to 300 °C at a ramp rate of 10 °C per min.

3.4.5. Gas Chromatography (GC)

This technique is used to determine the concentrations of individual gas components in a gas mixture. The gas mixture is passed through a column where gas

separation takes place. Gas species that do not interact with the column exit the column early on, whereas gas species that interact with the column are slowed down. In this way different gas species exit the column at different times. The amount of gas exiting the column is measured using a thermal conductivity detector (TCD).

A "carbon plot" column is used to separate CO_2/C_2H_4, and $CO_2/C_2H_2F_2$ gas mixtures. The GC parameters used for separating these gas mixtures are given in table 3.2. Before performing the separation of these gas pairs, the GC is calibrated for each individual gas to quantify the detector response.

Table 3.2. The GC parameters used in separating CO_2/CH_4, CO_2/C_2H_4, and $CO_2/C_2H_2F_2$ gas mixtures.

GC Parameter	CO_2/C_2H_4
Column Temperature	75 °C
Inlet Temperature	75 °C
Detector Temperature	200 °C
Split ratio	150:1
Inlet pressure	15 psi
Total flow	181 ml/min

3.5. References

1. Robertson, G.P., et al., *Structural determination of Torlon$^{(R)}$ 4000T polyamide-imide by NMR spectroscopy.* Polymer, 2004. 45: p. 1111.

2. Yokelson, H.B., et al., Amide-imide resin for production of heat-resistant fiber, 1992, U.S.Patent, 5,124,428.

3. Larlus, O., S. Mintova, and T. Bein, *Environmental synthesis of nanosized zeolites with high yield and monomodal particle size distribution.* Microporous and Mesoporous Materials, 2006. 96(1-3): p. 405.

4. II, R.W.C. and J.K. William, *Torlon(R) and silicalite mixed matrix membranes for xylene isomer purification*, in *School of Chemical and Biomolecular Engineering*. 2007, Georgia Institute of Technology: Atlanta.

5. Clausi, D.T. and W.J. Koros, *Formation of defect-free polyimide hollow fiber membranes for gas separations.* Journal of Membrane Science, 2000. 167: p. 79.

6. McKelvey, S.A., D.T. Clausi, and J.K. William, *A guide to establishing hollow fiber macroscopic properties for membrane applications.* Journal of Membrane Science, 1997. 124: p. 223.

7. Pesek, S.C. and W.J. Koros, *Aqueous quenched asymmetric polysulfone hollow fibers prepared by dry/wet phase separation.* Journal of Membrane Science, 1994. 88: p. 1.

8. Wallace, D. and W.J. Koros, *Crosslinked hollow fiber membranes for natural gas purification and their manufacture from novel polymers*, in *Department of Chemical Engineering*. 2004, The University of Texas at Austin: Austin.

9. Carruthers, S.B. and J.K. William, *Integral-skin formation in hollow fiber membranes for gas separations*, in *Department of Chemical Engineering*. 2001, University of Texas at Austin: Austin. p. 140-188.

10. Ekiner, O.M., R.A. Hayes, and P. Manos, Reactive post treatment for gas separation membranes, 1992, U.S. Patent, 5,091,216.

11. Ekiner, O.M. and S.S. Kulkarni, Process for making mixed matrix hollow fiber membranes for gas separation, 2003, U.S. Patent, 6663805.

12. O'Brien, K.C., W.J. Koros, and T.A. Barbari, *A New Technique for the Measurement of Multicomponent Gas Transport Through Polymeric Films.* Journal of Membrane Science, 1986. 29: p. 229.

13. Pye, D., H. Hoehn, and M. Panar, *Measurement of gas permeability of polymers. I. Permeabilities in constant volume/variable pressure apparatus.* Journal of Applied Polymer Science, 1976. 20(7): p. 1921.

14. Mulder, M., *Basic Principles of Membrane Technology*. 2nd edition ed. 2003, Boston: Kluwer Academic Publishers. 71-156.

15. Vu, D.Q., J.K. William, and S.J. Miller, *High pressure CO_2/CH_4 separation using carbon molecular sieve hollow fiber membranes.* Ind. Eng. Chem. Res., 2002. 41: p. 367.

16. Koros, W.J., Y.H. MA, and T. Shimidzu, *Terminology for membranes and membrane processes.* Journal of Membrane Science, 1996. 120: p. 149.

17. Peng, D.-Y. and D.B. Robinson, *A New Two-Constant Equation of State.* Industrial and Engineering Chemistry Fundamentals, 1976. 15(1): p. 59.

18. Crank, J., *The Mathematics of Diffusion*. 2nd edition ed. 2001, Britain: Oxford University Press. 44-68.

CHAPTER 4

FORMATION OF ASYMMETRIC HOLLOW FIBER MEMBRANES FROM TORLON®

4.1. Abstract

The first section of this chapter describes the main challenge in achieving the asymmetric membrane for the desired separation of CO_2 from a mixture of $scCO_2$ and C_2F_4. A solution to this problem is then suggested by selecting an appropriate polymer, Torlon® (a polyamide-imide). The reason for this selection will be explained in a detailed manner. After choosing Torlon®, the methods of making good asymmetric hollow fiber membranes from it will be covered. The challenges encountered in making these good membranes and the measures taken to overcome these challenges are illustrated. Gas permeation and scanning electron microscopy are used to characterize these membranes.

4.2. Main Challenge in $scCO_2$ separation

The partial pressures of CO_2 in supercritical carbon dioxide streams are greater than or equal to 1070psi. At these high CO_2 partial pressures, a large amount of CO_2 is absorbed onto the polymer. Such large concentration of CO_2 acts like a swelling agent for the polymeric chains and decreases their inter-segmental interactions. These decreased inter-segmental interactions result in increased polymeric segmental mobility, thereby enhancing the gas transport through the membrane. In fact, the transport of large gas species is increased more than that of small gas species, resulting in decreased

membrane selectivity. This undesired phenomenon is called plasticization[1-3]. The lowest CO_2 pressure at which the plasticization occurs is called the plasticization pressure. Typically, membranes provide selective separations below the plasticization pressure and for the pressures above the plasticization pressure, the separation performance drastically decreases. An indicator of plasticization, even in pure component CO_2 cases, is an upward inflection in CO_2 permeability versus CO_2 feed pressure.

4.2.1. Current polymers used for CO2 separation

Industrially, Matrimid® (a polyimide) and cellulose acetate are the two polymers that are used for CO_2 separations from natural gas. The structures of these two polymers are given in Figures 4.1 and 4.2 respectively. These polymers have plasticization pressures of 150 psi and 160 psi respectively,[1] so as such these two polymers cannot be used for separating $scCO_2$.

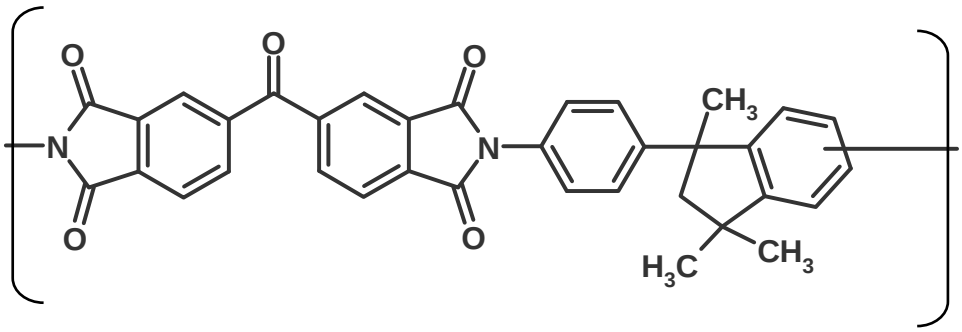

Figure 4.1: Chemical structure of Matrimid®, a polyimide polymer

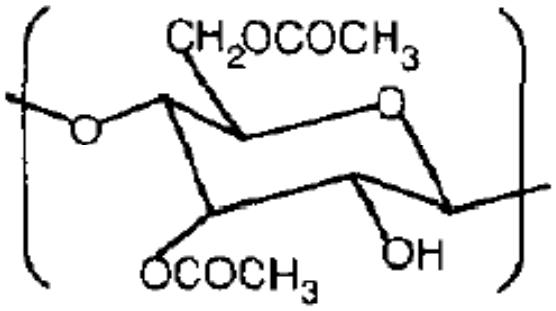

Figure 4.2: Chemical structure of cellulose acetate.

Other researchers are working on cross-linkable polymers to prevent plasticization,[4, 5] and successful formation of cross-linked hollow fiber membranes have been reported. These membranes show enhanced plasticization resistance up to 400 psi partial pressures of CO_2. This approach looks promising but further studies needs to be investigated to check the stability of such membranes for supercritical carbon dioxide pressures. The minor drawbacks of cross-linking strategy are that the cross-linkable polymers are expensive and the process for crosslinking involves an additional processing (cross-linking) step which makes the overall process even more expensive. Even though this strategy of chemically crosslinking the polymeric chains looks promising we have not pursued this approach for our application, and decided to explore other approaches. The approach of cross-linking the polymer chains using hydrogen bonding is investigated. The details of this approach are explained in the following section.

4.3. Choice of Torlon®

This study seeks to suppress the "plasticization" phenomenon by using Torlon®, a polyimide-amide polymer, which is resistant to many organic solvents because of its ability to form intra and inter chain hydrogen bonding. The structure of Torlon® is given in Figure 3.1. The amide groups of Torlon® facilitate hydrogen bonding between the N-H groups of a particular chain with either N-H or C=O groups of the neighboring chains. We expect that such hydrogen bonds can suppress CO_2 induced segmental mobility and thus suppress the plasticization effect.

To check the hypothesis of hydrogen bonding between the N-H groups and the N-H or C=O groups, transmission infrared studies were performed on Torlon® dense film. Figure 4.3 shows the infrared spectrum of the film in the N-H stretching region. A broad peak at 3359 cm^{-1} wave-number, corresponding to hydrogen bonded N-H stretching mode[6-8], indicates that the N-H groups are hydrogen bonded with varied intensity. In addition, the absence of peak at 3446 cm^{-1} wave-number, corresponding to "free" N-H stretching mode[6-8], indicates that all the N-H groups are involved in hydrogen bonding.

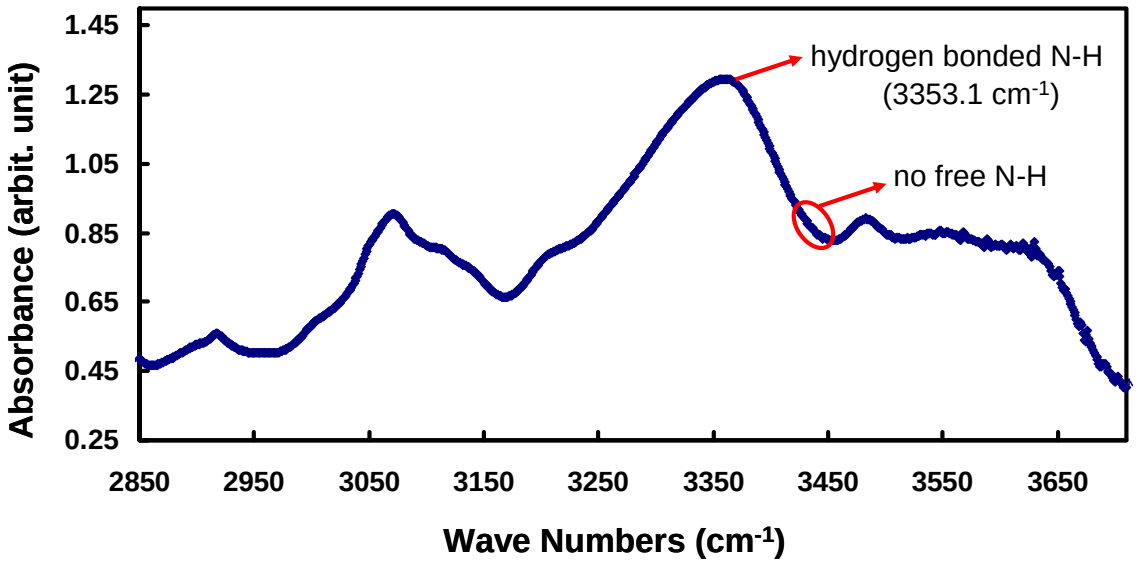

Figure 4.3: Infrared spectrum showing N-H stretching vibration modes in Torlon® film at 25 °C.

To further verify that the peak at 3353.1 cm-1 wave-numbers correspond to the hydrogen bonded N-H, infrared studies are performed on the Torlon® film at elevated temperatures of 100 °C, 200 °C, 300 °C and 450 °C, respectively. If the peak at 3359 cm^{-1} is due to the hydrogen bonded N-H then at elevated temperatures this hydrogen bonding becomes weak and the peak position moves towards the free N-H stretching mode position, 3446 cm^{-1}. The infrared spectra at these elevated temperatures along with the IR spectrum taken at 25 °C are shown in Figure 4.4. The temperature corresponding to each spectrum and their corresponding peak position of the N-H stretching vibration modes are also provided in the figure. The peak position has shifted gradually from 3353.1 cm^{-1} at 25 °C to 3371.5 cm^{-1} at 440 °C. This shift to higher wave-numbers with increase in temperature indicates that the N-H groups in the polymer are hydrogen bonded at 25 °C.

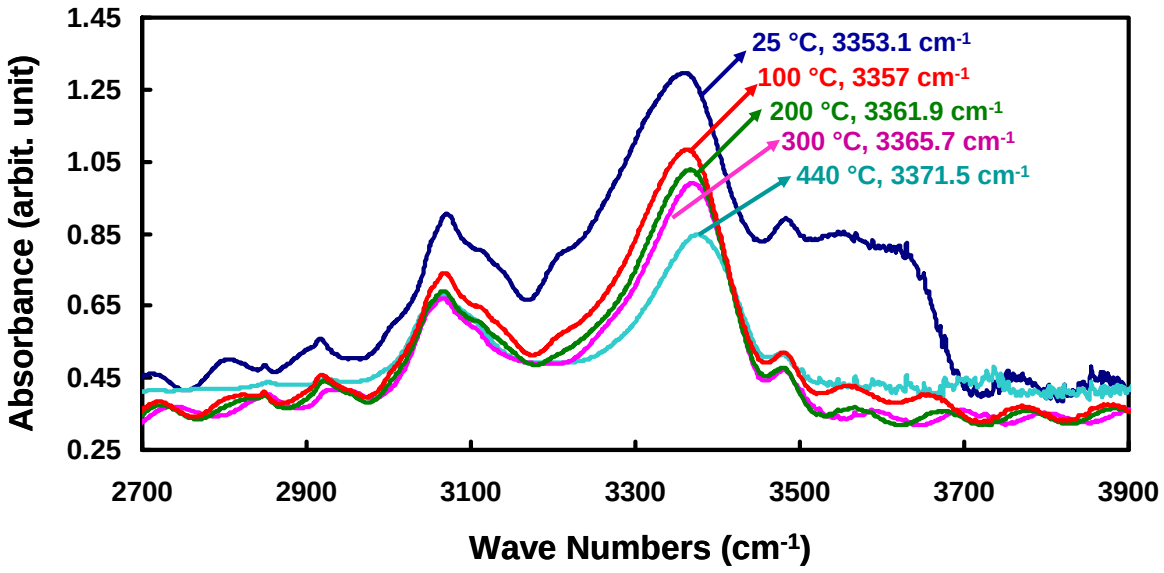

Figure 4.4: Infrared spectra of N-H stretching vibration modes in Torlon® film which is maintained at different temperatures. Corresponding temperature and the peak position of each spectrum are also shown in the figure.

In addition to the peak shifts, there are other changes that can also be observed in the spectra. The peak heights and the absorption area decreased with increase in temperature. This is due to the decrease in the IR absorption coefficient with increase in temperature. Also, there is a decrease in the IR absorption between 3500 and 3700 wave-numbers for the high temperature spectra compared to the spectrum at 25 °C. This is due to the presence of absorbed water in the Torlon® film at 25 °C. At temperatures of 100 °C and above, there is no IR contribution from the water as at those temperatures water desorbs from the film.

4.4. Intrinsic gas separation properties of Torlon®

Intrinsic gas permeabilities of Torlon® membranes are determined by making a dense film membrane and studying its gas transport properties. The dense film

membranes are made using the procedure described in Chapter 3 (section 3.2). Gas permeation properties of O_2, N_2, and He through the Torlon® dense film are also determined using the procedure described in Chapter 3. The measured permeabilities and selectivities are shown in Table 4.1. These gases are the standard non-interacting gases that are typically used to characterize the membranes. The permeabilities of these gases are later used to characterize the hollow fiber membranes.

Table 4.1: Intrinsic O_2, N_2, and He permeabilities and selectivities through Torlon® membrane at 35 °C. The permeabilities are given in barrers and the permeances are given in GPUs.

Intrinsic Permeability	Dense Film (Intrinsic)	Permeance	Hollow Fiber Membrane
P_{He}	4.4 ± 0.2	$\left(P/l\right)_{He}$	7.4 ± 0.3
P_{O_2}	0.12 ± 6E-3	$\left(P/l\right)_{O_2}$	0.26 ± 0.02
P_{N_2}	0.014 ± 7E-4	$\left(P/l\right)_{N_2}$	0.034 ± 2E-3
α_{He/N_2}	310 ± 15	α_{He/N_2}	215 ± 8
α_{O_2/N_2}	8.3 ± 0.4	α_{O_2/N_2}	7.7 ± 0.4

4.5. Making defect-free & macrovoid free asymmetric hollow fiber membranes

4.5.1. Initial attempt

The fiber spinning process is explained briefly in Chapter 3 (section 3.2). The first step in fiber spinning process is to make a dope/polymer solution. The selected low-volatile solvent, volatile solvent, and non-solvent for the dope composition are NMP, THF, and ethanol respectively. Determining the best percentage of each of these components is a critical step that requires a combination of experience and optimization based on observations (see Chapter 3). Based on conventional knowledge (related to spinnable viscosities and skin formation) acquired from spinning polyimides like Matrimid®[9], 27 wt% of polymer and NMP/THF ratio of 80/20 were chosen for the starting dope composition to begin the optimization process. Percent ethanol was determined such that the overall dope composition was close to the binodal curve of the phase diagram. Close proximity to the binodal curve is preferred for rapid phase separation during the quenching process. The "cloud-point technique", described in the experimental section (section 3.2), was used to determine the binodal curve and is shown in Figure 3.12. The so-determined dope composition that is close to the binodal curve was 27 wt% Torlon®, 50.4 wt% NMP, 12.6 wt% THF, and 10 wt% ethanol.

Based on our previous knowledge acquired from spinning polyimides, a bore fluid composition of 96 to 4 parts of NMP and H_2O mixture was chosen[9]. The selection of the preferred NMP to H_2O composition reflects the need to avoid internal skin formation while minimizing extraction of low molecular weight oligomer debris into the bore.

Asymmetric hollow fibers were spun at room temperature (22 °C) using the above mentioned dope and bore fluid compositions. As noted above, we used the spinning

parameters used for polyimide (Matrimid®) spinning as an initial basis for our investigation[10]. The dope flow rate, bore fluid flow rate, take up rate, quench bath temperature, and air gap used for the initial fiber formation are 180 ml/hr, 60 ml/hr, 32 m/min, 22 ^{o}C, and 8 cm respectively. SEM analysis of the fiber's cross-section (Figure 4.5) indicates that the fiber has many macrovoids, which reduce the mechanical strength of the fiber[11, 12]; and as such they should be eliminated for high pressure CO_2 applications.

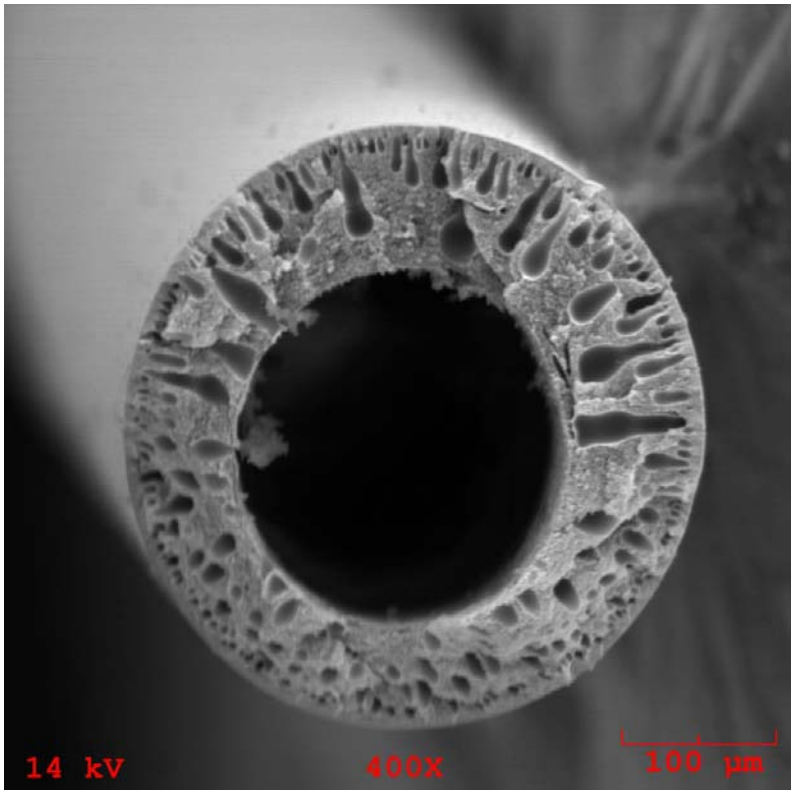

Figure 4.5: SEM cross-section of the fiber spun with 27 wt% of polymer concentration.

In addition to macrovoids, small particulate debris is also observed inside the bore of the fiber (Figure 4.5), due to extraction of oligomers by the bore fluid. Ideally, the bore fluid should be "neutral" to avoid such extraction, so the bore fluid composition had to be further optimized. Optimization showed that a composition of NMP(80)/water(20) was neutral to the polymeric solution (i.e. at this composition, small debris was not extracted nor was internal skin layer formed). This new optimized bore fluid composition was used for subsequent spins.

4.5.2. Reducing the macrovoids

Macrovoids are formed when the fiber is quenched in the water bath. During this quenching process, water from the bath enters the fiber and drives the composition into the 2-phase region where the phase separation occurs. This process is schematically shown in Figure 3.3 (previous chapter). This phase separation proceeds from the outside surface of the fiber towards the bore of the fiber. During the initial periods of phase separation, small nuclei of polymer lean phase are formed. This polymer lean phase is rich in non-solvent (either water or ethanol) and has a very high affinity towards the solvent (NMP). This forms the driving force for the solvent surrounding the nucleus to migrate into the non-solvent rich nucleus. Such solvent migration into the closed nucleus causes osmotic pressure which makes the nucleus grow. Since the front side of the nucleus (the side near the outer wall) is already vitrified, it has enough strength to withstand the osmotic pressure. On the other hand, the back side of the nucleus is still a homogeneous one phase which expands under the osmotic pressure to form a tear shaped

macrovoid. Schematic of this macrovoid growth due to solvent ingress is shown in Figure 4.6.

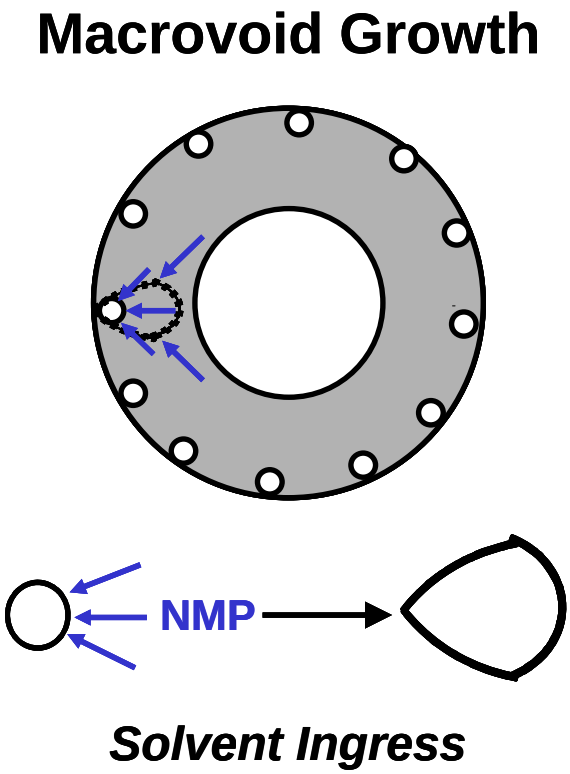

Figure 4.6: The figure schematically shows the macrovoid growth due to NMP diffusion into the nucleus.

The macrovoid formation can be suppressed if the newly formed nucleus is arrested in its original size before it grows into a macrovoid. This can be done by delaying the onset of osmotic pressure till the solution surrounding the nucleus is phase separated due to the incoming water. Such a delay can be achieved by reducing the diffusion of NMP from the surrounding polymer solution in to the nucleus. One of the

ways of decreasing the NMP diffusion is by increasing the viscosity of the polymer solution via increasing the polymer concentration in the dope.

We have increased the polymer concentration from 27 wt% to 34 wt% of Torlon® in the dope. In this new dope composition, NMP/THF ratio was maintained at 80/20. The dope composition that is close to the binodal curve at this new polymer concentration is 34 wt% Torlon®, 47.2 wt% NMP, 11.8 wt% THF and 7 wt% ethanol. Fibers were spun with this new dope using the original spinning conditions. Figure 4.7 shows a SEM of a fiber from this spin set. No macrovoids were observed, verifying our hypothesis that by reducing the diffusion of NMP into the nucleus, macrovoids are suppressed. The fiber now has the potential to withstand high pressures.

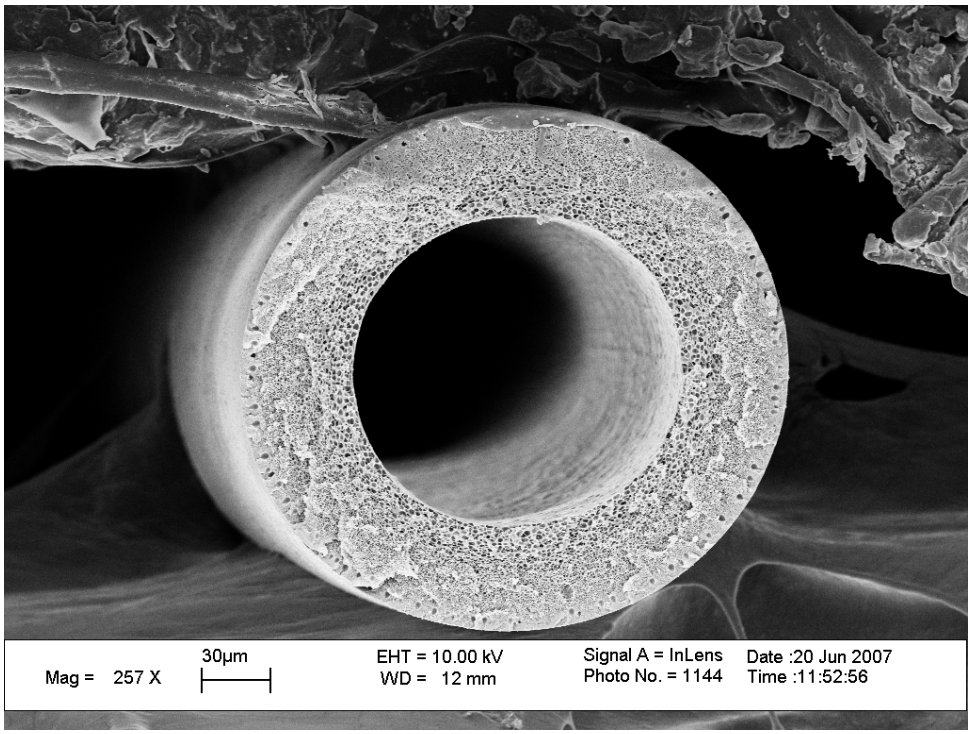

Figure 4.7: SEM of the fiber spun from a 34 wt% polymeric solution at a dope temperature of 25 ºC.

4.5.3. Making a defect-free fiber

To check whether the above macrovoid-free fiber has a defect-free skin layer, pure gas (N_2, O_2, and He) permeation tests were carried out. These fibers showed an O_2/N_2 selectivity of 4.0, which is well below the dense film selectivity of 8.3, thereby indicating that the fibers were defective. Defective skins can be formed if the composition of the outer surface of the fiber is not driven sufficiently close to the vitrified region during spinning through the air gap. We hypothesized that the fibers were defective due to the lack of adequate THF evaporation in the air gap from the outer surface of the fiber. THF evaporation can be increased by changing the spinning parameters such as air gap and dope temperature. Larger air gaps and higher dope temperatures favor defect-free skin formation.

To pursue formation of a defect-free skin layer, fibers were spun at room temperature with an increased air gap of 22 cm; however, the fibers were still defective with a selectivity of 4.3. Another set of fibers were spun at a dope temperature of 50 ^{o}C (less than the boiling point of THF, 65 ^{o}C) with an air gap of 22 cm. The spun fibers showed an O_2/N_2 selectivity of 7.7, which is about 90% of the intrinsic polymer selectivity of 8.3. At this level of selectivity, not only skin defects but also excessive substructure resistance can cause less than intrinsic selectivity[13-15]. To check whether the fiber skin was defect free or not, a post treatment test (described in the experimental section) was carried out. The fiber skin is defective if an increase in O_2/N_2 selectivity (close to intrinsic value of 8.3) is observed after the post treatment procedure. If such an increase is not observed then the fiber's selective layer is not defective and substructure resistance is most likely the cause of the lower than intrinsic selectivity. The selectivity

of the post treated fibers was measured to be 7.7, which was the same as that of the untreated fibers, indicating that the fibers' skin layer is defect-free. Furthermore, the permeabilities of the gases were decreased slightly after the post treatment procedure, indicating the presence of a small increase in skin layer resistance due to the post treatment.

The below-intrinsic selectivity (7.7) of the fiber can, therefore, be best explained in terms of the substructure resistance[14, 16]. Knudsen or bulk flow occurring in the substructure is less selective compared to the solution-diffusion occurring in the skin layer. When such less selective substructure resistance becomes comparable to the skin layer resistance then the overall selectivity of the membrane gets lowered from the intrinsic value. We believe that the observed low selectivity in our fibers is due to such substructure resistance.

The substructure resistance can be further verified by comparing the permeation of different "fast" (more permeable) versus "slow" (less permeable) gas species. The substructure would more significantly affect (decrease) the permeation of fast gas species compared to slow gas species[9, 16]. Among He, O_2, and N_2 gas species, the highly permeable He gets effected the most followed by O_2 and then N_2. Hence by measuring the He/N_2 and O_2/N_2 selectivities and comparing them with the intrinsic values, the existence of a substructure resistance can be identified. If the substructure resistance exists, then the $\frac{(He/N_2)_{measured}}{(He/N_2)_{\text{intrinsic}}}$ value will be considerably lower compared to the $\frac{(O_2/N_2)_{measured}}{(O_2/N_2)_{\text{intrinsic}}}$ value. The greater is this difference between these ratios for the He/N_2

and O_2/N_2 cases, the greater is the substructure resistance. This method is a useful indicator of substructure resistance, but not a simply interpreted one.

Measured permeances and selectivities of O_2, N_2, and He gases through hollow fiber membranes along with the intrinsic permeability and selectivity values (obtained from dense film measurements) are shown in Table 1. The calculated value for $\frac{(He/N_2)_{measured}}{(He/N_2)_{intrinsic}}$ is 0.69 ± 0.04, which is considerably lower than the $\frac{(O_2/N_2)_{measured}}{(O_2/N_2)_{intrinsic}}$ value of 0.92 ± 0.03. This supports the conclusions based on the post treatment study and strongly indicates that the fiber's lower O_2/N_2 selectivity is due to substructure resistance and that the fiber's skin is truly defect-free.

Approximate skin thickness of a defect-free fiber can be determined by taking the ratio of the intrinsic permeability of a particular gas through the polymer to the permeance of that gas through the fiber. This method provides a more accurate estimate if the gas has negligible substructure resistance compared to the skin resistance. Nitrogen, which has low substructure resistance, was used to determine the skin thickness of the defect-free fiber. The calculated skin thickness is ~ 410 nm.

The SEM of this membrane with a defect free skin, prepared at a dope temperature of 50 ºC and an air gap of 22 cm is shown in Figure 4.8. Small voids, again, start appearing at the outer surface of the fiber. This behavior is explained by a reduction in dope viscosity at high temperature spinning. To determine whether these small voids have any significant effect on the membrane's strength, we performed a collapse test using N_2 gas on the shell side. This test revealed that the fiber could withstand up to 2000 psi of N_2 before collapsing. Since this pressure is beyond the supercritical pressure of CO_2 (1100 psi), the fibers were studied up to scCO_2 pressure of 1100 psi without

further modification. These fibers are then investigated for the actual CO_2/C_2F_4 separations under supercritical conditions. The results of these studies are reported in the next chapter.

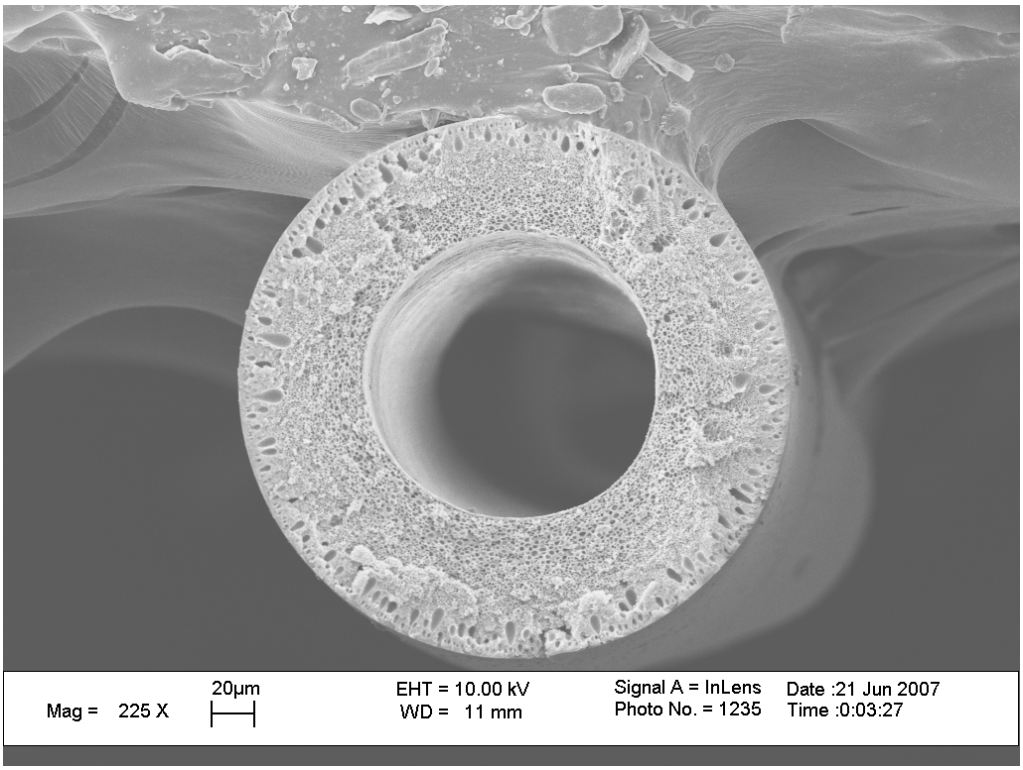

Figure 4.8: SEM of the fiber spun from 34 wt% polymeric solution and 50 ºC dope temperature.

4.5.4. Further reducing the macrovoids

Although the fiber shown in Figure 4.8 can withstand high pressures, we still are interested to reduce the existing small voids for the purpose of developing a better understanding on macrovoid formation. So, a parallel study of suppressing the macrovoids is performed along with the studies on characterizing the defect-free Torlon® membrane for supercritical CO_2 separations.

Based on the mechanism proposed earlier in this chapter (section 4.5.2), the macrovoids could be reduced by increasing the polymer weight percent in the dope. However increasing the polymer weight percent would further increase the substructure resistance of the fiber and thereby reduces the membrane's separation performance. Hence we haven't explored this possibility of increasing the polymer weight percent to reduce the macrovoids.

However, we still want to pursue the same strategy of suppressing the macrovoids by phase separating the solution surrounding the nascent nucleus before it grows into a macrovoid. In the previous method, this strategy is accomplished by decreasing the solvent influx into the nucleus by increasing the viscosity of the solution via increasing the polymer weight percent in the dope. In our new approach, we want to accomplish this strategy by bringing the dope solution quite close to its unstable (2-phase) state. This method of bringing the dope solution close to its unstable state is currently done by adding ethanol as a non-solvent to the dope. However ethanol doesn't maintain the dope solution in its unstable state based on the following argument.

When a water rich nucleus is formed (as shown in Figure 4.6), then not only NMP but also ethanol from the dope solution (surrounding the nucleus) enter the nascent nucleus resulting in macrovoid formation. When ethanol is diffused away from the dope solution (into the nucleus) then the dope composition (surrounding the nucleus) is driven away from the unstable state. Hence ethanol does not keep the dope solution (surrounding the nucleus) unstable. So, instead of ethanol we have chosen to add water to bring the dope solution close to the unstable state. Since water in the surrounding dope

solution does not diffuse into the water rich nucleus (as there is no driving force), the dope solution (surrounding the nucleus) is maintained in an unstable state.

So a new binodal point is determined for Torlon®, NMP, THF and water system with 34 wt% polymer and 4:1 ratio of NMP:THF. The dope composition close to this binodal point is 34 wt% polymer, 50.4 wt% NMP, 12.6 wt% THF, and 3 wt% water. The SEM cross-section of the fiber spun at this composition is shown in Figure 4.9.

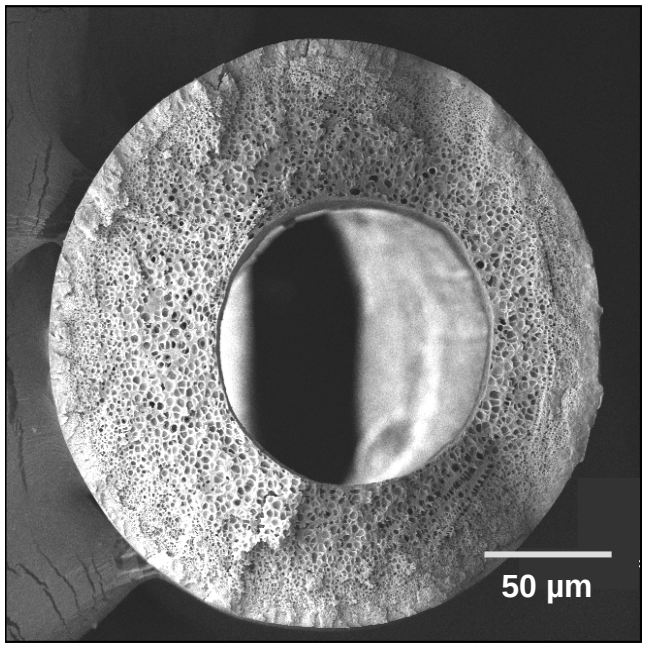

Figure 4.9: SEM of the fiber spun from 34 wt% polymeric solution with water as non-solvent (in the dope) and 50 ºC dope temperature.

During this spin, all the other spinning parameters which are used in making defect-free fibers are used. No macrovoids are observed indicating that our hypothesis of suppressing macrovoids is correct, i.e., using water (rather than ethanol) maintains the

dope in its unstable state which facilitates faster phase separation and thereby preventing the growth of macrovoids.

These fibers are then tested whether the skin layer is defect-free or not by performing oxygen and nitrogen permeation measurements. The measured O_2/N_2 selectivity of 2.8 indicates that the fibers are defective. As discussed previously, the lowering in selectivity could be because of either substructure resistance or defects in the skin layer. To determine which one of these factors is the reason for low selectivity, oxygen permeance is compared with the defect-free fibers. The O_2 permeance of these fibers (0.96 GPUs) is three times greater than the O_2 permeance of defect-free fibers (0.26 GPUs). This relatively high O_2 permeance indicates that the skin layer is defective. As explained earlier, defective fibers are formed due to lack of enough THF evaporation in the air gap. Especially in this particular case of fast phase separation, more THF evaporation is required to form a defect-free skin layer. Because of the fast phase separation, no densification of skin layer occurs during quenching and so a relatively thick dense skin layer needs to be formed prior to quenching. This can be achieved by promoting more THF evaporation in the air gap. This more THF evaporation can be accomplished by increasing the air gap and by using more THF in the dope formulation.

4.6. Summary and Conclusions

Torlon® was chosen for supercritical CO2 separations. Infrared spectroscopy studies show that Torlon® forms inter-chain hydrogen bonding. Initial attempts to spin resulted in defective and macrovoid containing hollow fibers. After subsequent optimization of dope composition and spinning parameters, defect-free asymmetric

hollow fiber membranes were successfully made. The reason for macrovoid formation is hypothesized. Based on the proposed hypothesis macrovoids are initially reduced and subsequently were completely eliminated.

4.7. References

1. Bos, A., et al., *CO_2-induced plasticization phenomena in glassy polymers.* Journal of Membrane Science, 1999. 155: p. 67-78.

2. Donohue, M.D., B.S. Minhas, and S.Y. Lee, *Permeation behavior of carbon dioxide-methane mixtures in cellulose acetate membranes.* Journal of Membrane Science, 1989. 42: p. 197-214.

3. Wessling, M., et al., *Plasticization of gas separation membranes.* Gas Separation & Purification, 1991. 5(4): p. 222-228.

4. Wind, J.D., D.R. Paul, and W.J. Koros, *Natural gas permeation in polyimide membranes.* Journal of Membrane Science, 2004. 228: p. 227-236.

5. Wind, J.D., et al., *The effects of crosslinking chemistry on CO_2 plasticization of polyimide gas separation membranes.* Ind. Eng. Chem. Res., 2002. 41: p. 6139-6148.

6. R., S.L. and S.L. Cooper, *Hydrogen bonding in polyamides.* journal of applied physics, 1976. 47(10): p. 4310-4317.

7. Skrovanek, D.J., et al., *Hydrogen bonding in polymers: Infrared temperature studies of an amorphous polyamide.* Macromolecules, 1985. 18: p. 1676-1683.

8. Skrovanek, D.J., P.C. Painter, and M.M. Coleman, *Hydrogen bonding in Polymers. 2. Infrared temperature studies of Nylon 11.* Macromolecules, 1986. 19: p. 699-705.

9. Clausi, D.T. and W.J. Koros, *Formation of defect-free polyimide hollow fiber membranes for gas separations.* Journal of Membrane Science, 2000. 167: p. 79-89.

10. Carruthers, S.B., G.L. Ramos, and W.J. Koros, *Morphology of integral-skin layers in hollow-fiber gas separation membranes.* Journal of Applied Polymer Science, 2003. 90: p. 399-411.

11. McKelvey, S.A. and W.J. Koros, *Phase separation, vitrification, and the manifestation of macrovoids in polymeric asymmetric membranes.* Journal of Membrane Science, 1996. 112: p. 29-39.

12. McKelvey, S.A. and J.K. William, *Formation and Characterization of Hollow Fiber Membranes for Gas Separation*, in *Department of Chemical Engineering*. 1997, PhD Thesis, University of Texas at Austin: Austin.

13. Bauer, C.J.M., J. Smid, and J. Olijslager, *The resistance towards gas transport of the sublayer of asymmetric PPO hollow fiber membranes determined by plasma-etching.* Journal of Membrane Science, 1991. 57: p. 30-320.

14. Henis, J.M.S. and M.K. Tripodi, *Composite hollow fiber membranes for gas separation: the resistance model approach.* Journal of Membrane Science, 1981. 8: p. 233-246.

15. Pinnau, I., et al., *Gas permeation through composite membranes.* Journal of Membrane Science, 1988. 37: p. 81-88.

16. Pinnau, I. and W.J. Koros, *Structures and gas separation properties of asymmetric polysulfone membranes made by dry, wet and dry/wet phase inversion.* Journal of Applied Polymer Science, 1991. 43: p. 1491-1502.

CHAPTER 5

CHARACTERIZING TORLON® MEMBRANES FOR $scCO_2/C_2H_4$ & $scCO_2/C_2H_2F_2$ SEPARATIONS

5.1. Abstract

In this chapter I utilize Torlon® hollow fiber membranes for the desired separation of CO_2 and C_2F_4 mixtures. However due to the explosive nature of C_2F_4, the intended separation of CO_2 and C_2F_4 is not studied experimentally. Instead, the separations of CO_2/C_2H_4 and $CO_2/C_2H_2F_2$ gas mixtures are studied to predict the separation of CO_2/C_2F_4. The reason for selecting these two gas pairs are described in this chapter. The separation performance and the stability analysis of the Torlon® membranes under supercritical conditions are also investigated.

5.2. Predicting the CO_2/C_2F_4 separation

5.2.1. Hypothetical reasoning behind the selection of C_2H_4 & $C_2H_2F_2$

As explained in the introduction section (chapter 1), C_2F_4 is explosive in nature and needs special handling equipment. Since we do not have those facilities, we could not use C_2F_4 in our laboratories. Instead of experimentally measuring the CO_2/C_2F_4 separations, we chose an alternative approach of predicting them. We intend to do this by measuring CO_2/C_2H_4 and $CO_2/C_2H_2F_2$ separations.

C_2H_4 is chosen because of its smaller size and similar shape compared to C_2F_4. As a result, the diffusion of C_2H_4 is going to be greater than C_2F_4. The critical temperatures of these two gases (C_2F_4: 306.5 °C and C_2H_4: 282.4 °C)[1] are similar, and since the critical temperatures are rough indicators of sorption, both the gases are

estimated to have similar sorption capacities.[2] These trends in sorption and diffusion indicate that the permeability of C_2H_4 is going to be greater than C_2F_4. This suggests that the selectivity of CO_2/C_2F_4 will be greater than the selectivity of CO_2/C_2H_4, i.e. if the membrane can selectively separate CO_2/C_2H_4 then it should separate CO_2/C_2F_4 with a selectivity of greater or equal to that of CO_2/C_2H_4.

The gas sorption depends on the chemical interactions between the gas molecules and the polymer. Since C_2H_4 and C_2F_4 have different chemical compositions, the actual sorption of these gases on the membrane could be different. The critical temperature is only an approximate estimator of relative gas sorption and is not always a reliable one, so to exactly estimate the sorption of these two gases, one needs some experimental evidence. For this reason we have chosen $C_2H_2F_2$ to determine the effect of fluorine on the gas sorption.

$C_2H_2F_2$ is chosen because its structure is intermediate between C_2H_4 and C_2F_4 and the diffusion and sorption coefficients of $C_2H_2F_2$ would also be between those of C_2H_4 and C_2F_4. Moreover $C_2H_2F_2$ is not highly hazardous and so it can be used in our laboratories. The effect of fluorines on the sorption can now be experimentally determined by measuring the sorption of $C_2H_2F_2$. In addition, by knowing the selectivities of CO_2/C_2H_4 and $CO_2/C_2H_2F_2$, one could roughly estimate the selectivities of CO_2/C_2F_4.

5.2.2. Sorption of C_2H_4 and $C_2H_2F_2$ on Torlon®

C_2H_4 and $C_2H_2F_2$ sorption measurements are performed on a thin Torlon® dense film of thickness 1 mil. Such a small thickness is used because thin films reach

equilibrium much quicker compared to thicker ones. The sorption measurements are performed as discussed in the experimental section (section 3.4.2). The sorption and diffusion coefficients of C_2H_4 and $C_2H_2F_2$ are calculated from these measurements and are shown in Table 5.1. The details of the calculations are provided in chapter 3 (section 3.4.2.1 and 3.4.2.2). The measurements are performed at a pressure of 27 psi and the gas phase non-idealities are corrected using virial equation of state.

Table 5.1: Sorption and diffusion coefficients of C_2H_4 and $C_2H_2F_2$ through Torlon® dense film measured at 27 psi and 35 °C.

Gas type	Sorption Coefficient $\frac{cm^3 gas(STP)}{cm^3 polymer.cmHg}$	Diffusion Coefficient (cm^2/sec)	Permeability (Barrer) $10^{-10}\frac{cm^3 gas(STP).cm}{cm^2.cmHg.\sec}$
C_2H_4	0.04 ± 0.003	$(2.1 \pm 0.2)\times 10^{-11}$	$(8.2 \pm 1.5)\times 10^{-3}$
$C_2H_2F_2$	0.035 ± 0.003	$(6.0 \pm 0.6)\times 10^{-12}$	$(2.1 \pm 0.4)\times 10^{-3}$

The data reported in table 5.1 indicates that both C_2H_4 and $C_2H_2F_2$ have similar sorption coefficients on Torlon® which is consistent with our predictions based on critical temperatures. The presence of fluorine on $C_2H_2F_2$ seems to have minimal effect on sorption when compared to C_2H_4. As expected, the diffusion of $C_2H_2F_2$ is smaller compared to C_2H_4; the diffusion coefficient of $C_2H_2F_2$ is measured to be about 3.5 times smaller than C_2H_4. Overall, the permeability of $C_2H_2F_2$ is about 3.9 times lower than

C_2H_4. These observations also indicate that the permeability of C_2H_4 will definitely be higher than C_2F_4, validating our choice of using C_2H_4 to predict the separation of CO_2/C_2F_4 mixture.

5.3. Characterizing Torlon® hollow fiber membranes for scCO_2 permeation

As mentioned in Chapter 4 (section 4.2), high pressures of CO_2 plasticize the polymeric membranes and reduce their separation performance. So, before studying the actual CO_2/C_2H_4 separation, preliminary tests on membrane's separation ability are carried by measuring pure gas CO_2 permeances at various CO_2 pressures. An upward swing in the permeance with increase in pressure is an indicator of swelling. The amount of upward swing determines the degree of swelling and a higher degree of swelling results in plasticization which affects the separation ability of the membrane, so the pure gas CO_2 permeance measurements are good predictors of membrane's separation ability. Nevertheless, actual test of a membrane's separation performance require mixed gas CO_2/C_2H_4 selectivity measurements, which are shown later in this chapter.

Defect-free hollow fiber membranes that can withstand high pressures are prepared as explained in Chapter 4 and these membranes are tested for pure CO_2 permeances at pressures up to 2000 psi, well into supercritical region (supercritical pressure of CO_2 is 1070 psi). Steady state permeances are measured at various pressures and are plotted in Figure 5.1. These permeances are measured after steady state CO_2 permeation is reached. Measurements are typically made after equilibrating the membrane for 3-4hrs and this duration is sufficient for CO_2 to reach steady state because

3-4 hrs are much longer than the time lag of CO_2 which is 30 sec through an asymmetric Torlon® membrane.

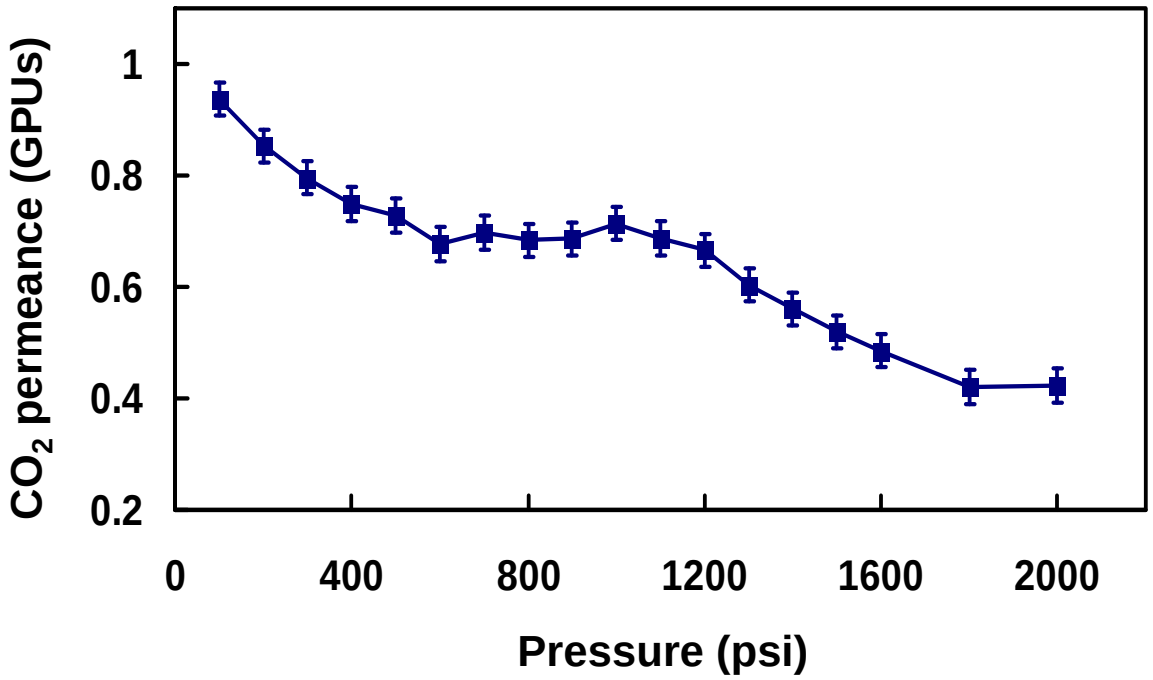

Figure 5.1: CO_2 permeances through Torlon® hollow fiber membranes at various pressures measured at 35 °C.

Figure 5.1 indicates that the CO_2 permeances initially decrease with increase in pressure from 100 psi to 600psi and then the permeances remain constant up to 1200 psi and with further increase in the CO_2 pressure, the permeances start decreasing again. This behavior is not only due to membrane material characteristics but also due to the gas phase non-idealities of CO_2. As explained in chapter 3 (section 3.4.1.2), the non-idealities of CO_2 are considered in calculating permeances by using fugacities instead of CO_2 pressures. The fugacity corrected CO_2 permeances are plotted in Figure 5.2.

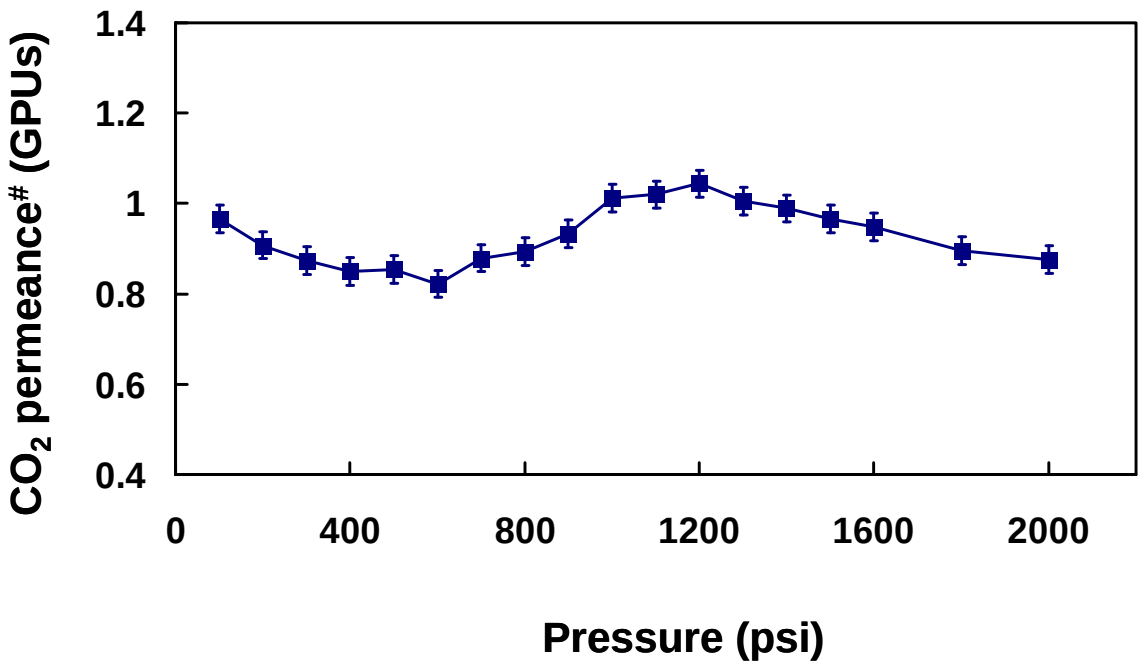

Figure 5.2: Fugacity corrected CO_2 permeances through Torlon® hollow fiber membranes at various pressures measured at 35 °C.

The fugacity corrected permeances also show an initial decrease in permeance with increase in pressure from 100 psi to 600 psi. However, the percent decrease is smaller for the case of fugacity corrected permeances. When no non-ideal gas effects are considered, the permeances showed a decrease of about 28% where as when the non-ideal effects are considered (fugacity corrected permeances) the decrease is only 14%. This 14% reduction is primarily due to saturation of inter-segmental Langmuir sites at higher pressures. These sites favor CO_2 sorption; however they are fixed in number. At low pressures, they enhance CO_2 sorption and thereby enhance CO_2 permeance. But at higher pressures, these sites get saturated resulting is no additional sorption contribution from the Langmuir sites. As a result, both the CO_2 sorption and permeances are lowered at higher pressures.[3]

For pressures between 600 psi to 1200 psi, the fugacity corrected permeances slightly increased with increase in pressure. This increase can be attributed to swelling of the membrane which results in increase in polymer chain mobility and thereby increase in CO_2 permeance. However, the overall increase in permeance from 600 psi to 1200 psi is only about 27% which is not very substantial and so this swelling may not have a significant affect on the membrane's separation performance. The best way to check whether this small degree of swelling has a profound effect on separation performance or not, is, by performing mixed gas CO_2/C_2H_4 selectivity measurements. These measurements will be covered later in this chapter.

To verify whether the observed increase in permeance from 600 psi to 1200 psi is due to the swelling of the membrane, a pressurization and a de-pressurization study was performed. The membrane is pressurized to 1000 psi and then de-pressurized back to 100 psi; during this process the permeances are measured and are plotted in Figure 5.3. Hysteresis in permeance is observed during the de-pressurization step, which is a good indicator that the membrane is in a highly swelled state at 1000 psi. The swelling occurs because of high sorption of CO_2, which increases the net volume of the polymer sample. During the de-pressurization step, when the pressure is decreased, the CO_2 desorbs from the membrane leaving extra free volume which enhances the CO_2 permeance.

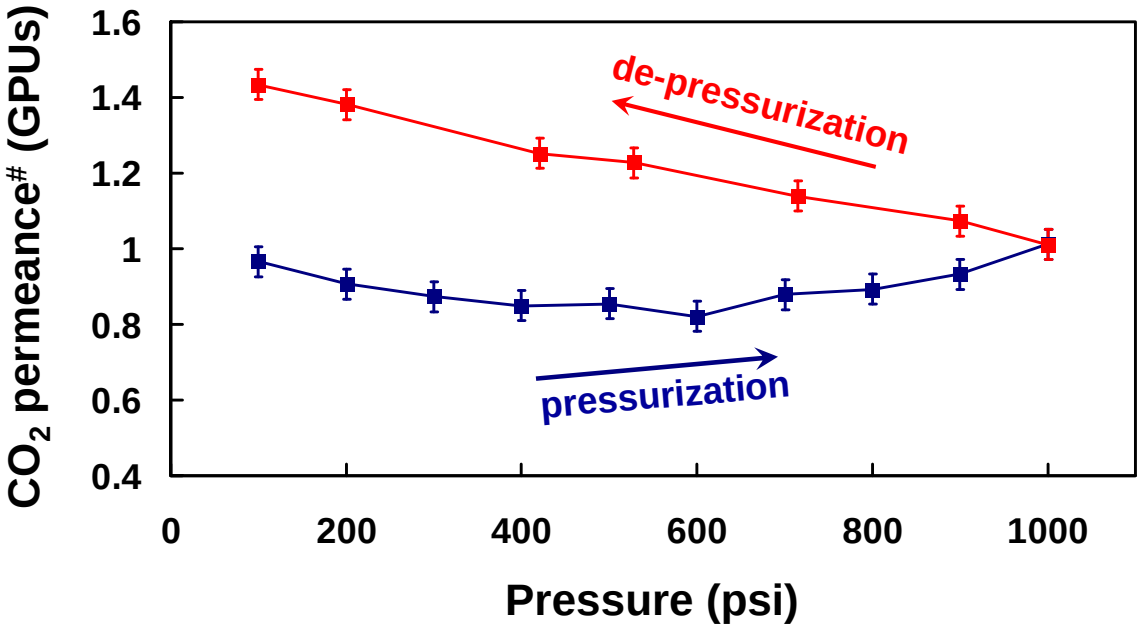

Figure 5.3: Fugacity corrected CO_2 permeances through Torlon® hollow fiber membranes during pressurization (from 100 psi to 1000 psi) and de-pressurization (from 1000 psi to 100 psi). The measurements are performed at 35 °C.

Beyond 1200 psi, the fugacity corrected permeances (Figure 5.2) decrease with increase in pressure. This behavior could be because of membrane compaction at high pressures. At high pressures, the substructure of the membrane may collapse giving rise to additional resistance to CO_2 permeance. This collapse could also be aided by the swelling of the membrane due to supercritical CO_2. Swelling decreases the strength of the polymer and when high pressures are applied, the swelled substructure compresses resulting in substructure resistance. To determine whether the membrane is swelled under these high pressure conditions, a depressurization study is performed from 1800 psi. The permeances during depressurization step along with the pressurized ones are plotted in Figure 5.4. Hysteresis in CO_2 permeance is observed indicating that the membrane is swelled under these conditions. So swelling and substructure collapse are

the two phenomena taking place under these high pressure $scCO_2$ conditions. Both of these factors can have a profound affect on the separation performance[4-7] and to determine the exact effect of these two factors, mixed gas CO_2/C_2H_4 selectivity measurements are performed.

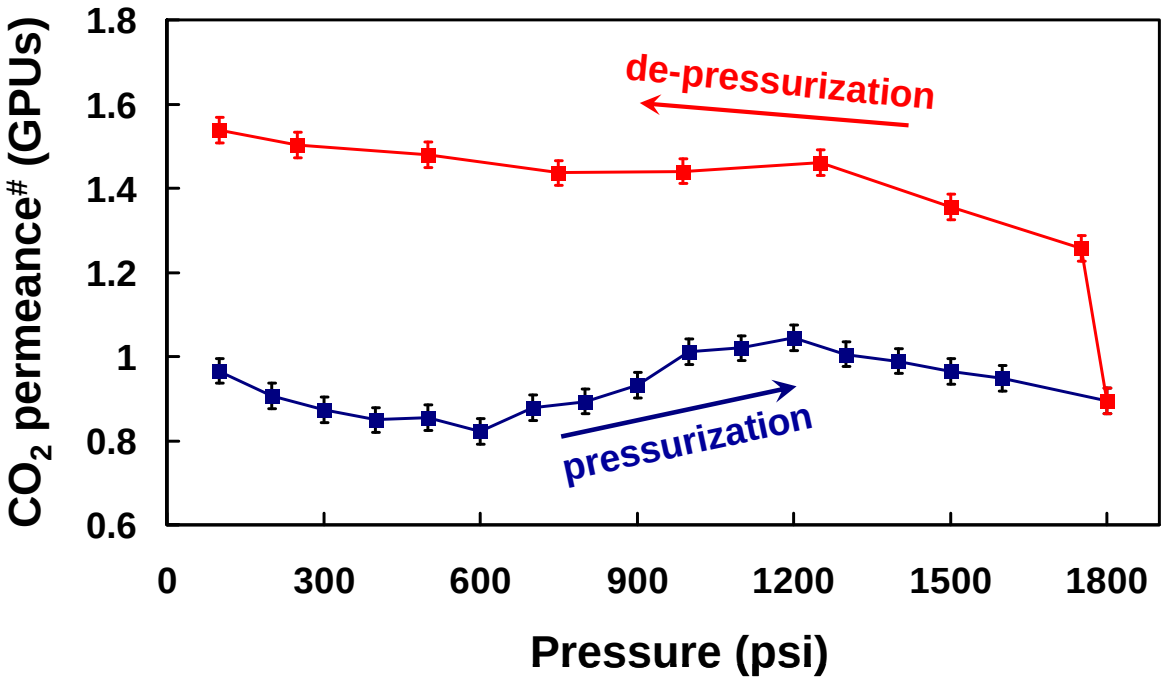

Figure 5.4: Fugacity corrected CO_2 permeances through Torlon® hollow fiber membranes during pressurization (from 100 psi to 1800 psi) and de-pressurization (from 1800 psi to 100 psi). The measurements are performed at 35 °C.

5.4. CO_2/C_2H_4 separation by Torlon® membrane

5.4.1. CO_2/C_2H_4 selectivity at various CO_2 pressures

To study whether Torlon® can actually provide selective separations at high pressures of CO_2, the defect-free fiber was tested using a mixed gas of CO_2 and C_2H_4 (90

mol% CO_2 and 10 mol% C_2H_4) up to a total pressure of 1700psi at 35 °C. This upper limit of 1700 psi is in the supercritical regime since the partial pressure of CO_2 at this pressure is ~1530 psi , which is beyond the critical pressure of CO_2 (1070 psi). The reason for testing the membrane only up to 1700psi is explained later in this section.

The selectivity of CO_2/C_2H_4 at various partial pressures of CO_2 is shown in Figure 5.5. The selectivities gradually decreased with increase in CO_2 partial pressures from 180 psi to 1260 psi. During this period, the selectivities decreased from 39 (at 180 psi of CO_2) to 24 (at 1260 psi of CO_2) which is about 38% decrease. Beyond 1260 psi partial pressures of CO_2, the selectivity dropped quite drastically from 24 (at 1260 psi of CO_2) to 8.4 (at 1530 psi of CO_2) which is about 65% decrease. This drastic decrease in selectivity could be due to excessive swelling of the membrane (plasticization). Moreover, the substructure collapse, that starts happening at pressures beyond 1260 psi (Figure 5.2), could also be the reason for such a drastic decrease in selectivity. A substructure collapse results in an additional non-selective substructure resistance. This substructure resistance, as explained in Chapter 2, hinders the transport of fast moving gas (CO_2) more than the slow gas (C_2H_4) and as a result the CO_2/C_2H_4 selectivity decreases. Because the membrane showed such a drastic selectivity loss at 1530 psi of CO_2 (i.e. when the total pressure is 1700 psi), 90/10 CO_2/C_2H_4 mixed gas studies beyond 1700 psi were not pursued.

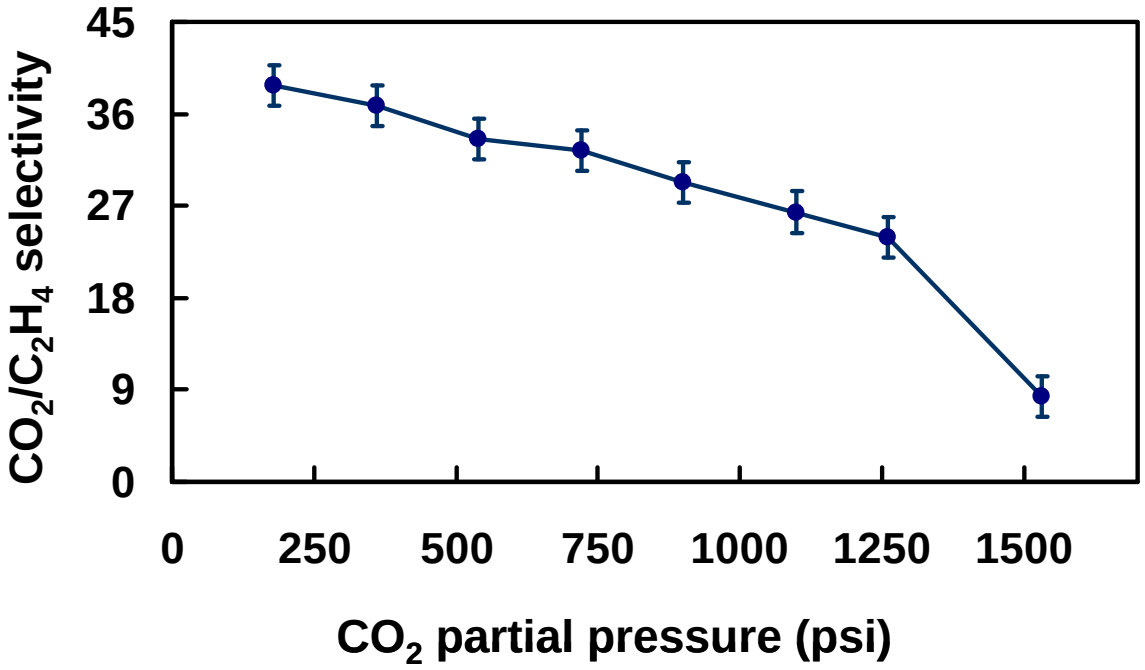

Figure 5.5: Mixed gas CO_2/C_2H_4 selectivities of Torlon® asymmetric hollow fiber membrane at various partial pressure of CO_2. These measurements are made with a feed gas composition of 90% CO_2 and 10% C_2H_4 at 35 °C.

The selectivity trend plotted in Figure 5.5 is not only due to the membrane material behavior but also due to the non-ideal gas phase effects.[8] These non-ideal gas phase effects are taken into account by using fugacities of CO_2 and C_2H_4 instead of their partial pressures. This procedure of accounting non-ideal gas phase effects is described in Chapter 3 (section 3.4). The fugacity corrected selectivities are plotted at various partial pressures of CO_2 in Figure 5.6.

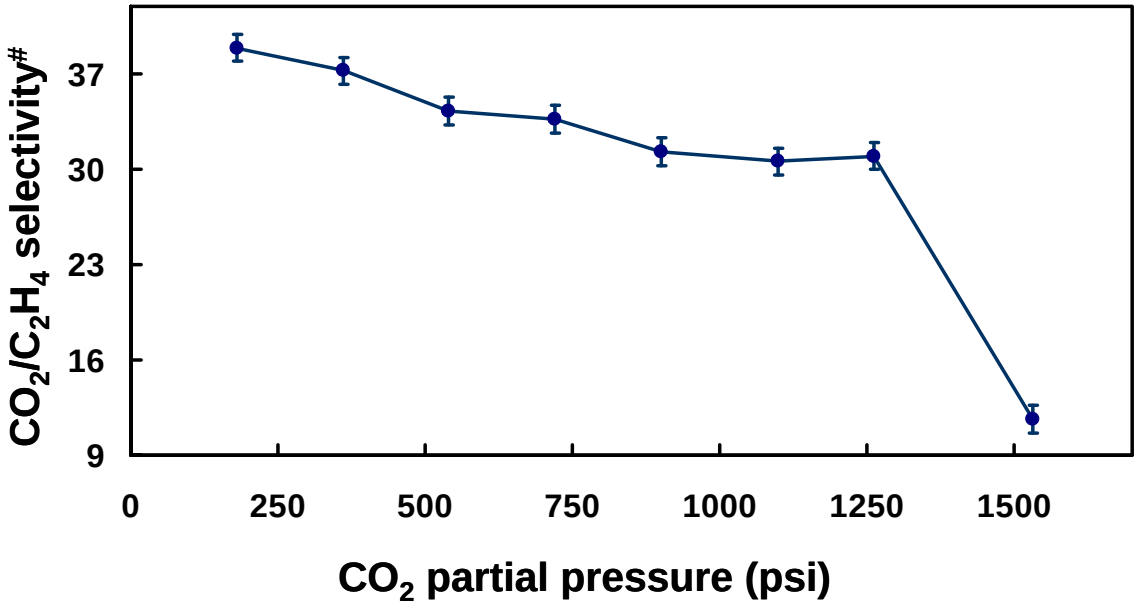

Figure 5.6: Fugacity corrected mixed gas CO_2/C_2H_4 selectivities of Torlon® membranes at various partial pressure of CO_2. These measurements are made with a feed gas composition of 90% CO_2 and 10% C_2H_4 at 35 °C.

In comparison with the un-corrected selectivities (Figure 5.5), the fugacity corrected selectivities show a smaller decrease from 39 (at 180 psi partial pressure of CO_2) to 31 (at 900 psi partial pressure of CO_2). This decrease is only about 20% compared to the 38% decrease in the case of un-corrected selectivities. This 20% decrease could be either due to the saturation of Langmuir sites or due to the swelling of the membrane.

For CO_2 partial pressures between 900 psi to 1260 psi, the fugacity based selectivities remained constant without any decrease in selectivity. However based on the pure CO_2 permeability measurements (Figure 5.2), the membrane is found to have slightly swelled under these conditions. This indicates that the membrane retains its size discrimination ability for CO_2 and C_2H_4 pair even when the membrane is in a slightly

swelled state. From this argument we speculate that the initial decrease in selectivity from 180 psi to 900 psi may not be due to the membrane swelling. The saturation of Langmuir sites is probably the main reason for that initial selectivity decrease. Langmuir sites favor CO_2 sorption compared to C_2H_4 and hence their presence increases the CO_2/C_2H_4 selectivity of a membrane. At low pressures, when these Langmuir sites are available, the CO_2/C_2H_4 selectivity of a membrane is increased. At high pressures, when these Langmuir sites are fully saturated and there are no new sites available, the CO_2/C_2H_4 selectivity is lowered. This phenomenon has been studied quite extensively by previous researchers and the reader is referred to them for more details.[3, 8-10]

Beyond 1250 psi, the selectivity of the membrane is drastically decreased from 31 (at 1260 psi) to 11.6 (at 1530 psi) which accounts to about 62% decrease. As previously stated, we speculate that the reason for this decrease is the combination of both plasticization and the substructure collapse (occurred due to the combination of both plasticization and high pressures). To estimate the effect of substructure collapse on the membrane selectivity, CO_2 permeances during this mixed gas permeation experiment are plotted in Figure 5.7. The CO_2 permeance has dropped from 0.97 GPUs (at 1250 psi partial pressure of CO_2) to 0.67 GPUs (at 1530 psi partial pressure of CO_2) which accounts to about 31% decrease. As an approximation, if we assume that the C_2H_4 permeance doesn't change at all during the substructure collapse and the CO_2 permeance is the only gas that is affected, then the upper-estimate of the selectivity loss because of the collapse will be 31%. So the substructure collapse could account for up to 50% of the total selectivity loss (which is 62%) during the pressurization from 1260 psi CO_2 partial pressures to 1530 psi. The remaining 50% loss is due to plasticization.

These effects of substructure collapse and plasticization can be independently verified by reducing the total pressure difference (Δp_{tot}) across the membrane while maintaining the upstream CO_2 partial pressures of 1530 psi. By reducing the total pressure difference to below 1400 psi, the substructure collapse can be prevented and the affects of plasticization can be independently determined. We haven't performed these experiments but we propose to do them in the future.

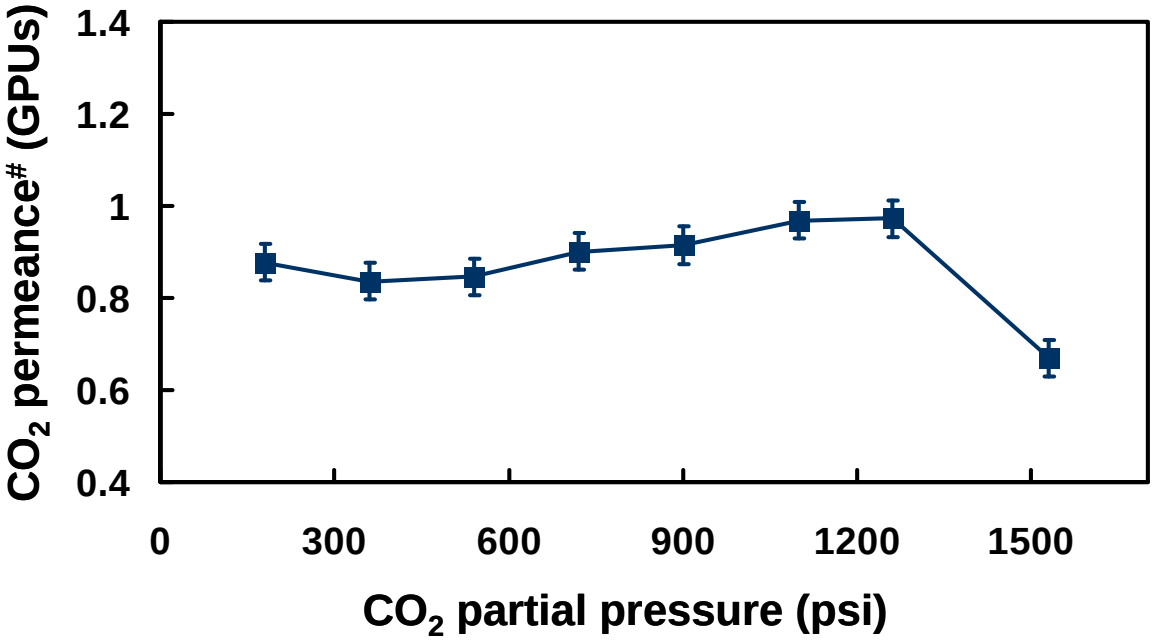

Figure 5.7: CO_2 permeances during the mixed gas (CO_2(90%) and C_2H_4(10%)) permeation.

5.4.2. Stability of Torlon® membranes at 1250psi partial pressure of CO_2

In the previous section, we have shown that the membrane provides selective separations up to 1260 psi partial pressures of CO_2 and the membrane fails beyond this

pressure. Long term stability of these membranes is an important factor that needs to be determined before commercializing them for industrial applications. This long term stability test is performed by monitoring the separation performance using a 90/10 mixture of CO_2/C_2H_4 at a total pressure of 1400 psi for a period of about 5½ days.

The CO_2/C_2H_4 selectivity and CO_2 permeances over this period is shown in Figures 5.8 and 5.9, respectively. The CO_2 permeances increased about 66% in 5½ days from 0.86 to 1.4 GPUs. Most of this increase (about 80% of the total increase) is observed in the first 2 days and then the permeances asymptotically approached saturation by 5½ days. This implies that the membranes reach an equilibrium swelling state over time. The increase in CO_2 permeance could be because of the increase in either CO_2 sorption or CO_2 diffusion. As the membrane is being swelled, more carbonyl groups of the polymeric chains are accessible for CO_2 sorption resulting in more CO_2 absorption into the membrane. And also as the membrane is being swelled, the inter-chain distance of the polymeric molecules increase, possibly resulting in large scale thermal fluctuations of the polymeric chains which enhances CO_2 diffusion. So with an increase in either CO_2 sorption or diffusion, the permeance could increase. If the second factor, which is increase in thermal fluctuations of the polymeric chains is significant then it would also increase the C_2H_4 permeances resulting in decreased membrane separation efficiency. On the other hand, if the CO_2 sorption is the main contributing factor in CO_2 permeance increase and the increase in thermal fluctuations of the polymeric chains are minimal then the separation ability of the membrane is either increased or at least preserved.

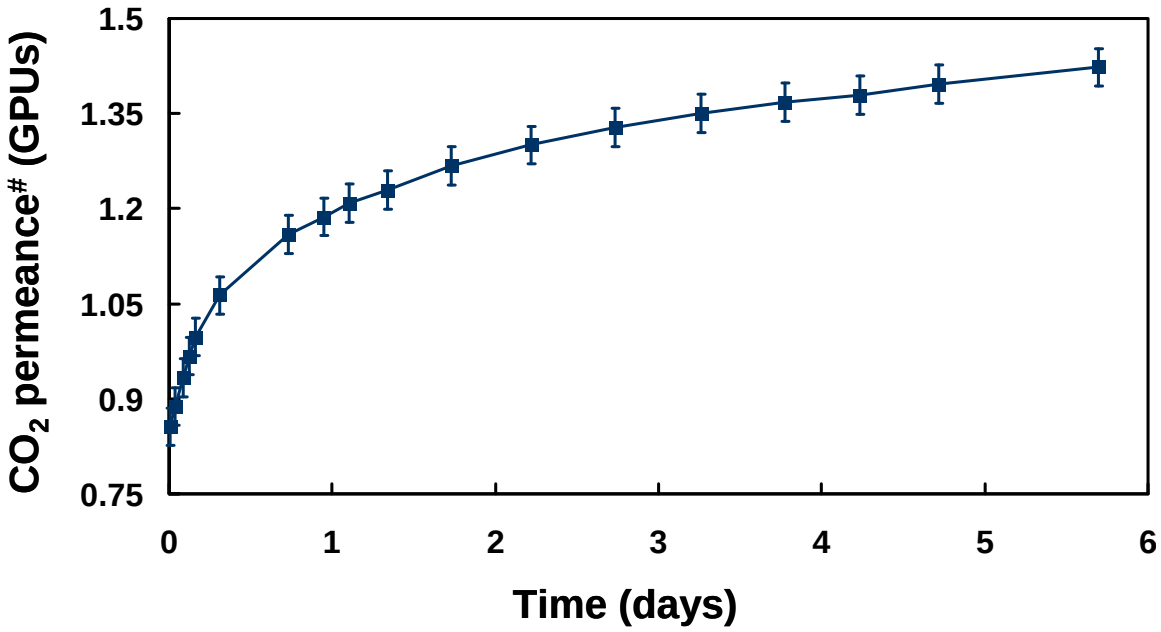

Figure 5.8: CO_2 permeances measured over time during a mixed gas CO_2/C_2H_4 permeation through Torlon® at 1250 psi partial pressures of CO_2.

During this swelling period, the selectivity of CO_2/C_2H_4 remained constant at 31 (Figure 5.9), indicating that large scale thermal fluctuations of the polymeric chains are minimal. This constant selectivity also indicates that the membrane provides stable CO_2/C_2F_4 separations. Moreover, these small thermal fluctuations would have a lesser effect on a bigger molecule compared to a smaller one. Hence, C_2F_4 (whose size is bigger than C_2H_4) is also not going to get affected due to swelling, so the membrane will also provide stable CO_2/C_2F_4 separations at 1260 psi partial pressures of CO_2.

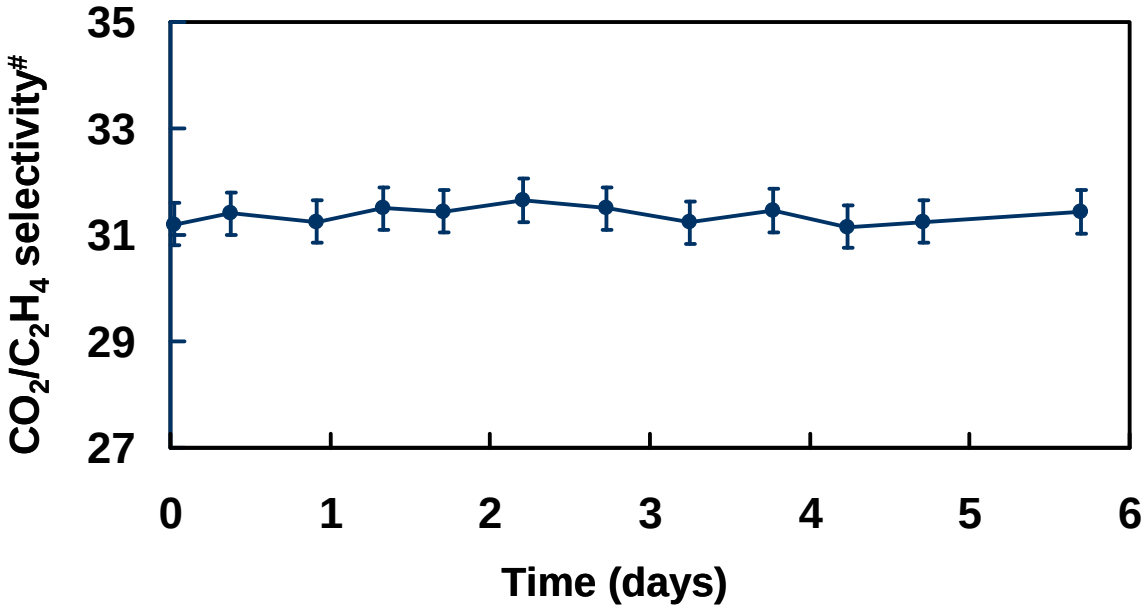

Figure 5.9: CO_2/C_2H_4 selectivity measured over time during a mixed gas CO_2/C_2H_4 permeation through Torlon® at 1250 psi partial pressures of CO_2.

5.4.3. Determining whether the swelling is reversible

Understanding whether the swelling is reversible or not is important to determine if the membranes exposed to these high partial pressures of CO_2 (1250 psi of CO_2) can still be used for separating low partial pressures of CO_2 feeds. So, a depressurization is performed from 1250 psi partial pressures of CO_2 to 180 psi using CO_2/C_2H_4 (90/10) mixed gas. Depressurization is carried out at a controlled rate that is slower than the CO_2 desorption from the fiber in order to prevent the fiber from being damaged due to rapid depressurization. Since the time lag of CO_2 in our Torlon® asymmetric membrane is less than 30 seconds, a depressurization rate of 1 psi per min is sufficient to prevent the fiber from being damaged.

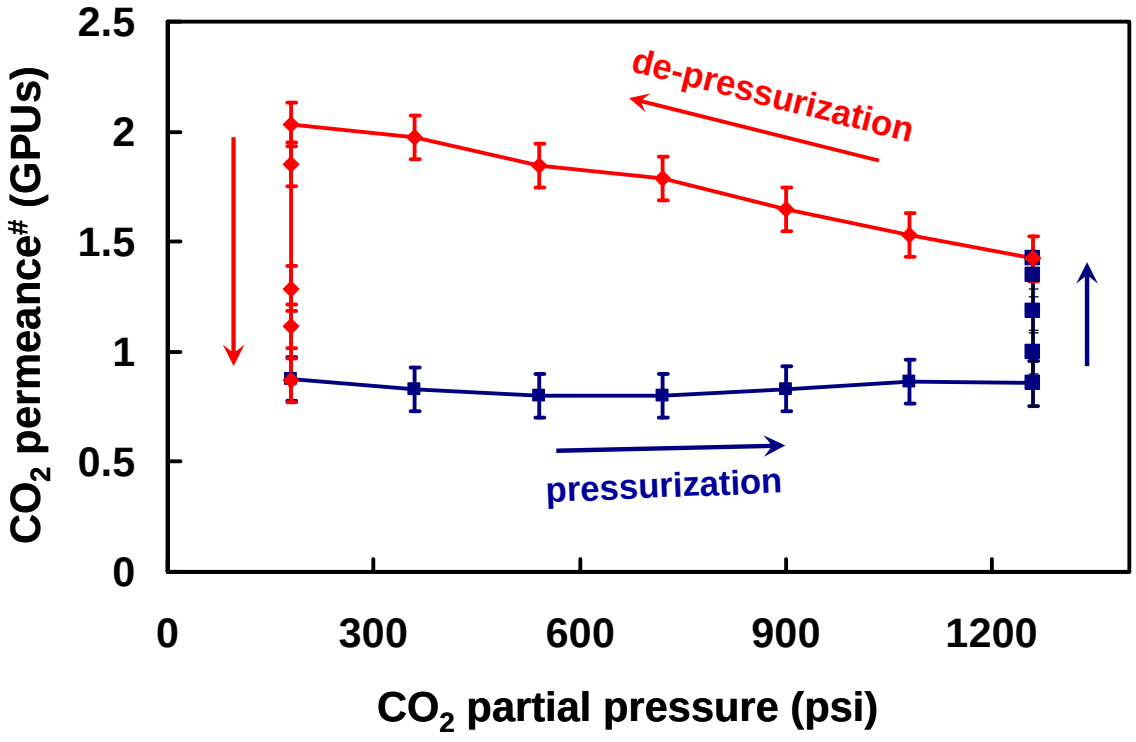

Figure 5.10: CO_2 permeances measured during pressurization and de-pressurization of mixed gas CO_2/C_2H_4 (90/10) through Torlon® membrane

The CO_2 permeances and CO_2/C_2H_4 selectivities during this depressurization step are plotted along with the values measured during the pressurization step in Figures 10 and 11 respectively. CO_2 permeances followed a hysteresis behavior similar to the ones observed during pure gas CO_2 depressurization (Figures 5.3 & 5.4). This hysteresis occurs because of the above mentioned membrane swelling phenomenon occurring at 1250 psi of CO_2. The CO_2 permeance at 180 psi soon after the depressurization step is 2 GPUs which is about 130% more than the original permeance of 0.88 GPUs (before pressurization) at 180psi. After de-pressurization step, the membrane is studied periodically for about two months. The CO_2 permeances during that period are also plotted in Figure 5.10. The CO_2 permeance has reached to its original

permeance value indicating that the swelling process is reversible. The CO_2/C_2H_4 selectivities (Figure 5.11) during pressurization and depressurization steps also showed a similar trend indicating that the swelling is reversible. Hysteresis is observed in CO_2/C_2H_4 selectivities during de-pressurization step and this hysteresis is due to the excess free volume that is created when CO_2 is desorbed from the membrane. This excess free volume increases the diffusion of both CO_2 and C_2H_4 gas species. In fact the percentage increase in C_2H_4 gas is more than CO_2 resulting in a decrease in selectivity. The CO_2/C_2H_4 selectivity at 180 psi soon after the depressurization step is 27 which is about 23% smaller than the original selectivity of 38 (before pressurization) measured at 180 psi. However, over a period of two months after de-pressurization, the membrane selectivity came back to its original value of 38 (shown in Figure 5.11), indicating that the membrane swelling is reversible. This behavior of reversible CO_2 induced swelling is also observed by Jordan et al. in polycarbonates.[11]

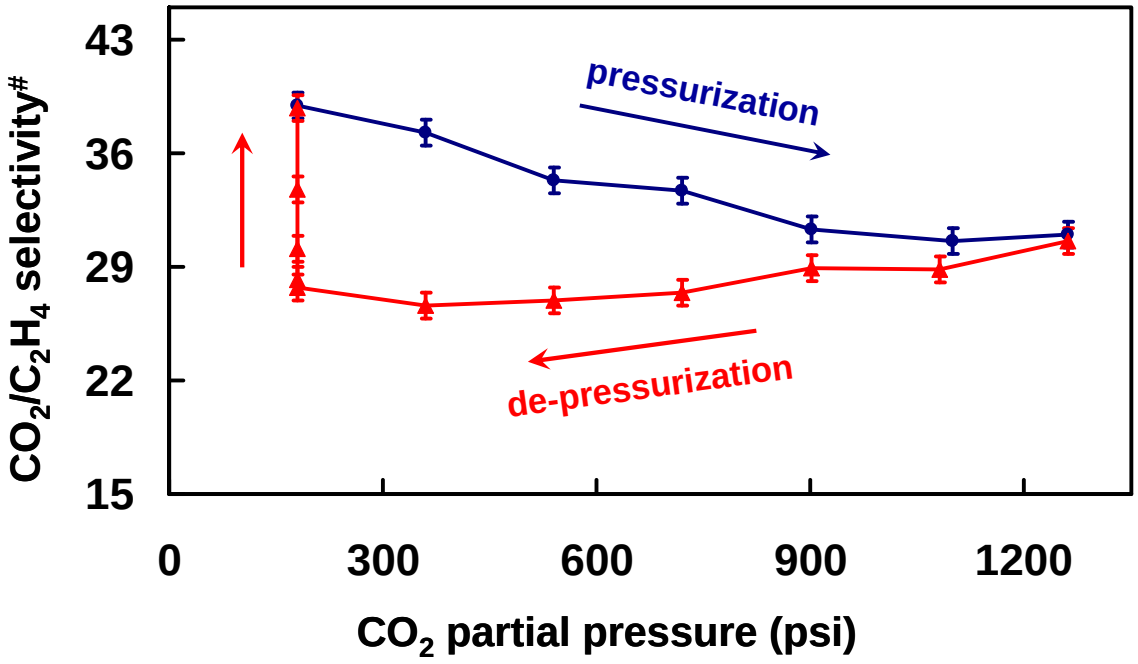

Figure 5.11: CO_2/C_2H_4 selectivities measured during pressurization and depressurization of mixed gas CO_2/C_2H_4 (90/10) through Torlon® membrane.

5.4.4. $CO_2/C_2H_2F_2$ separation at high partial pressures of CO_2

In the previous section we have shown that the Torlon® membranes provide CO_2/C_2H_4 separations with a selectivity of 31 even at 1250 psi partial pressures of CO_2. As mentioned in section 5.2.2., the sorption experiments showed that the $CO_2/C_2H_2F_2$ selectivity is about 3.9 times the selectivity of CO_2/C_2H_4 at 27 psi partial pressures of CO_2. Since the actual separations are performed under supercritical pressures, it becomes important to determine whether the selectivity of $CO_2/C_2H_2F_2$ is similarly greater than the selectivity of CO_2/C_2H_4 under the $scCO_2$ conditions. So, the mixed gas selectivities of $CO_2/C_2H_2F_2$ are measured using $CO_2/C_2H_2F_2$ (96/4) gas mixture at various increasing

pressures up to 1400 psi partial pressures of CO_2. The pressurization and depressurization selectivities are plotted in Figure 5.12.

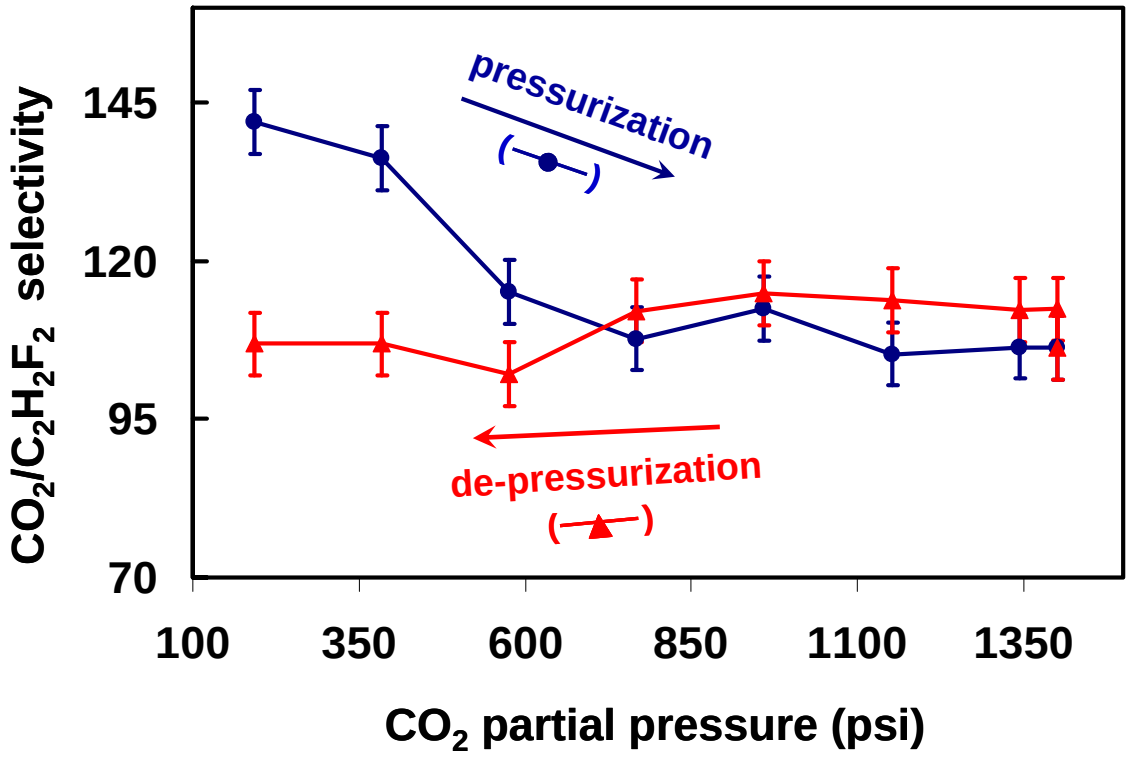

Figure 5.12: $CO_2/C_2H_2F_2$ selectivities measured during pressurization and depressurization of mixed gas $CO_2/C_2H_2F_2$ (96/4) through Torlon® membrane.

These selectivities are calculated by using partial pressures of CO_2 and $C_2H_2F_2$ instead of their fugacities. Since the interaction parameters between CO_2 and $C_2H_2F_2$ are not reported in the literature, we could not use any of the equations of states to correct for the gas phase non-idealities. But even without taking into the account of non-ideal gas phase effects, the membrane provides quite high $CO_2/C_2H_2F_2$ selectivities. The selectivities remained constant at high partial pressures of CO_2 from 800 psi to 1400 psi indicating

that the swelling doesn't affect the $CO_2/C_2H_2F_2$ separation. The selectivity of $CO_2/C_2H_2F_2$ under supercritical conditions (1260 psi partial pressures of CO_2) is 106 which is about 3.4 times the selectivity of CO_2/C_2H_4 measured under the same partial pressures of CO_2. By analogy, the selectivity of CO_2/C_2F_4 might similarly be about 3.4 times the selectivity of $CO_2/C_2H_2F_2$. This makes the predicted CO_2/C_2F_4 selectivity to be about 360 or at least equal to the $CO_2/C_2H_2F_2$ selectivity of 106. In any case, we have shown that Torlon® membranes will provide selective separations of CO_2/C_2F_4 even up to 1250 psi partial pressures of CO_2.

5.5. References

1. Reid, R.C., J.M. Prausnitz, and B.E. Poling, *The Properties of Gases and Liquids*. Fourth ed. 1987: McGraw-Hill, Inc., p: 656-732.

2. Lin, H. and B.D. Freeman, *Gas solubility, diffusivity and permeability in poly(ethylene oxide).* Journal of Membrane Science, 2004. 239(1): p. 105-117.

3. Sanders, E.S., et al., *Pure and mixed gas sorption of carbon dioxide and ethylene in poly(mehtyl methacrylate).* Journal of Membrane Science, 1984. 18: p. 53-74.

4. Bos, A., et al., *CO_2-induced plasticization phenomena in glassy polymers.* Journal of Membrane Science, 1999. 155: p. 67-78.

5. Clausi, D.T., S.A. McKelvey, and W.J. Koros, *Characterization of substructure resistance in asymmetric gas separation membranes.* Journal of Membrane Science, 1999. 160: p. 51-64.

6. Pinnau, I. and W.J. Koros, *Relationship between substructure resistance and gas separation properties of defect-free integrally skinned asymmetric membranes.* Industrial and Engineering Chemistry Research 1991. 30: p. 1837-1840.

7. Wessling, M., et al., *Plasticization of gas separation membranes.* Gas Separation & Purification, 1991. 5(4): p. 222-228.

8. Chern, R.T., et al., *Selective permeation of CO2 and CH4 through Kapton polyimide: Effects of penetrant competition and gas-phase non-ideality.* Journal of Polymer Science. Part B: Polymer Physics, 1984. 22: p. 1061-1084.

9. Chern, R.T., et al., *"Second component" effects in sorption and permeation of gases in glassy polymers.* Journal of Membrane Science, 1983. 15(2): p. 157-170.

10. William, J.K., D.R. Paul, and A.A. Rocha, *Carbon dioxide sorption and transport in polycarbonate.* Journal of Polymer Science. Part B: Polymer Physics, 1976. 14(4): p. 687.

11. William, J.K., S.M. Jordan, and G.K. Fleming, *Processes to condition gas permeable membranes*, U.S.Patent:19880705, Editor. 1988, Board of Regents, The University of Texas System, Austin, Tex.

CHAPTER 6

MIXED MATRIX MEMBRANES OF TORLON® AND ZEOLITE 4A

6.1. Abstract

In the previous chapter (Chapter 5), the plasticization pressure of Torlon® is measured to be around 1250 psi partial pressure of CO_2 at 35 ºC. This plasticization pressure can potentially be increased by incorporating rigid molecular sieves in the polymer matrix with strong bonding between the sieves and the polymer. Also by using highly selective sieves with permeability properly matched to that of the desired component in the matrix, the overall selectivity and the permeability of the membrane can be enhanced. Zeolite 4A was chosen as the molecular sieve of our choice and the reason behind this selection is explained in this chapter.

As noted above, to obtain enhancement in the plasticization resistance or selectivity, good bonding between the sieve and matrix is crucial, so this topic is covered in this chapter. Initial studies indicated that the interface between Torlon® and neat zeolite 4A was defective. To improve this interface, a novel surface modification technique was investigated and the interface between the so modified zeolite and Torlon® was studied using different characterization techniques. These studies indicate that the interface is still defective at the sub-nanometer scale. To determine the size of these interfacial defects, 3-phase Maxwell modeling of the gas transport though mixed matrix membranes was performed. The model suggests that not only are the sieves blocked, but also 4-5 Å size defects at the polymer-sieve interface. A path forward to address these issues (pore blockage and interfacial defects) is suggested.

6.2. Choice of zeolite 4A

Zeolite 4A was chosen as the sieve material for the separation of CO_2 and C_2F_4 gas mixtures because its 3.8 Å pore openings should allow CO_2 molecules (whose size is 3.3 Å) to diffuse while blocking C_2F_4 molecules (whose size is greater than 3.8 Å). Since the size of the C_2F_4 molecules is greater than the pore openings, the selectivity of the 4A sieves for the CO_2/C_2F_4 gas mixture should approach infinity. By incorporating such a highly selective zeolite 4A in Torlon®, the overall selectivity of the membrane should be enhanced significantly.

The permeability of CO_2 through zeolite 4A is estimated to be on the order of 15 barrers[1] which is more than an order of magnitude greater than the permeability of Torlon (which is 0.47 barrers). By incorporating zeolite 4A in Torlon, the CO_2 permeability of the overall membrane should also be enhanced.

6.3. Zeolite-4A and Torlon® mixed matrix membranes

Initially we speculated that the hydrogen bonding between the amide groups of Torlon® and the hydroxyl groups of zeolite 4A might promote a good sieve-polymer interface. To verify our speculation, a mixed matrix membrane was made from the untreated zeolite 4A and Torlon®. The membrane was investigated for its interfacial characteristics and the results are explained in the following sections. Since this study seeks to investigate the interfacial properties, only a 20wt% zeolite loading in the polymer was used for making mixed matrix membranes, thereby minimizing agglomeration issues that may arise at higher zeolite loading dopes.

6.3.1. Procedure for making good mixed matrix membranes

In our first attempt, mixed matrix membranes were formed according to the procedure described in Chapter 3. In this procedure, the membranes were casted on a hot plate at 110 °C in a hood. At this temperature, the solvent (NMP) slowly evaporates forming a membrane. The SEM cross-section of the membrane is show in Figure 6.1.

Agglomeration of the zeolite particles can be observed in this figure, which is detrimental for mixed matrix membranes as they create inter-particle gaps. These gaps offer low resistance to gas transport and are not selective, so improved separation performance of the sieves is not achieved. Particle agglomeration also reduces the strength of a membrane, and the resulting membrane may not withstand the high pressures encountered in supercritical carbon dioxide separations. Clearly, to address these problems, the agglomeration issue needs to be addressed.

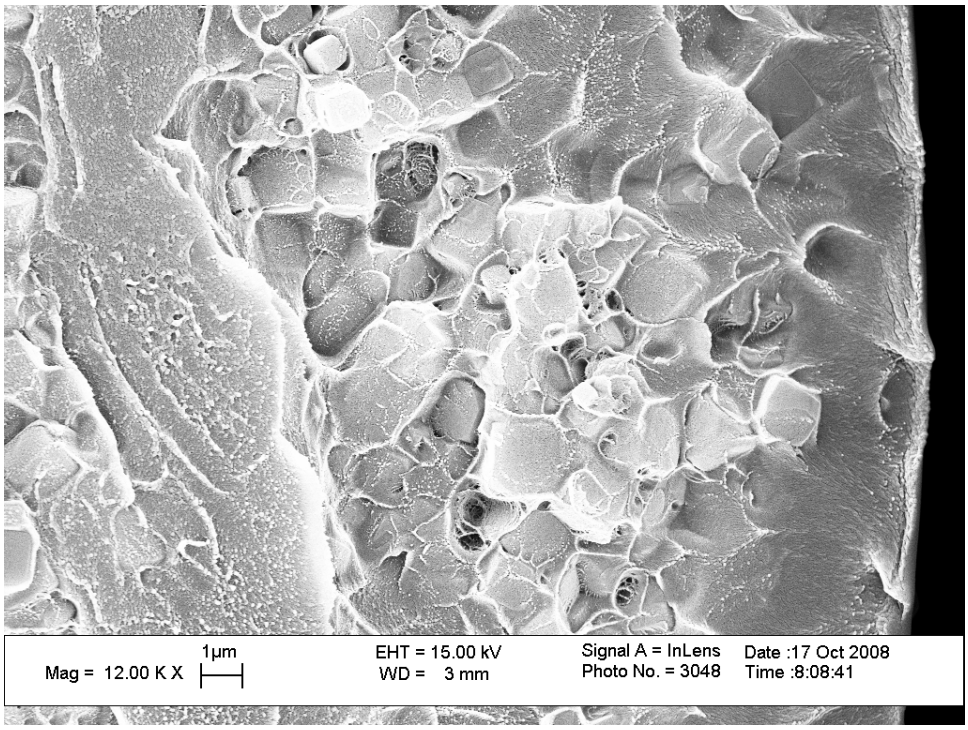

Figure 6.1: SEM cross-section of a mixed matrix membrane of Torlon® and unmodified zeolite 4A casted on a hot plate.

We speculated that the agglomerates were mostly occurring during the membrane casting step. When a membrane is cast on a hot plate, the liquid below the top surface is hotter than the top surface (top surface refers to the film-air interface). Hotter liquid (because it is less dense) tends to rise, while cooler fluid (because it is more dense) circulates downward resulting in a circulating convective flow. The convective flow drags the zeolite particles along with it and when the zeolite particles come in contact with each other, particle agglomerates are formed. Therefore, the hot plate casting procedure tends to result in a convective flow which in turn causes particle agglomeration.[2]

To prevent these agglomerates, the membrane can be heated from the top surface instead of heating from the bottom surface. This process results in hotter surface at the

top compared to the bulk. The hot fluid being less dense continues to be at the top and the cold fluid being more dense continuous to be at the bottom suppressing the convective flow and agglomeration.

Heating from the top surface is done by casting the membrane on a glass plate (which is at room temperature) and then transferring it to a preheated oven. Inside the oven, the glass plate is kept on a wooden block. This wooden block (which is initially under room temperature conditions) is introduced into the oven along with the glass plate. The purpose of the wooden block is to act like a heat insulator to the bottom surface of the glass plate. This way the casted membrane is mainly being heated from the top surface and not from the bottom surface. During this heating procedure, the evaporated solvent is removed from the oven using a continuous nitrogen purge.

The SEM cross-section of the membrane so casted is shown in Figure 6.2. No particle agglomerations are observed. The particles are fairly well dispersed indicating that our hypothesis is in-fact true and the membrane casting procedure is important in obtaining an agglomeration free mixed matrix membrane. From hereon, this procedure of heating the membrane from the top surface is used in making mixed matrix membranes.

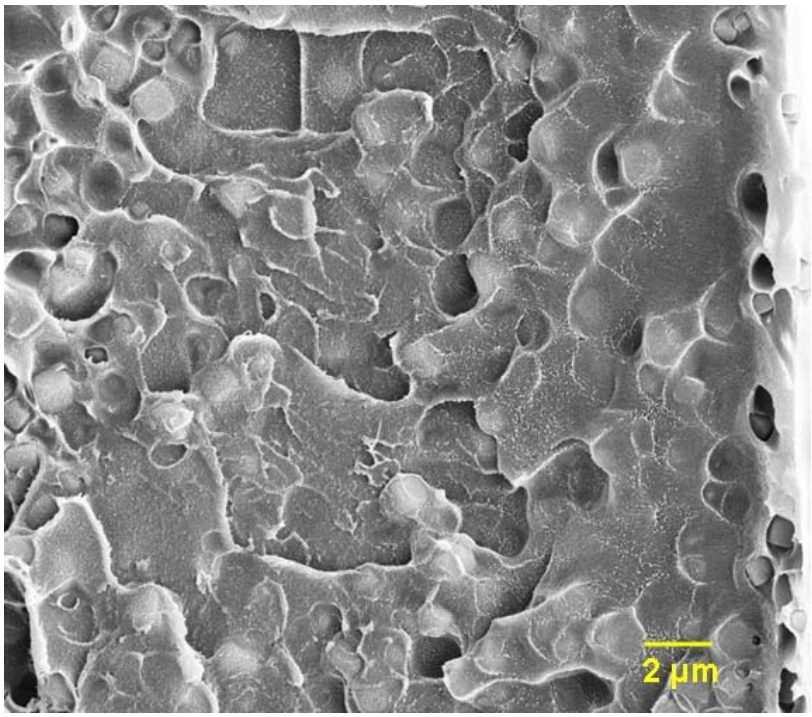

Figure 6.2: SEM cross-section of a mixed matrix membrane of Torlon® and unmodified zeolite 4A casted by heating the membrane from the top surface.

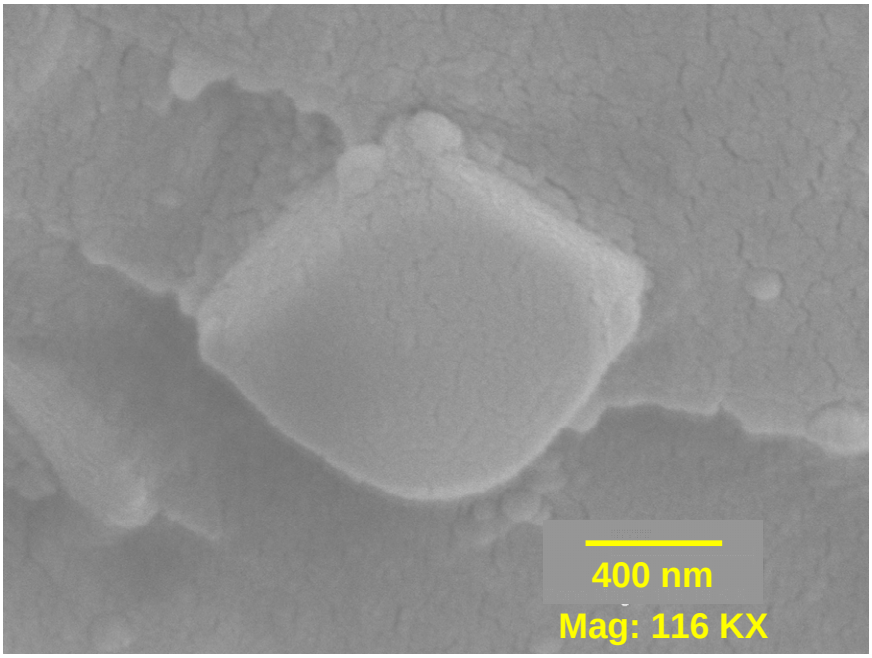

Figure 6.3: A higher magnification SEM image showing the interface between the polymer and zeolite.

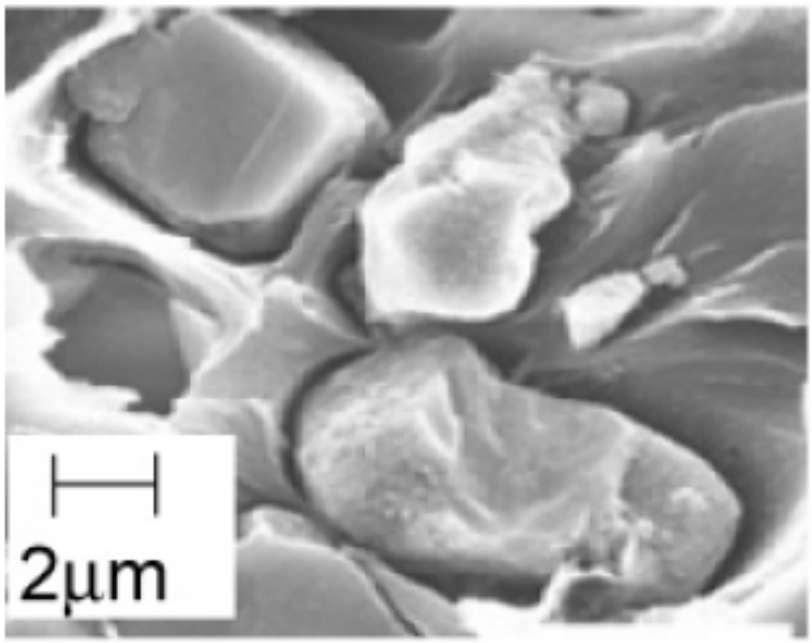

Figure 6.4: SEM cross-section of Ultem® (a polyimide that does not have any hydrogen bonding capability) and zeolite 4A mixed matrix membrane. Defective interface can be clearly seen. The picture adopted from Shu et al article.[3]

6.3.2. Characterizing the polymer-sieve interface

A high magnification SEM image (Figure 6.3) shows that the polymer appears to adhere well to the zeolite surface. For comparison, SEM image of a mixed matrix membrane from Ultem® (a polyimide with a Tg of 230 ºC and which does not have any hydrogen bonding capability) and unmodified zeolite 4A, adopted from Shu et al. work[3], is shown in Figure 6.4. Apparent sieve in cage morphology is observed indicating that Torlon®, a polymer with relatively higher Tg, forms a better interface. This validates our speculation that hydrogen bonding between Torlon® and zeolite 4A helps in improving the interface. However, SEM images do not provide information about the quality of an interface on a molecular scale. If the hydrogen bonding is not uniform across the sieve surface, then gas molecules could bypass the sieve resulting in a

failure of the mixed matrix membrane. So a uniform good interface is necessary to observe the mixed matrix affect. To probe whether such a good interface exists in our membranes, gas transport measurements are performed. If the polymer-zeolite interface is good then the superior gas transport properties of the zeolites will be captured and in that situation, the overall desired gas permeabilities and selectivities of the mixed matrix membranes will be enhanced. So the quality of the interface can be probed by comparing the measured permeabilities and selectivities of the mixed matrix membranes with those of the predicted values.

As long as the gases do not plasticize the membrane or adversely affect the interface, any gas pair can be used for probing the interface. In our measurements, non-interacting gases, oxygen and nitrogen, are used as the probing molecules. The O_2 and N_2 permeabilities and selectivities of Torlon® and zeolite 4A are given in Table 6.1. The measured selectivity and permeabilities of the mixed matrix membranes along with the predicted values are also provided in this table. To predict the mixed matrix properties, the Maxwell model (as described in Chapter 3) is used. Zeolite loading of 20wt% is used in the Maxwell model predictions. The zeolite framework density of 1.55 g/cm^3 and the polymer density of 1.33 g/cm^3 are used in determining the volume fraction of zeolites in the polymer.

Table 6.1: Measured O_2 and N_2 permeabilities and selections through pure Torlon® membrane, zeolite 4A[4] and mixed matrix membranes (MMM). The predicted values through the mixed matrix membrane are also given. Permeabilities are given in Barrers.

Permeability /Selectivity	Pure Torlon® membrane	Zeolite 4A[4]	Measured MMM properties	Predicted MMM properties
P_{O_2} (Barrers)	0.12 ± 6E-3	0.77	0.16±2E-3	0.166
P_{N_2} (Barrers)	0.014 ± 7E-4	0.021	0.03±2E-3	0.016
α_{O_2/N_2}	8.3 ± 0.4	37	5.7±0.4	10.7

The measured O_2/N_2 selectivity (5.7) of the mixed matrix membranes is quite low compared to the predicted value of 10.7. This indicates that the interface is bad and the gas molecules are bypassing the sieve and therefore the selectivity enhancement is not observed. Not only the measured selectivity value is lower than the predicted value, it is even lower than the selectivity of pure Torlon®. Lower selectivity, below the intrinsic polymer selectivity, is observed when a small leaky interface (in the order of angstroms) is present between the polymer and the zeolite surface.[4] Through this interface, the gas molecules diffuse with a selectivity roughly equal to Knudsen selectivity. As the Knudsen selectivity is lower than the pure Torlon® selectivity, the overall selectivity of the membrane is lowered. (see section 6.5)

In order to improve the polymer-zeolite interface, the surface of the zeolite 4A is modified using a new modification technique. This technique is explained in the following section.

6.4. Phosphonic acid treated Zeolite-4A and Torlon® mixed matrix membranes

We wanted to modify the surface of the zeolites so that it can have better interactions with Torlon®. Earlier researchers have used silane coupling agents to modify the zeolite surfaces.[5, 6] However, since silane coupling agents are expensive, we wanted to pursue an alternative approach. Marder et al. have shown that metal oxide surfaces (such as barium titanate) can be modified using phosphonic acid (PA) ligands.[7] Since PA ligands are less expensive, we wanted to see whether this technique can be used to modify zeolite 4A surface.

6.4.1. Modifying the zeolite surface with penta-fluoro benzyl phosphonic acid ligand

We wanted to use a PA ligand that has good interactions with Torlon®. In this regard, we have chosen penta-fluoro benzyl phosphonic acid ligand (PFBPA) and its structure is shown in Figure 6.5. The reason for selecting this ligand is that the fluorine atoms attract the electrons from the benzene group of PFBPA, making the benzene group electron deficient. This electron deficient benzene group will now have greater affinity towards the electron rich benzyl groups of Torlon®. The strength of such interactions is reported by Ashley et al. [8]

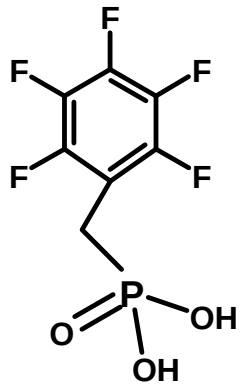

Figure 6.5: The chemical structure of penta-fluoro benzyl phosphonic acid.

The zeolites are treated with PFBPA ligands. This work is done in collaboration with Prof. Marder and exact details of the treatment procedure are reported in Dr. Hotchkiss's PhD thesis[9]. (Dr. Hotchkiss was a PhD student with Prof. Marder). In this treatment, the zeolites are treated with PFBPA ligands at 80 ºC for one hour in a solvent mixture of ethanol/water (volume ratio of 95/5). X-ray photoelectron spectroscopy (XPS) on these treated zeolites indicates the presence of fluorines on the surface. The XPS spectrum is shown in Figure 6.6. The presence of fluorines suggests that the treatment yielded a PFBPA terminated surface. Solid state NMR (^{31}P MAS NMR) studies on the PFBPA modified zeolites indicated the presence of phosphorous, which further supports the successful modification of the zeolite surface. It is believed that a monolayer coverage of all –OH's was achieved based on TGA studies with octadecyl phosphonic acid ligands (ODPA) on the zeolite surface.[9] Previous studies on metal oxide surfaces show that the nature of the groups attached (flourinate vs. hydrocarbon) do not significantly affect the phosphonic acid reactivity with hydroxyl groups.[7]

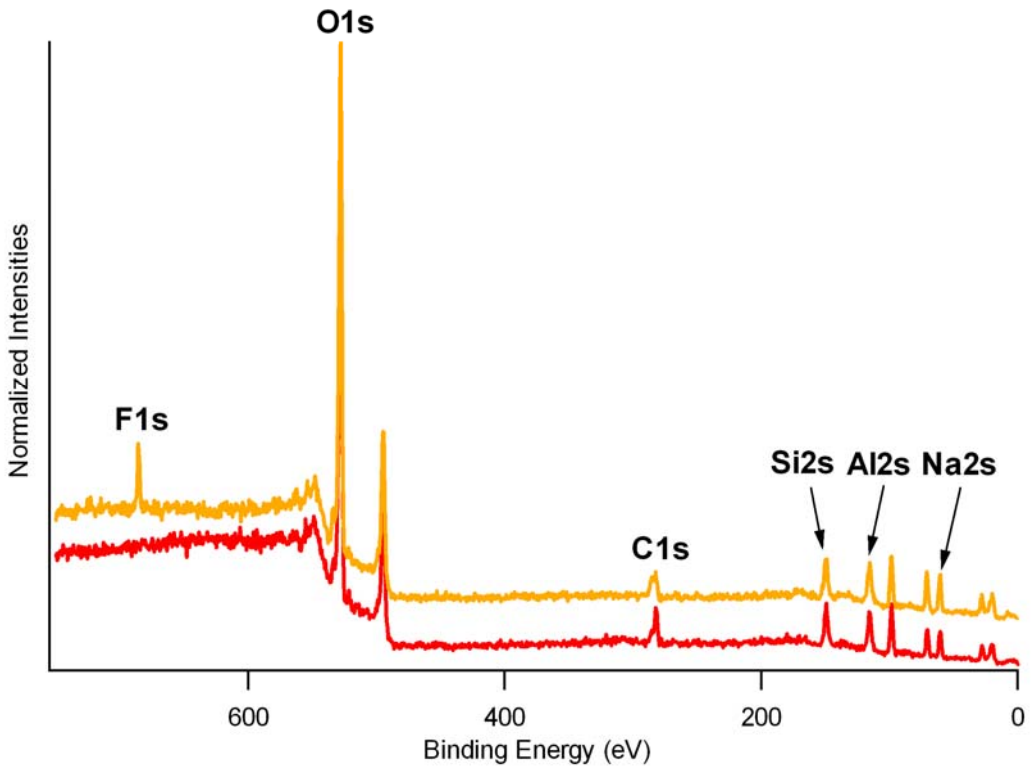

Figure 6.6: XPS spectra of unmodified zeolites (red) and the PFBPA modified zeolites (orange). Both the spectra are normalized using O(1s) peak and are offset for clarity. This figure is adapter from Dr. Hotchkiss's PhD thesis.[9]

To determine whether the inner microstructure of the zeolites is preserved during the surface treatment procedure, BET and sorption studies are performed. The BET analysis showed that the total surface area (both internal and external) of the zeolites is preserved even after the surface treatment procedure. The total surface area of the PFBPA treated zeolite 4A is 492.6± 8.3 m^2/g which is similar to that the unmodified 4A (481.4 ± 8.2 m^2/g). The CO_2 sorption capacity of the PFBPA treated zeolite is also same as that of the unmodified zeolite. These observations indicate that the inner microstructure of the zeolite is maintained and the pores are also not blocked during the

treatment procedure. After surface treatment, however, the sieves were exposed to NMP with ultrsonication. As discussed later, this NMP/sonication treatment may have occluded surface pores in the treated zeolite.

Following the modification of the zeolite surface using PFBPA ligands, the PFBPA modified zeolites were treated to probe the interface with Torlon®. The following section details the mixed matrix work.

6.4.2. Mixed matrix membranes with PFBPA modified zeolite

Mixed matrix membranes are made from PFBPA treated zeolites by heating the casted membrane from the top surface as explained earlier in this chapter. The SEM cross-sections of the membrane are shown in Figures 6.7a and 6.7b. The overall morphology of the membrane (Figure 6.7a) indicates that the particles are fairly well dispersed. A relatively larger magnification image (Figure 6.7b) indicates that the polymer is well adhered to the zeolite and there is no apparent gap between the zeolite and the polymer matrix.

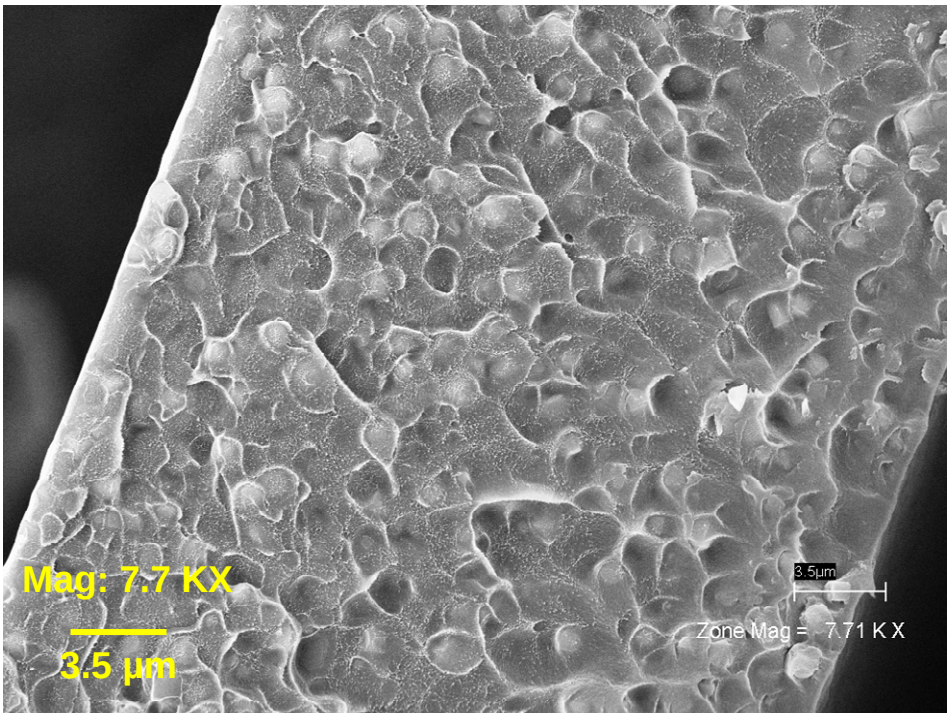

Figure 6.7a: SEM of the mixed matrix membrane with PFBPA modified zeolites. Good dispersion of zeolites in the polymer matrix is observed.

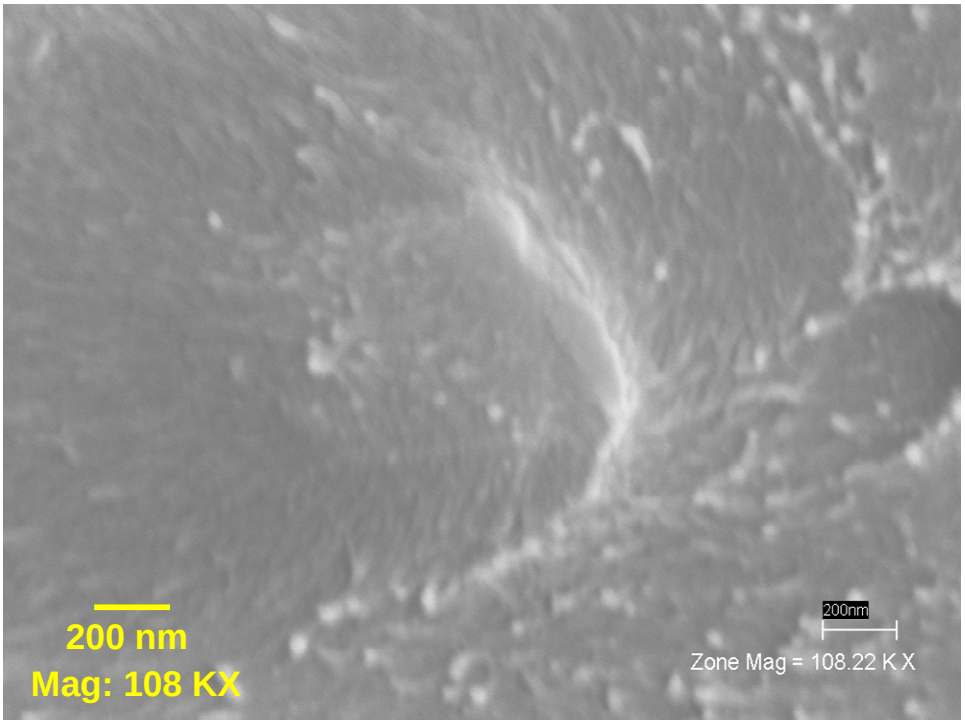

Figure 6.7b: High magnification SEM image of the zeolite and polymer interface. Good adhesion between the PFBPA treated zeolites and the polymer is apparently observed.

Gas permeation measurements are made to probe the interface on a molecular scale. O_2 and N_2 permeabilities through the mixed matrix membranes (20wt% zeolite loading) are reported in Table 2. The values predicted using Maxwell model are also given in that table and once again, the selectivity is found not only to be lower than the predicted value but also lower than the selectivity of Torlon® membrane. This result again indicates that subnanometer gaps still exist between the polymer and the zeolite.

Table 6.2: Measured and predicted O_2 and N_2 permeabilities and selections of the mixed matrix membranes with PFBPA modified zeolites. Permeabilities are given in barrers.

Permeability /Selectivity	Measured MMM properties	Predicted MMM properties
P_{O_2}	0.11 ± 6E-3	0.166
P_{N_2}	0.02 ± 2E-3	0.016
α_{O_2/N_2}	5.5 ± 0.4	10.7

6.5. Modeling the mixed matrix membrane

For a more in-depth understanding about factors responsible for lowering of selectivity, the membranes were modeled using a 3-phase Maxwell model[4]. This model takes into consideration the interface properties along with the zeolite and polymer properties. Mahajan et al. have successfully shown the applicability of this model to the mixed matrix membranes with leaky interfaces[4], and this 3-phase Maxwell model was used to probe the characteristics of the leaky interface of our mixed matrix membrane system.

The schematic of a membrane with such subnanometer gaps is given in Figure 6.8. The three-phase model considers the membrane to be made of three different phases: polymer, zeolite and interface.

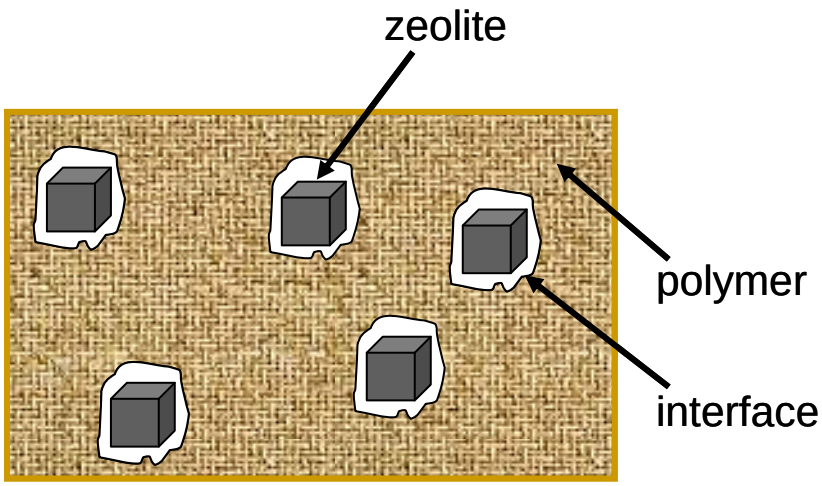

Figure 6.8: Schematic of a mixed matrix membrane with a leaky interface.

6.5.1. Details of the 3-phase Maxwell model

The overall properties of these 3 phases are determined by initially applying a 2-phase Maxwell model (given in chapter 2, equation 2.11) on the zeolite and the interface phases. In this model, the interface phase is considered as a continuous phase and the zeolite phase as the dispersed phase. From this 2-phase model, the effective properties of the zeolite and the interface phases are determined.

Another 2-phase Maxwell model is then applied considering the polymer phase as the continuous phase and the combined "zeolite and interface" phase as the dispersed phase. This second 2-phase Maxwell model predicts the overall properties of the three phases.

For applying the Maxwell model, the volume fractions of the zeolite, the interface, and the polymer are required. Densities of zeolite 4A (1.55 g/cm^3) and Torlon® (1.33 g/cm^3) are used in determining the zeolite and polymer volume fractions from the experimentally measured weight fractions. The size of the sieve used in our experiments was 1.5 μm and in this model the sieve particle is approximated to be a sphere of diameter 1.5 μm. By assuming a size for the void, the volume fraction of the void can also be estimated.

The permeabilities and selectivities of the polymer and the zeolite are known and are given in Table 6.1. In order to use the 3-phase model, the selectivity and permeabilities of the void needs to be determined. The transport mechanism through the void is assumed to be Knudsen. As the void in our case is in the order of angstroms (i.e. it is in the order of gas molecules), a slightly modified Knudsen diffusion equation (Equation 6.1) is used.[10]

$$D_{A.K} = 9.7 \times 10^{-5} \cdot r \cdot \sqrt{\frac{T}{M_A}} \cdot \left[1 - \frac{d_g}{2 \cdot r}\right]. \tag{6.1}$$

Where $D_{A.K}$ is the diffusion coefficient in cm^2/sec; r is the pore radius in Å; T is the temperature in Kelvin; M_A is the molecular weight in grams, and d_g is the diameter of the gas molecule in Å. For oxygen, the kinetic diameter of 3.46 Å is used.[11] The partition coefficient (K) of gas on to the void is given by[10] Equation 6.2. It has a strong dependence on pore dimensions. For example, the partition coefficient for oxygen in a 4 Å pore opening is 0.018 compared to 0.7 for 20 Å opening.

$$K = \left(1 - \frac{d_g}{2 \cdot r}\right)^2. \tag{6.2}$$

The concentration of gas inside the pore, when the external gas pressure is p atmospheres, is given by Equation 6.3.

$$C = K \cdot \left({}^{p}\!\!\diagup\!\!{}_{R \cdot T} \right) \cdot 22400 . \tag{6.3}$$

Where C is the concentration of gas in $cm^3 (STP) / cm^3$, R is universal gas constant in $atm \cdot cm^3 / mol \cdot K$. The sorption coefficient of the gas (S) is then given by

$$S = \frac{C}{p}. \tag{6.5}$$

Based on these sorption and diffusion coefficients, the permeability of the void can be estimated.

The modified Knudsen diffusion and sorption equations are applicable when the pores are rigid. When the pores are not rigid, these equations may not provide accurate predictions, and this is particularly true in predicting selectivities. For example, when the pore dimension is 4 Å, the modified Knudsen equations predict O_2/N_2 selectivity of 9.0 which is greater than the selectivity of neat polymer (intrinsic selectivity of Torlon® is 8.3). Such selective pores are possible only when the pores are rigid. In our case, as the pores are not rigid (as part of the pore is made of polymer which is flexible), the O_2/N_2 selectivity is not estimated using the modified Knudsen equations. Instead, we consider the pores are non-selective and assume O_2/N_2 selectivity of 1.

On the other hand, the permeabilities predicted using the modified Knudsen equations are only slightly affected when the criteria of rigid pores is relaxed. For example, the predicted O_2 permeability through a rigid 4 Å pore is 51 barrers. In case of a non-rigid pore, this predicted permeability could increase because of the fluctuations of polymer chains. However, since Torlon® is relatively rigid, the increase in O_2

permeability due to chain fluctuations is negligible. (Recall that the O_2 permeability of Torlon, a good indicator of chain fluctuations effect, is only 0.11 barrers). So the modified Knudsen equations are used in predicting O_2 permeabilities and the O_2/N_2 selectivity is assumed to be 1 for approximate calculations here.

6.5.2. Predicting the membrane properties using a 3-phase Maxwell model

The size of the characteristic void was varied from 3.46 Å to 15 Å and the overall oxygen permeability and O_2/N_2 selectivity of the membrane are determined using the above mentioned 3-phase Maxwell model. The O_2 permeability and O_2/N_2 selectivity are plotted in Figure 6.9 and Figure 6.10, respectively. The void size of 3.46 Å is used as a starting point because the Knudsen diffusion equation (Equation 6.1) is only applicable when the void size is greater than the size of the diffusing gas species.

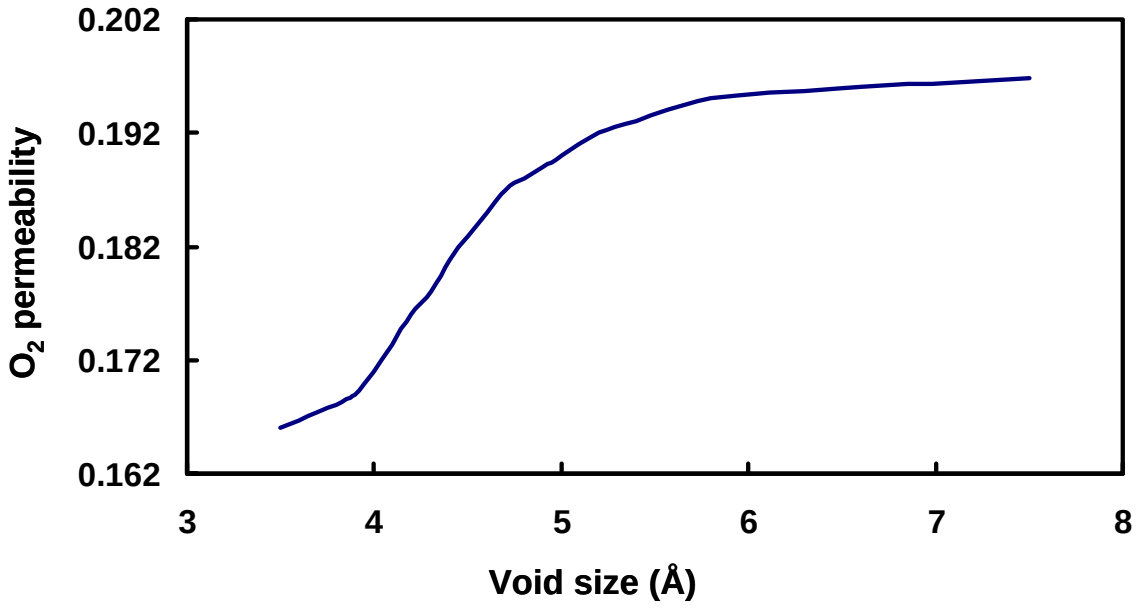

Figure 6.9: Three-phase Maxwell model prediction of oxygen permeability as a function of void size.

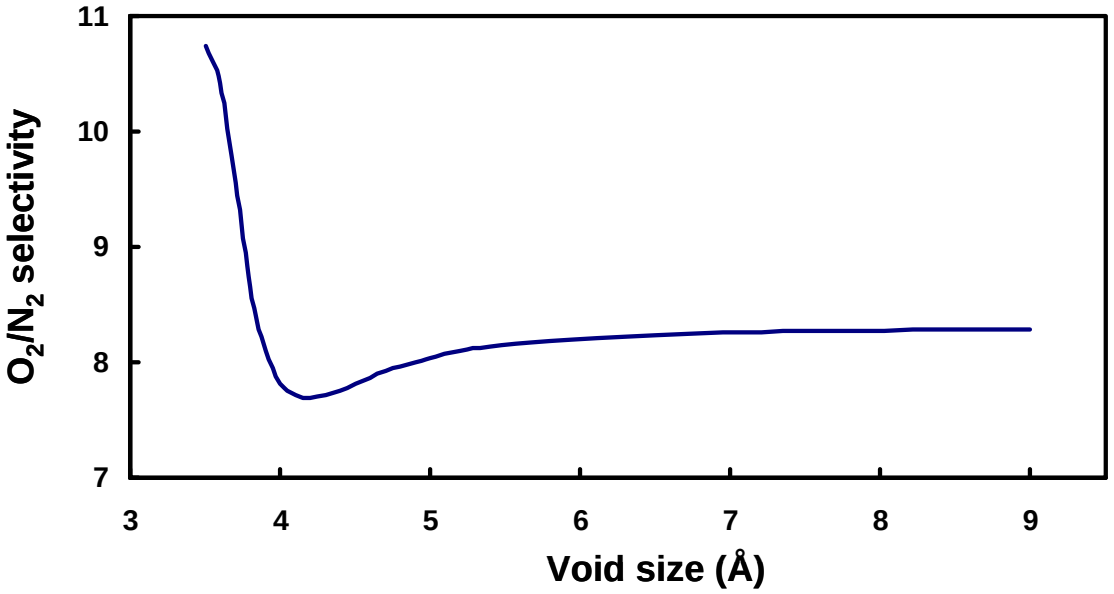

Figure 6.10: Three-phase Maxwell model prediction of O_2/N_2 selectivity as a function of void size.

As reported by Mahajan et al.[4], the O_2/N_2 selectivity of the mixed matrix membranes decreased below the intrinsic value of the polymer. The maximum decrease occurred when the void size is about 4Å. The selectivity at this maximum decrease is 7.7. However, the observed selectivity (5.5) for the mixed matrix membranes is much lower than the predicted value. So the model suggests that the presence of voids alone does not explain the observed selectivity decrease. Along with the voids, another significant factor may be affecting the membrane's performance.

The measured O_2 permeability of the mixed matrix membrane (particularly the one with PA treated zeolites) is *lower* compared to the predicted O_2 permeabilities. (Compare the O_2 permeability reported in Table 6.2 and the predicted values shown in Figure 6.9). This low observed permeability suggests that the zeolites may be blocked, so the mixed matrix membranes were modeled by considering that the zeolites are

blocked. Again a 3-phase Maxwell model is used in determining the O_2 permeabilities and O_2/N_2 selectivities with varied void sizes. Figures 6.11 and 6.12 show the plots.

The model now predicts a selectivity of 5.7 which matches our observed selectivity values. This low selectivity occurred when the void size is 3.85 Å for plugged sieves. The good agreement between the measured and predicted values indicates that the zeolites are effectively blocked and small voids (in the order of angstroms) are present between the polymer and the zeolite interfaces. The measured O_2 permeability (for the case MMM with PA treated zeolites) also matched well with the predicted value. (Compare the O_2 permeability value reported in Table 6.2 and the predicted value shown in Figure 6.11 for the void size of 3.85 Å). This further validates the model predictions.

In the case of untreated zeolite mixed matrix membranes, the O_2 permeability is high compared to the model predictions. (See table 6.1 and Figure 6.11). This could be because of the presence of some occasional bonding defects which increased the overall permeability of the membrane. Such occasional bonding defects can be seen in Figure 6.2 and are mainly observed in mixed matrix membranes with unmodified 4A and are rarely observed in phosphonic treated 4A. However, the overall selectivity of the membrane is low because of the presence of the subnanometer voids and blocked sieves.

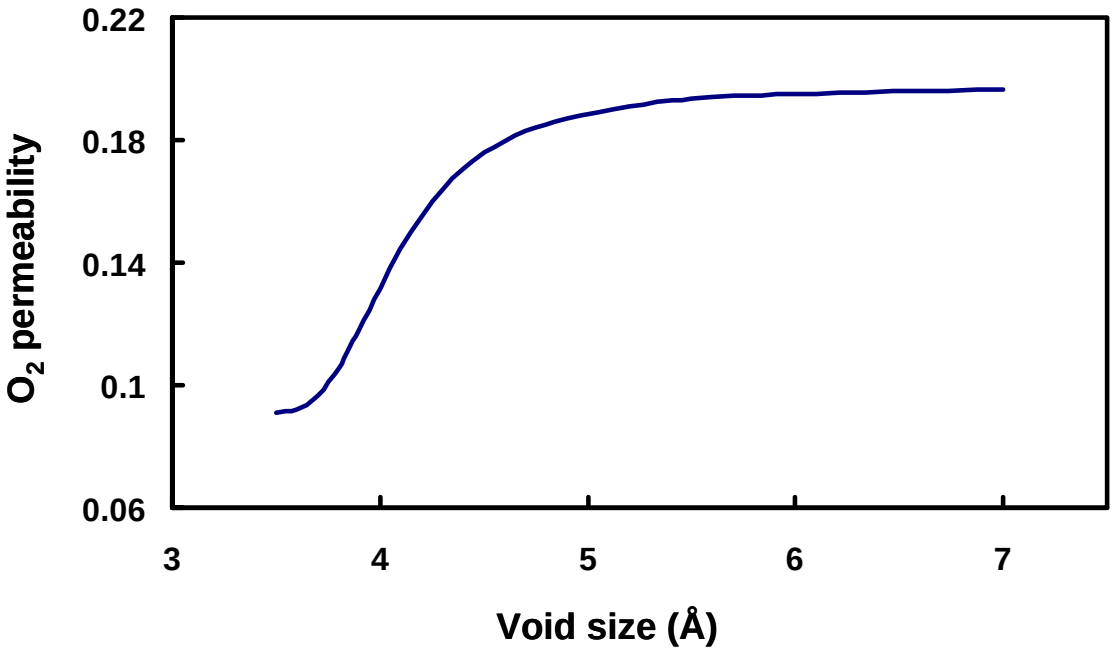

Figure 6.11: Three-phase Maxwell model prediction of oxygen permeability as a function of void size with the zeolites assumed to be blocked.

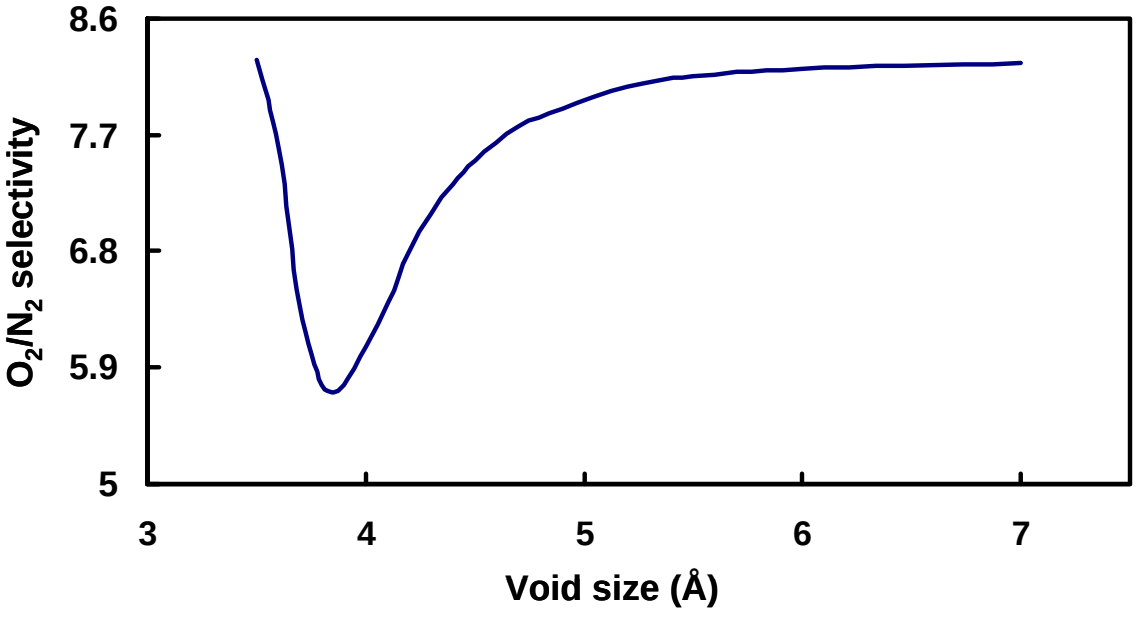

Figure 6.12: Three-phase Maxwell model prediction of oxygen permeability as a function of void size. The zeolites are assumed to be blocked.

6.6. Suggestions on zeolite blocking and interface issues

6.6.1. Investigating zeolite blocking

To determine whether or not the sieves are blocked by water, water sorption experiments were performed on the mixed matrix membranes. A membrane was heated to 220 ºC in a vacuum oven over night to remove any absorbed water from the membrane. After the high temperature water desorption, the membrane was cooled down to room temperature. The membrane was then removed from the oven and allowed to equilibrate with the moisture in air at ambient conditions. The weight of the membrane was monitored during this process to determine the moisture uptake kinetics. From this information, the moisture uptake of the zeolites can be determined by correcting for the moisture uptake of the polymer. Detailed calculations regarding the moisture uptake of the zeolites are provided in appendix B. The moisture uptake of the zeolites was measured to be 22 wt% which is similar to the reported water sorption capacity of the zeolites (26 wt%).[11, 12] The slight observed decrease in capacity could be because of the moisture uptake during the sample transfer from the oven to the weighing scale.

During the usual testing procedure, the membrane is removed from the oven (after high temperature desorption) and masked onto a cell and later loaded in a permeation system. The masking of the membrane takes about 30 min and during this time, the moisture from air could be absorbed by the zeolites, thereby saturating them. Experimental studies show that 65% of the zeolites are saturated with moisture from air during the 30 minute masking period. Further studies also indicate that essentially all the water is desorbed from the membrane after pulling vacuum overnight on the membrane in the permeation system at 35 ºC. Appendix B contains more detailed explanation on

these moisture uptake and desorption experiments. Since degassing is typically done for at least a day before the actual permeation, essentially all the water is believed to be removed from the zeolites by the start of actual permeation.

These above two sets of experiments suggest that the zeolites are not blocked; however, the permeation measurements (results from 3-phase Maxwell modeling) suggest that the zeolites are blocked, so these findings seem to contradict each other. In fact, if the gas transport through the zeolites is slowed down sufficiently, then the zeolites appear to be blocked, whereas, in terms of equilibrium uptake the sieve capacity is not greatly affected, consistent with our findings. I speculate, therefore, that the gas transport through the zeolites may be slowed down greatly, and this reduction in gas transport is possible if solvent (NMP) molecules reside in outer pores of the zeolites. The transport through the zeolites could be significantly hindered even if one outer layer of the zeolite pores is filled with NMP molecules. As the size of NMP molecule is slightly greater than the zeolite 4A pore dimensions (3.8 Å), diffusion of NMP molecules in and out of the zeolites is difficult; however, during the sonication step, the zeolite particles collide with each other quite strongly producing high local temperatures which could drive NMP molecules into the pores of the zeolite.[13, 14] Once NMP is driven into the zeolites by sonication, it is hard for it to diffuse out and therefore it gets stuck inside the zeolite. These stuck NMP molecules may reduce the transport through the zeolite.

6.6.2. Suggestions to improve the transport properties of sieves

To determine the effect of NMP on the zeolite transport properties, one could perform CH_4 (or any other gas that diffuse through the zeolite) sorption kinetics on the

neat zeolites and also on the zeolites sonicated in NMP. By comparing the CH_4 diffusion coefficients through them, one could determine the effect of NMP.

If NMP is found to be the reason for the slow kinetics then one could use alternate solvents such as dimethyl sulfoxide (DMSO) or dimethyl acetamide (DMAc). However, these solvents are similar in size and so similar pore blocking affects may be encountered even with these solvents. Moreover, the environmental and health hazards of these solvents make them less attractive for practical purposes.[15, 16] Another approach would be to use zeolite 5A instead of zeolite 4A. Since zeolite 5A has 4.4 Å pore openings [11], NMP could come out relatively easily at high temperatures. More importantly, zeolite 5A also has good CO_2/C_2F_4 selectivity as the pore size of zeolite 5A is still smaller than C_2F_4 (kinetic diameter ~ 5.3 Å). So using zeolite 5A appears to be a more practical approach to this blocking issue.

6.6.3. Suggestions to improve the interface

As shown previously, the permeation experiments indicate the presence of subnanometer voids between the polymer and the zeolite. I speculate that these voids are formed because Torlon® is a rigid polymer (T_g = 270 °C). For rigid polymers, energy (similar to activation energy) is required to move their polymer segments so that they can interact with the zeolite surface. This activation can be provided by heating the membrane beyond its glass transition temperature in a vacuum oven. If the interactions between the polymer and the zeolite can be promoted, the voids may be removed by this heat treatment procedure.

Another possible reason for the occurrence of subnanometer voids in the case of PFBPA treated zeolites may be the structure of PFBPA ligand. PFBPA ligand (shown in Figure 6.5) has an intermediate carbon atom between the phosphonic acid group (that attaches to the zeolite) and the benzene group (that interacts with the polymer). This carbon atom may provide 2-3 Å packing defects around the sieve surface, resulting in a non-selective pathway. To probe this, a phosphonic acid ligand without the intermediate carbon atom (i.e. a pentafluro benzene group attached directly to the phosphonic acid group) may eliminate the observed angstrom size defects, and this certainly merits investigation.

6.7. Summary and conclusions

Mixed matrix membranes were formed with 20wt% zeolite loading in Torlon® without any particle agglomerations. Hydrogen bonding between the amide groups of Torlon® and hydroxyl groups of zeolite 4A were expected to help forming a good interface, and so the mixed matrix membranes with untreated zeolite 4A were studied to probe this possibility. SEM images indicate good apparent interaction between Torlon® and untreated zeolite 4A. On the other hand, gas permeation measurements using O_2 and N_2 gases show that the O_2/N_2 selectivity of the mixed matrix membrane is lower than the intrinsic value of the polymer, suggesting the presence of subnanometer defects between the polymer and the zeolite surfaces.

To eliminate these defects and improve the interface, the zeolite surfaces were modified using phosphonic acid chemistry. Penta-fluoro benzyl phosphonic acid (PFBPA) ligands were used. Based on SEM images, PFBPA coated zeolites

appeared to form good interface with the polymer. Unfortunately, O_2/N_2 selectivity is still lower than the intrinsic value of Torlon® suggesting that the subnanometer size defects are still present.

The mixed matrix membranes were analyzed further by modeling with a 3-phase Maxwell model. The model not only indicates the presence of voids but also suggests that the zeolites are blocked. The most likely source of the apparent sieve blockage is sonication-induced intrusion of NMP into the surface pores of the zeolite. This hypothetical surface pore blockage (even in a small layer of the zeolite surface) could provide adequate reductions in effective sieve transport, lowering the effective permeability without substantially inhibiting equilibrium uptake. Sorption kinetic study of NMP-sonicated sieves followed by re-calcining could help verify this hypothesis. If this analysis is correct, successful mixed matrix membranes require resolution of both these issues (subnanometer interfacial defects and pore blockage), and the potential methods to address these issues were suggested.

6.8. References

1. Moore, T.T. and J.K. William, *Effect of materials, processing and operating conditions on the morphology and gas transport properties of mixed matrix membranes*, in *Department of Chemical Engineering*. 2004, PhD Thesis, University of Texas at Austin: Austin.

2. Mahajan, R., *Formation, characterization and modeling of mixed matrix membrane materials*, in *Department of Chemical Engineering*. 2000, PhD Thesis, The University of Texas at Austin: Austin.

3. Shu, S., S. Husain, and J.K. William, *A general strategy for adhesion enhancement in polymeric composites by formation of nanostructured particle surfaces.* The journal of physical chemistry C, 2007. 111(2): p. 652-657.

4. Mahajan, R. and W.J. Koros, *Mixed matrix membrane materials with glassy polymers. Part 1.* Polymer Engineering and Science, 2002. 42(7): p. 1420-1431.

5. Duval, J.-M., et al., *Preparation of zeolite filled glassy polymer membranes.* Journal of Applied Polymer Science, 1994. 54: p. 409-418.

6. Vankelecom, I.F., et al., *Incorporation of zeolites in polyimide membranes.* The journal of physical chemistry 1995. 99(35): p. 13187-13192.

7. Kim, P., et al., *Phosphonic acid-modified barium titanate polymer nanocomposites with high permittivity and dielectric strength.* Advanced Materials, 2007. 19: p. 1001-1005.

8. Ringer, A.L., et al., *The effect of multiple substituents on sandwich and T-shaped $\pi-\pi$ interactions* Chemistry a european journal, 2006. 12: p. 3821-3828.

9. Hotchkiss, P. and S. Marder, *The design, synthesis, and use of phosphonic acids for the surface modification of metal oxides*, in *Chemistry and Biochemistry*. 2008, PhD Thesis, Georgia Institute of Technology: Atlanta.

10. Neogi, P., *Diffusion in Polymers*. 1996, New York: Marcel Dekker, Inc.

11. Breck, D.W., *Zeolite molecular sieves*. 1974, New York: J. Wiley and Sons. 636-637.

12. Moore, T.T. and J.K. William, *Gas sorption in polymers, molecular sieves, and mixed matrix membranes.* Journal of Applied Polymer Science, 2007. 104: p. 4053-4059.

13. Moore, T.T. and J.K. William, *Sorption in zeolites modified for use in organic-inorganic hybrid membranes.* Ind. Eng. Chem. Res., 2008. 47(3): p. 591-598.

14. Ramesh, S., Y. Koltypin, and A. Gedanken, *Ultrasound driven aggregation and surface silanol modification in amorphous silica microshpheres.* J. Mater. Res., 1997. 12(12): p. 3271-3277.

15. Brayton, C.F., *Dimethyl sulfoxide (DMSO): a review.* The Cornell Veterinarian, 1986. 76(1): p. 61-90.

16. Kennedy, G.L.J., *Biological effects of acetamide, formamide, and their monomethyl and dimethyl derivatives.* CRC Crit. Rev. Toxicol., 1986. 2: p. 129-182.

CHAPTER 7

SUMMARY, CONCLUSIONS AND FUTURE DIRECTION

7.1. Summary and conclusions

Torlon® membranes are shown to provide selective separations of CO_2/C_2F_4 under supercritical CO_2 conditions (up to 1250 psi partial pressures of CO_2). Torlon®, a polyamde-imide, was chosen as the membrane material because of its ability to form inter and intra chain hydrogen bonding. These hydrogen bonds provide resistance to CO_2 plasticization and therefore provide selective separations under supercritical conditions. Successful spinning of asymmetric hollow fiber membranes from Torlon® is an important step towards making practical membranes. An initial attempt of spinning Torlon® resulted in hollow fibers with defective skins and macrovoids that make the membranes nonselective and cause the fibers to collapse at high pressures. After subsequent optimization of both dope composition and spinning parameters, defect-free asymmetric hollow fiber membranes and macrovoid free fibers are successfully made.

The successful asymmetric hollow fiber membranes were then studied for the separation of CO_2/C_2H_4 and $CO_2/C_2H_2F_2$ gas mixtures. The membrane provides mixed gas selectivities of 34 and 106, respectively, for CO_2/C_2H_4 and $CO_2/C_2H_2F_2$ gas mixtures at 1250 psi partial pressures of CO_2. This increasing trend in selectivity with the addition of fluorine atoms suggests that the selectivity of CO_2/C_2F_4 will be more than 106. Even a selectivity of 100 would be very attractive, so one of the overarching goals of this work was achieved. Another key goal was to achieve a highly stable membrane, and the

membrane created here show stable separations under high CO_2 partial pressure feed conditions without being plasticized, so this goal is achieved as well.

To further improve the plasticization resistance of Torlon® and to further improve its separation performance, the so-called mixed matrix approach was explored. In the process of improving the polymer-zeolite interface, we identified that the zeolite surface can be modified using phosphonic acid (PA) ligands. As these ligands are relatively inexpensive, this surface modification process appears commercially attractive. Unfortunately, experimental and modeling studies indicate that both the untreated 4A and PA treated 4A zeolites formed defective membranes. Based on the experimental evidence and 3-phase Maxwell modeling, I tentatively conclude that the mixed matrix membranes contained subnanometer sized defects between the polymer and sieve surfaces. Based on these findings, I also tentatively conclude that the sieves are blocked. It was speculated, but not proven definitively that the casting solvent (NMP) was irreversibly driven into the outer region of the sieves. Such an outcome could result during the ultrasonication of zeolites in NMP. Since NMP is close to the critical window size of 4A sieves, significant local heating (during sonication process) could facilitate superficial NMP uptake with no clear way to remove such contaminant. After identifying the above interfacial defects and NMP contaminants, I suggest heating these membrane above glass transition of the polymer (>280 ºC) and using zeolite 5A (instead of 4A) to solve these issues. The larger sieve size will allow easy in and out movement of the solvent, thereby preventing plugging.

7.2 Future directions

7.2.1. Modifying the Structure of Torlon®

As shown earlier in this thesis, Torlon® provides high resistance to CO_2 plasticization compared to other CO_2 separating polymers. However, Torlon® is a low permeable polymer. CO_2 permeability of Torlon® is 0.47 barrers compared to Matrimid®[1] (12.5 barrers), Cellulose acetate[1] (6 barrers). The relatively simple aryl groups in Torlon® (Figure 7.1) allow the polymer chains to pack close together. This results in reduced free volume in the membrane causing low gas permeabilities.

Torlon® type polymers can be made more permeable by having bulky aryl and bulky pendant groups in its structure which disrupt the close chain packing and increase the free volume of the membrane.

7.2.1.1. Predicting CO2 permeabilities in the modified Torlon®

Gas permeabilities through the new modified polyamide-imide polymers can be estimated using a model reported by Paul et al.[2] According to the model, the permeability of a gas (P) is calculated using the following expression:

$$P = A\exp\left(-B/FFV_n\right), \tag{7.1}$$

where A and B are constants for a particular gas. FFV_n represents fractional free volume of the membrane for a particular gas n. This FFV_n depends not only on the membrane material but also on the diffusing gas molecule and is given by:

$$FFV_n = \left[V - (V_o)_n\right]/V\,, \tag{7.2}$$

where V and $(V_o)_n$ represent the specific volume of the polymer and the volume occupied by the polymer chains, respectively. $(V_o)_n$ also depends on the type of gas n. Both these volumes are empirically estimated used the following expressions.

$$(V_o)_n = \sum_{k=1}^{K} \gamma_{nk} (V_w)_k , \tag{7.3}$$

$$\text{and } V = \sum_{k=1}^{K} \beta_k (V_w)_k . \tag{7.4}$$

Where V_w represent the van der Wall volume of group k of the polymer. β_k, and γ_{nk} are the constants for a particular group k and gas n. All the values (A, B, V_w, β_k, and γ_{nk}) are reported in the publication by Paul et al.[2]

Two different polyamide-imide structures are considered (shown in Figure 7.1) along with Torlon® 4000T to understand the effect of structural groups on the polymer permeability. The estimated CO_2 permeabilities of these polymers are given in Table 7.1. The reason for modeling CO_2 permeability of Torlon® 4000T is to determine whether the model yields reasonable predictions or not. The estimated CO_2 permeability of Torlon® (0.45 barrers) is quite close to the experimental value (0.44 barrers) validating the accuracy of the model. The predicted permeabilities of the two different polyamide-imide polymers are greater than Torlon® (more than one order of magnitude) indicating that the Torlon® can be made more permeable by modifying its structure.

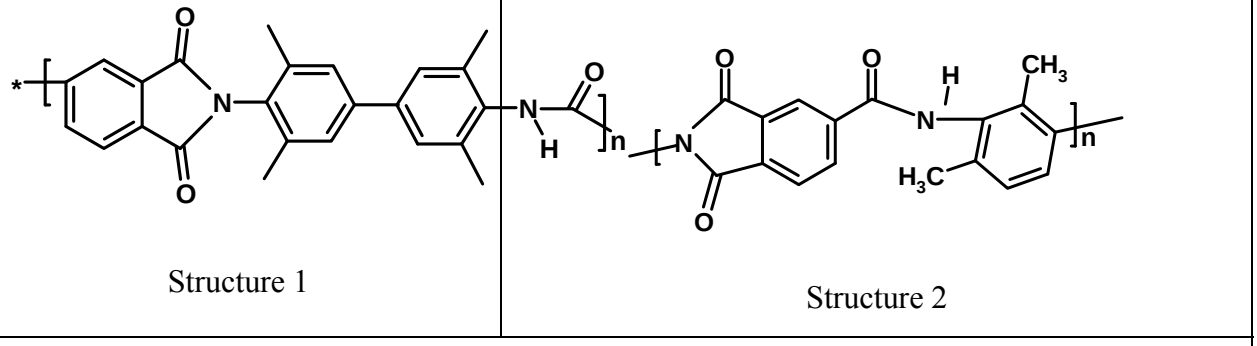

Structure 1

Structure 2

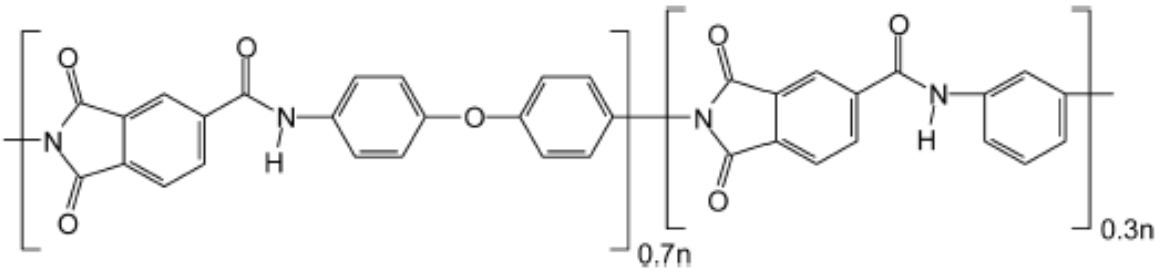

Torlon® 4000T

Figure 7.1: This figure shows the comparison between the structures of Torlon® 4000T and other polyamide-imide polymers that have bulky groups.

Table 7.1: The predicted CO_2 permeabilities of Torlon® 4000T and other polyamide-imides polymers.

Type of Polymer	Predicted CO_2 Permeability (Barrers)
Torlon® 4000T	0.45
Structure 1	30
Structure 2	10

7.2.1.2. Previous studies on different polyamide-imide polymers

Recent researchers[3-5] have studied different polyamide-imides for gas separations. The structures of these polymers are given in Figure 7.2. These polymers have bulky groups compared to Torlon® as thus they are predicted to have higher permeabilities. Oxygen and CO_2 permeabilities through these polymers have been measured and are given in Table 7.2.[3-5] These values confirm our previous predictions that CO_2 permeabilities can be greatly enhanced (even by two orders of magnitude) by appropriately modifying the structure.

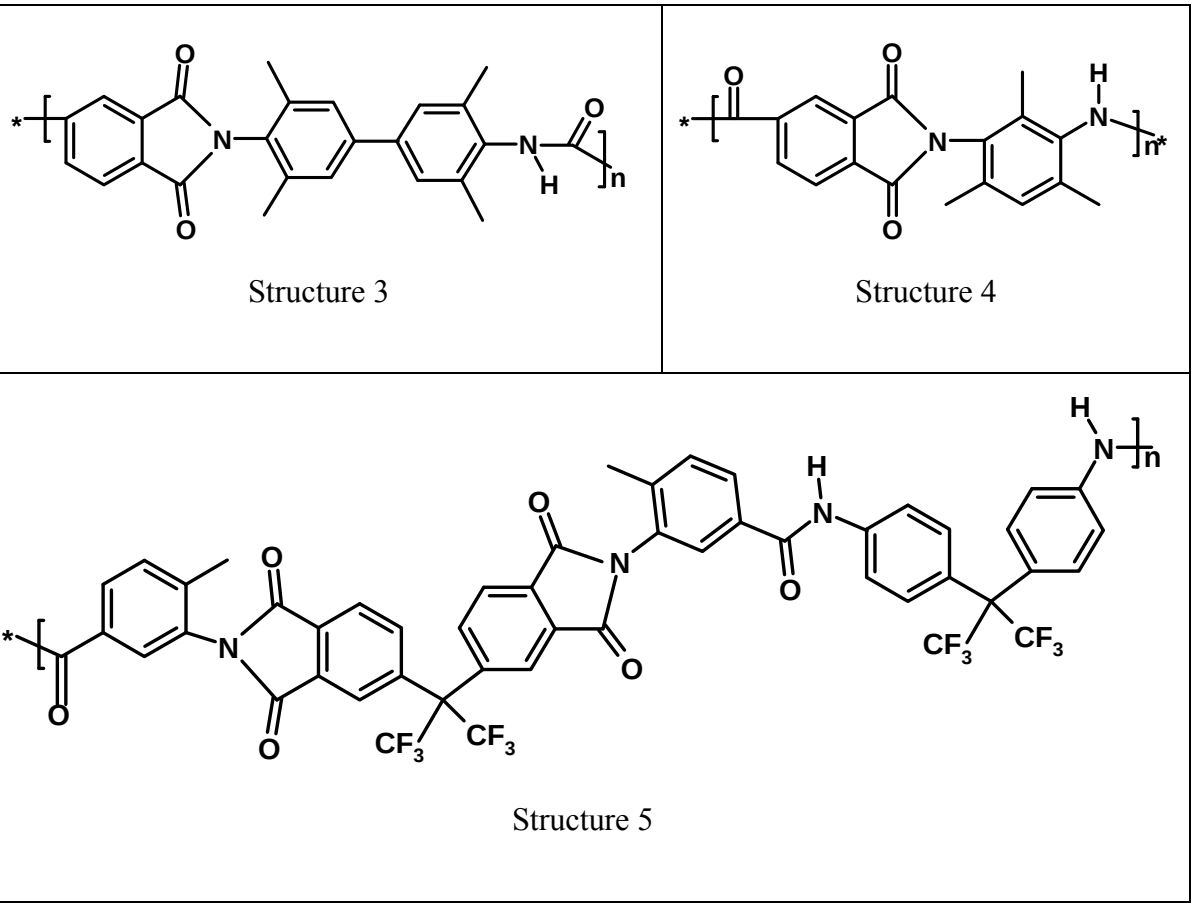

Figure 7.2: Polyamide-imide polymers that are synthesized by previous researchers

Table 7.2: Pure gas permeability values of different polyamide-imides measured at 35 °C, at pressures less than 10bar.

Type of Polymer	Permeability of CO_2 (Barrers)	Permeability of O_2 (Barrers)
Torlon® 4000T	0.47	0.12
Structure 3		0.9
Structure 4		4.8
Structure 5	72.7	10.5

7.2.1.3. Discussion on Structure Modification

Findings in the above sections indicate that the structure of the Torlon® can be engineered to enhance the permeabilities. The new modified structures (Figures 7.1 and 7.2) still have the **same number of hydrogen bonds per repeat unit** and hence should maintain the potential to provide outstanding resistance to plasticization. We expect, therefore, that the diffusion selectivity can be preserved under aggressive conditions. The ether groups in the original Torlon® (Figure 7.1) make the polymer chains flexible, and by having more rigid aryl groups in the back bone (like the structures shown in Figures 7.1 and 7.2), both the resistance to plasticization and the selectivity can hopefully be further enhanced or at least can be preserved.

Depending on the size and chemistry of these modified aryl and pendant groups, the permeabilities and selectivities of the modified polymer will be affected. Larger

pendant groups will cause greater disruption in polymer segmental packing and therefore result in greater gas permeabilities. Similarly, if the chemistry of the pendant group favors the absorption of CO_2, then again the CO_2 permeability will be increased. However, if the polymer chains are greatly disrupted, or if CO_2 absorption is greatly enhanced then the polymer may become susceptible to plasticization and the diffusion selectivity may go down. So there exists a tradeoff between the permeability and the plasticization resistance of the polymer. This tradeoff can be studied by performing a systematic study which involves identifying a permeable polymer based on the model predictions. Once a highly permeable polymer is identified, the polymer can be synthesized and studied for its plasticization pressure. This systematic study will yield a polymer with optimal permeability and plasticization resistance properties.

7.2.2. Exploring the relation between the macrovoid formation and the hydrophobicity of the polymer.

The presence of macrovoids in hydrophobic polymers such as Torlon®, Matrmid® and Ultem® and the absence of macrovoids in relatively less hydrophobic polymers such as cellulose acetate indicate that the hydrophobicity of the polymers plays an important role in determining the macrovoid formation. If the polymer is hydrophobic then the interfacial energy between the polymer and the "polymer lean phase" (which is rich in water) is high. When the interfacial energy is high, the macrovoids are formed to minimize the interfacial area. On the other hand, if the polymer is less hydrophobic, then the interfacial energy between the polymer and the "polymer lean phase" is low and no macrovoids are formed.

So if the structure of Torlon® is modified and the resulting polymer is less hydrophobic then the macrovoid formation may be restricted. The hydrophobicity of the polymer can be characterized by measuring contact angles on the polymer film. This study of hydrophobicity of the polymer and the tendency for macrovoid formation will open an opportunity to modify the polymer structure to suppress macrovoids.

7.2.3. Extending the performance of Torlon® membranes beyond 1250 psi of CO_2

As shown in Chapter 5 of this thesis, Torlon® membranes get plasticized and their substructure collapses at pressures beyond 1250 psi partial pressures of CO_2. Because of these effects, the performance of the membrane is drastically decreased. This failure happens because of the high sorption of CO_2 under those high CO_2 partial pressure conditions.

If the sorption of CO_2 is decreased then the membrane can withstand higher partial pressures without being plasticized. This can be done by increasing the temperature of the separation. At higher temperatures, less CO_2 is absorbed in the membrane and the membrane may withstand higher pressures if its intrinsic modulus and permselectivity of the unplasticized polymer does not drop precipitously.

Presumably an optimum temperature exists at which the membranes have high plasticization resistance to withstand high CO_2 pressures and increasing the temperature may be attractive if the first effect (less CO_2 sorption) is more dominant than the second effect associated with thermally driven reductions in intrinsic permselectivity and modulus. On the other hand, decreasing the temperature will help if the second effect is more dominant than the first effect. Experimentation is the best way to determine the

interplay of these effects. This can be done by measuring the plasticization pressures at various temperature conditions and finding the optimal temperature.

7.2.4. Functionalized nanowhisker morphology for better interface

In the previous chapter we found that the "penta fluoro benzyl phosphonic acid (PFBPA)" modified zeolite 4A forms angstrom sized interfacial defects with Torlon®. We hypothesize that these defects are formed because Torlon® is rigid and so it is energetically unfavorable for the polymer coil to deform and form good interactions with the zeolite surface. If the polymer coil can interact with the zeolite surface in its natural state (i.e. without the need for it to stretch) then a better interface could be formed. This can be achieved by having whisker morphology on the zeolite surface. If the whisker morphology is of the same dimensions as that of the polymer then the polymer can interact with the whiskers in its natural state. Moreover, whisker morphology increases the interfacial contact area between the polymer and the zeolite and hence a stronger interface can be created if a favorable interaction exists between the polymer and the whisker surface.

Some of our previous group members were successfully able to create $Mg(OH)_2$ nanowhiskers on the zeolite surfaces.[6, 7] This whisker technology can be used in our mixed matrix membranes in obtaining a good polymer-zeolite interface. In addition, these whiskers can be functionalized with PA ligands that have good interactions with Torlon®. Such a functionalized nanowhiker surface would have both the entropic advantage of nanowhiskers and the favorable enthalpic interactions of PA ligands. With this new approach, a good polymer-zeolite interface can be created.

7.2.5. Addressing the NMP contamination

Based on the experimental observations and modeling results, the zeolites appear to be blocked. I speculate that this blockage is due to the presence of NMP in the outer layer of the zeolite surface which significantly hinders the gas transport. As NMP size is close to the window size of zeolite 4A (3.8 Å), it is driven inside the zeolite during the sonication process. Once inside the pores, NMP is stuck and is difficult to remove. Even heating the membranes to 220 ºC is not sufficient to remove the absorbed NMP. Using alternate solvents such as DMSO or DMAc do not appear promising because of their similarity in size to NMP and as such similar blocking issues may be encountered with these solvents.

The issue of NMP contamination may be solved by using zeolite 5A instead of zeolite 4A. Since zeolite 5A has a critical window size of 4.4 Å (greater than the size of zeolite 4A), removing the absorbed NMP will be relatively easy. Moreover, the pore size of zeolite 5A is still large enough to block C_2F_4 (kinetic diameter ~ 5.3 Å) and provide high selectivity for CO_2/C_2F_4 gas pair.

7.3. References

1. Bos, A., et al., *CO_2-induced plasticization phenomena in glassy polymers.* Journal of Membrane Science, 1999. 155: p. 67-78.

2. Park, J.Y. and D.R. Paul, *Correlation and prediction of gas permeability in glassy polymer membrane materials via a modified free volume based group contribution method.* Journal of Membrane Science, 1997. 125(1): p. 23-39.

3. Choi, K.-Y., et al., *Polyamide-imide having head-to-tail backbone*. 2000, US Patent: 6,433,184 B1, Korea Research Institute of Chemical Technology.

4. Fritsch, D. and K.-V. Peinemann, *Novel highly permselective 6F-poly(amide-imide)s as membrane host for nano-sized catalysts.* Journal of Membrane Science, 1995. 99: p. 29-38.

5. Gao, X. and F. LU, *Structure/permeability relationships of polyamide-imides.* Journal of Applied Polymer Science, 1994. 54: p. 1965-1970.

6. Shu, S., S. Husain, and J.K. William, *A general strategy for adhesion enhancement in polymeric composites by formation of nanostructured particle surfaces.* The journal of physical chemistry C, 2007. 111(2): p. 652-657.

7. Shu, S., S. Husain, and J.K. William, *Formation of nanostructured zeolite particle surfaces via a halide/grignard route.* Chemistry of materials, 2007. 19(16): p. 4000-4006.

APPENDIX A

A.1. Determining compressibility factors

The deviation of a gas from its ideal behavior is often represented by compressibility factor (Z) and is defined as

$$Z = \frac{P \times v}{R \times T}, \tag{A.1}$$

where P, T, and v represent the pressure, temperature and specific volume, respectively. To determine the compressibility factor, one needs to know all these three quantities: temperature, pressure, and specific volume. Out of these three quantities, the pressure and temperature of a gas can be experimentally measured. The remaining quantity, specific volume, is determined from an equation of state. For gases at low pressures, ideal gas law is used in determining this specific volume. For high pressures, ideal gas law is not applicable and more advanced equations of states such as virial equation of state, Peng-Robinson equation of state are needed. Peng-Robinson (PR) equation of state is used for non-polar molecules such as CO_2, C_2H_4 etc. PR equation of state is not applicable for polar molecules such as $C_2H_2F_2$. For such polar molecules, virial equation of state is used instead. Both of these equations of state are briefly summarized below.

A.1.1. Peng Robinson Equation of State[1]

Peng-Robinson equation of state is a cubic equation with respect to volume and is given below:

$$P = \frac{RT}{V - b} - \frac{a}{V^2 + 2bV - b^2}, \tag{A.2}$$

where $b = \dfrac{0.07780 \times R \times T_C}{P_C}$,

$a = \dfrac{0.45724 R^2 T_C^2}{P_C}\left[1 + f\omega\left(1 - T_r^{1/2}\right)\right]^2$ and $f\omega = 0.37464 + 1.54226\omega - 0.26992\omega^2$.

Where P, V, T, R, ω, P_C, T_C, and T_r represent pressure, volume, temperature, universal gas constant, acentricity, critical pressure, critical temperature, and reduced temperature respectively. The reduced temperature is the ratio between the actual temperature and the critical temperature of the gas.

The equation (A.1) can also be represented in terms of the compressibility factor (Z) and is given below:

$$Z^3 - \left(1 + B^* - 2B^*\right)Z^2 + \left(A^* - 3B^{*2} - 2B^*\right)Z - A^*B^* + B^{*2} + B^{*3} = 0, \qquad \text{(A.3)}$$

where $A^* = \dfrac{aP}{R^2T^2}$ and $B^* = \dfrac{bP}{RT}$.

Solving the equation (A.2) gives the compressibility factors. The compressibility factors for CO_2 and C_2H_4 are determined using this approach. The critical parameters along with the acentricity (ω) for CO_2 and C_2H_4 species are provided in Table A.1.

A.1.2. Virial Equation of State[1]

The virial equation of state provides a relationship between pressure, volume, and temperature of the gas. It is given by the following expression:

$$Z = \frac{P \times v}{R \times T} = 1 + \frac{B \times P}{R \times T}, \qquad \text{(A.4)}$$

where B is called the second virial coefficient and is calculated from the established correlations. Depending on the polarity of the species, different correlations exist and are

detailed in the following sections. This Virial equation of state is used only when the specific volume of the gas is more than twice the critical volume $\left(V > 2V_C\right)$.

A.1.2.1. Non-polar molecules

For non-polar molecules, the value B is defined as[1]

$$\frac{BP_C}{RT_C} = B^{(0)} + \omega B^{(1)}, \tag{A.5}$$

where $B^{(0)} = 0.083 - \frac{0.422}{T_r^{1.6}}$ and $B^{(1)} = 0.139 - \frac{0.172}{T_r^{4.2}}$

A.1.2.2. Polar molecules

In case of polar molecules, the second virial coefficient (B) is determined using group contribution method proposed by McCann et al.[2] For each group, there are two contributions: the primary and the secondary. From these contributions, B is calculated using the following expressions:

$$B = \sum_{pri} n_i \Delta B_i + \sum_{\text{sec}} \left(n_i - 1\right)^2 \Delta B_i \tag{A.6}$$

$$\text{and } \Delta B_i = a_i + \frac{b_i}{T_r} + \frac{c_i}{T_r^3} + \frac{d_i}{T_r^7}. \tag{A.7}$$

Where n_i represent the number of occurrences of a particular group in the molecule. The terms a_i, b_i, c_i, and d_i are the group contribution coefficients for a particular i^{th} group. The reduced temperature (T_r) is the ratio of the experimental temperature and the critical temperature ($T_r = T/T_C$).

A.1.2.2.1. Compressibility factor for $C_2H_2F_2$

The above virial equation of state for polar molecules is used in determining the compressibility factor for polar $C_2H_2F_2$. Group contribution method as described above is used in estimating the second virial coefficient. Two groups, -CH_2 and –CF_2, are identified in the molecule. Both these groups have only primary contributions and have no secondary contributions. The expression for B is

$$B = \left(\Delta B_{CH_2} + \Delta B_{CF_2}\right)_{pri}. \tag{A.8}$$

The group contribution coefficients for –CH_2 and –CF_2 groups are listed in Table A.2. After substituting the coefficients, the final equation is given below:

$$B = 93.56 - \frac{208.51}{T_r} - \frac{61.46}{T_r^3} - \frac{0.104}{T_r^7}. \tag{A.9}$$

The units of B are cm^3/g-mol. The critical temperature required to evaluate T_r for $C_2H_2F_2$ is provided in Table A.1.

Table A.1. This table lists the critical values (both the critical temperatures and pressures) and the acentricity values for CO_2, C_2H_4 and $C_2H_2F_2$ gas molecules.

Gas Name	critical temperature (T_C in K)	critical Pressure (P_C in bars)	Acentricity (ω)
CO_2	304.1	73.8	0.239
C_2H_4	282.4	50.4	0.089
$C_2H_2F_2$	302.9	44.6	0.14

Table A.2. The group contribution coefficients for the two groups that are present in $C_2H_2F_2$: $-CH_2$ and $-CF_2$.

Coefficients	$-CH_2$	-CF2
a_i	36.25	57.31
b_i	-83.11	-125.40
c_i	-32.56	-28.90
d_i	-0.2862	0.1822

A.2. References

1. Reid, R.C., J.M. Prausnitz, and B.E. Poling, *The Properties of Gases and Liquids*. Fourth ed. 1987: McGraw-Hill, Inc., p: 656-732.

2. McCann, D.W. and R.P. Danner, *Prediction of Second Virial Coefficients of Organic Compounds by a Group Contribution Method.* Ind. Eng. Chem. Process. Des. Dev, 1984. **23**: p. 529-533.

APPENDIX B

MOISTURE UPTAKE KINETICS OF THE MIXED MATRIX MEMBRANES

B.1. Moisture uptake by zeolites in the mixed matrix membranes

Before the moisture uptake measurements, the membrane is heated to 220 ºC overnight to remove any absorbed water. The membrane is then cooled down to room temperature and transferred from the oven immediately to a weighing scale. The membrane is then equilibrated with the moisture in air at ambient conditions and the weight gain during this time is recorded manually. Figure B.1 shows the percentage increase in weight with time. The relative humidity and the temperature during the course of experiment are 23% and 21 ºC, respectively.

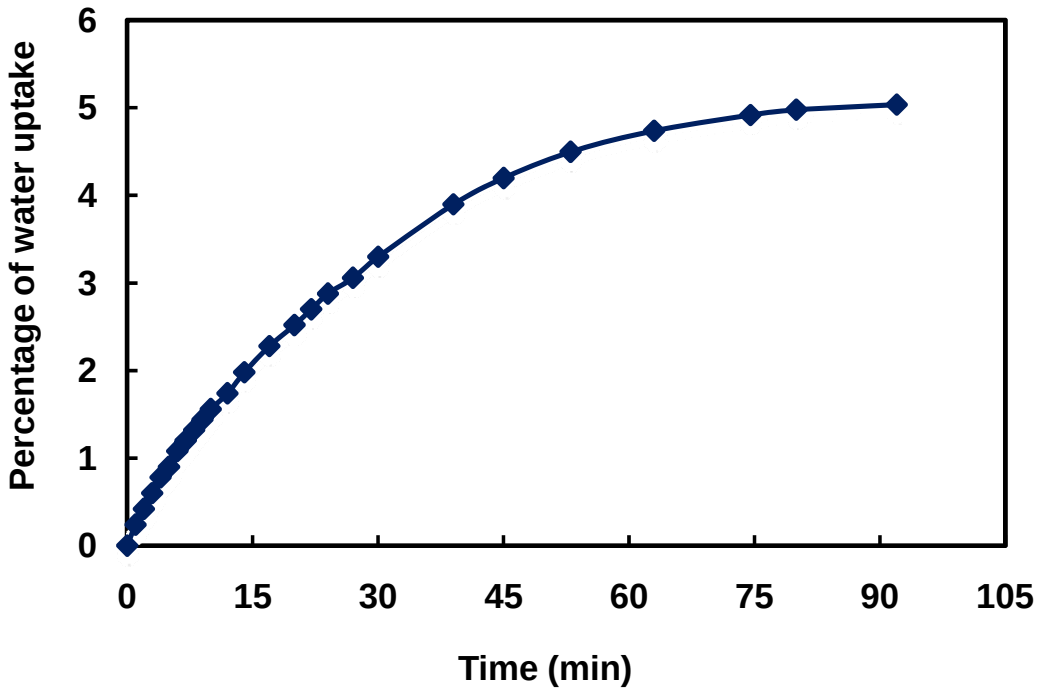

Figure B.1: Percentage of water uptake by the mixed matrix membrane of Torlon and zeolite 4A. The membrane consists of 20 wt% zeolite loading.

The above increase in weight by the membrane is due to the absorption of moisture both by the polymer and the zeolite materials. To decouple the moisture uptake of these materials, moisture uptake by a neat polymer film is studied independently. The percentage increase in weight of the Torlon® film with time is plotted in Figure B.2.

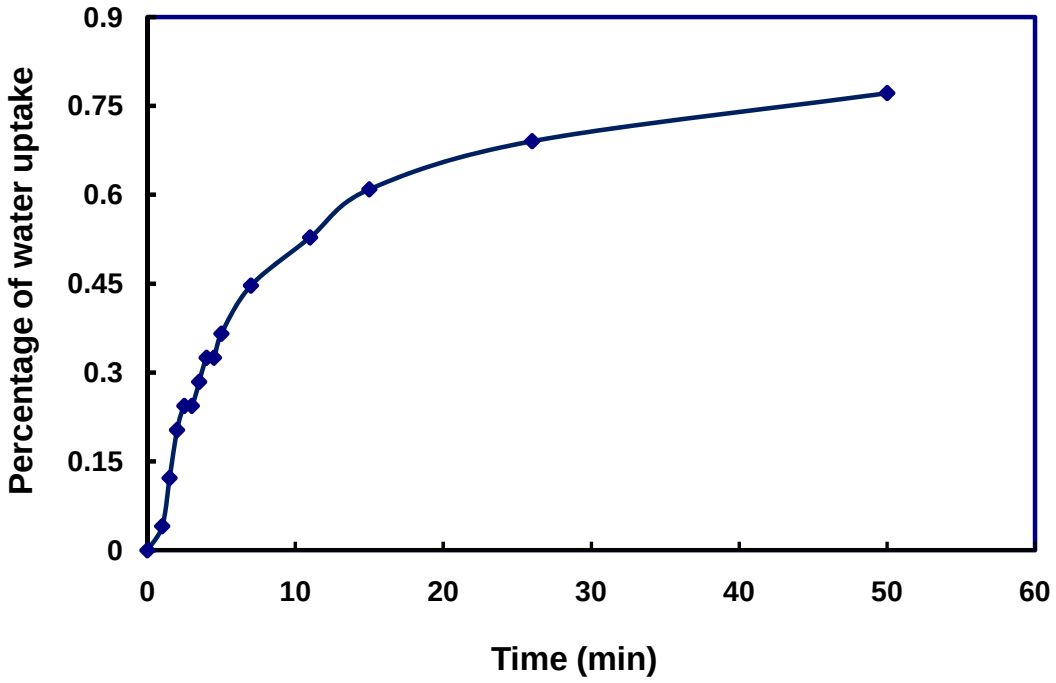

Figure B.2: Water uptake by Torlon® film as a function of time.

By subtracting the moisture uptake of Torlon® film from the mixed matrix membrane (on a weight average basis), the moisture uptake of the zeolites is determined. The percent moisture uptake by the zeolites is shown in Figure B.3. At saturation, zeolite 4A gains about 22 wt% of its weight and this amount is similar to the reported saturation value for zeolite 4A (26 wt% at relative humidity of 23%)[1, 2]. This similarity between the observed and expected values indicate that we are capturing the moisture uptake kinetics quite reasonably by these simple measurements.

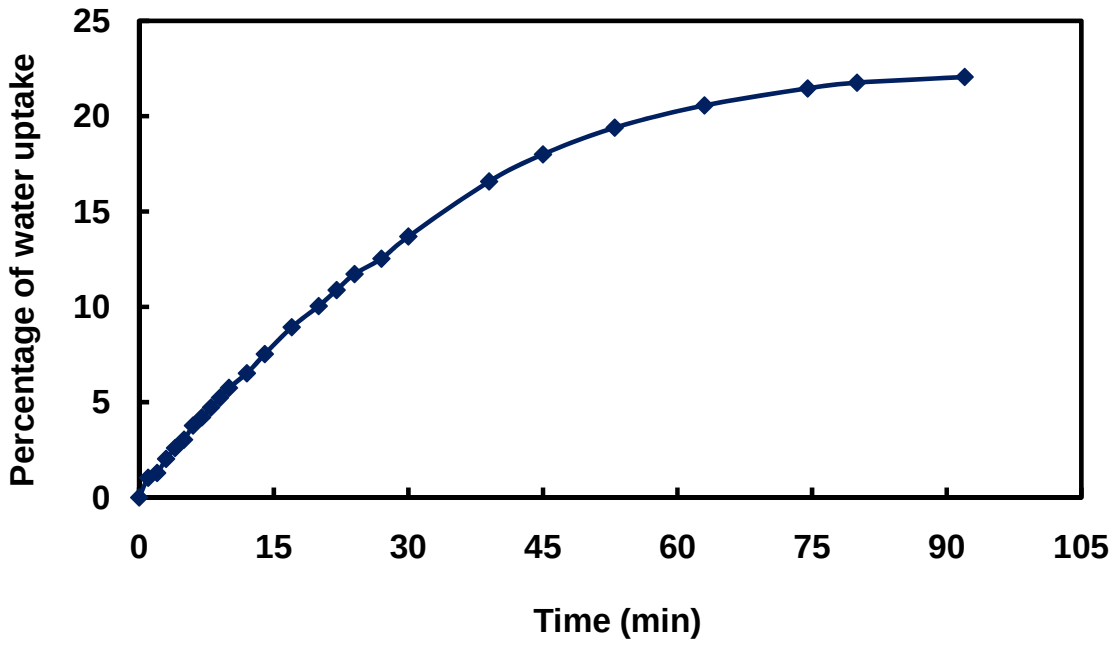

Figure B.3.: Percent moisture uptake by the zeolites

The above experiments also indicate that zeolite 4A (in mixed matrix membranes) becomes saturated with moisture within 60 min of its exposure to ambient conditions. Particularly, during the membrane masking step, which typically takes about 30 min, the zeolites could absorb up to 62% of their saturation value. This absorbed moisture could affect the transport properties of the zeolites. However, before the permeation test, the membrane is degassed overnight under vacuum at 35 ºC in the permeation system. So we wanted to see whether degassing the membrane under the exact same conditions would remove the water from the zeolites. So the following experiment is performed.

A membrane is intentionally saturated with moisture by keeping it in the ambient conditions and then the membrane is degassed in the permeation system at 35 ºC overnight. After this degassing step, the membrane is removed and immediately transferred to the balance to capture the moisture uptake kinetics. The final moisture

uptake of the zeolites is measured to be 22% , which is similar to the saturation value obtained after 220 º C heating. This indicates that the zeolites become active even after an overnight 35 ºC degassing step.

B.2. References

1. Breck, D.W., *Zeolite molecular sieves*. 1974, New York: J. Wiley and Sons. 636-637.

2. Moore, T.T. and J.K. William, *Gas sorption in polymers, molecular sieves, and mixed matrix membranes.* Journal of Applied Polymer Science, 2007. **104**: p. 4053-4059.